ADDIS ABABA UNIVERSITY

ADDIS ABABA INSTITUTE OF TECHNOLOGY

SCHOOL OF CIVIL AND ENVIRONMENTAL ENGINEERING

Assessment of Current Non-linear Analysis Models used in Earthquake Engineering

A Thesis in Structural Engineering

By: Anur Oumer

September, 2019

Addis Ababa

A Thesis

Submitted in Partial Fulfillment of the Requirements for the Degree of Master of Science

The undersigned have examined the thesis entitled '**Assessment of Current Nonlinear Models used in Earthquake Engineering**' presented by **Anur Oumer**, a candidate for the degree of **Master of Science** and hereby certify that it is worthy of acceptance.

Dr. Ing. Adil Zakaria		
Advisor	Signature	Date
Dr. Esayas G/Yohanes		
Internal Examiner	Signature	Date
Dr. Ing. Girma Zerayohanes		
External Examiner	Signature	Date
Dr. Ing. Mebruk Mohammed		
Chair person	Signature	Date

UNDERTAKING

I certify that research work titled "**Assessment of Current Nonlinear Models used in Earthquake Engineering**" is my own work. The work has not been presented elsewhere for assessment. Where material has been used from other sources, it has been properly acknowledged / referred.

Signature of Student

Anur Oumer

ABSTRACT

The study aims to evaluate existing numerical nonlinear modeling techniques used in the seismic analysis to provide a common ground for applications of the models in earthquake engineering. Comparative analysis carried out to further asses the existing nonlinear numerical finite element modeling techniques for beam-column elements subjected to lateral loading. First, experimentally tested RC bridge column specimens downloaded from peer structural performance database and modeled in OpenSees finite element software.

The study shows, for sections exhibiting strain hardening behavior, the distributed force-based fiber models provide a more accurate response. The response computed using the distributed displacement-based fiber models overestimate the capacity of the members. Therefore, to accurately describe the inelastic response, several displacement-based elements are required.

For the section exhibiting strain-softening behavior, the localization issue affected both the displacement-based and force-based formulations. Therefore, material regularization is required to overcome mesh dependent response. Furthermore, for section showing softening behavior, the regularization of both concrete and steel materials is required. The concentrated force-based plastic hinge model adequately captures the nonlinear response. The lumped plasticity with zero-length hinge model captures the initial stiffness adequately, but, inadequate to capture the cracking and onset of overall yielding. Furthermore, the model underestimates the ultimate capacity in terms of base shear.

Finally, to evaluate the numerical accuracy of the models, two-story and three-story RC frames modeled in OpenSees finite element software. For nonlinear analysis of the RC frames, the distributed force-based fiber models capture the inelastic response accurately. Increasing the axial load on the two-story RC frame exhibits mesh dependent results. For the frame under strain-softening behavior, the material regularization techniques successfully tackle the localization issue.

ACKNOWLEDGMENTS

First and foremost, I would like to express my deepest gratitude to my thesis advisor Dr. Adil Zakaria, of the School of Civil and Environmental Engineering at the University of Addis Ababa. I greatly admire his patience, motivation, and support throughout the year in writing this thesis. The door to Dr. Adil's office was always open whenever I ran into a trouble spot or had a question about my research.

I would also like to thank Dr. Esayas Gebreyouhannes of the School of Civil and Environmental Engineering at the niversity of Addis Ababa for the very relevant comments.

Last but not least, I thank the valuable support of my family and friends, for making me put things in perspective and helping me keep a balanced life. To my parents, role models who provided me with the education, motivation, loving guidance and unconditional support that lead me successfully through this journey, I am forever grateful.

Table of Contents

List of Tables

List of Figures

List of Notations

$\mathrm{a}_s(y,z)$	Section kinematic matrix
b_s	Strain Hardening
E_s	Modulus of elasticity
$\mathrm{b}(x)$	Section force interpolation function matrix
$e(x)$	Section deformation vector at x distance in the member
f	Element flexibility matrix
f_c	Maximum unconfined Concrete strength
f_{cc}	Maximum confined Concrete strength
f'_{c20}	Crushing stress of unconfined Concrete strength
f'_{cc20}	Crushing stress of confined Concrete strength
f_u	Ultimate strength of steel
f_y	Yield strength
G_s	Steel hardening energy
G_f^c	Fracture energy of concrete in compression
k_e	Elastic element stiffness matrix in basic system
k_S	Section stiffness matrix
L_{IP}	Length of integration point
L_p	Plastic hinge length
N	Sectional axial force
N_p	Number of element integration points

$N(x)$	Displacement interpolation function
M_y	Sectional moment about Y-axis
M_z	Sectional moment about Z-axis
q	Element basic force vector
$s(x)$	Sectional vector force
v	Element deformation vector;
ξ	Integration point location
ε_u''	Rapture strain
ε_a	Sectional normal strain
ε_o	Peak strain at maximum unconfined concrete
ε_y	yield strain steel
ε_{cc}	Peak strain at maximum confined concrete
ε_{cu20}	strain of the unconfined concrete at 80% strength loss
ε_{ccu20}	strain of the confined concrete at 80% strength loss
ω	Integration point weight
κ_y	Curvature along y-direction
κ_z	Curvature along z-direction

List of Abbreviations

ACI	American Concrete Institute
ASCE	American Society of Civil Engineers
DDB	Distributed Displacement-Based
DFB	Distributed Force-Based
EBCS	Ethiopian Building Code Standard
FEMA	Federal Emergency Management Agency
RC	Reinforced Concrete

1 Introduction

1.1 Background

Nowadays, it is most common to design structures using elastic analysis; however, under maximum earthquakes, structures experience significant inelastic deformations. The numerical nonlinear analysis of beam-column models play an important role in the performance-based design. Previously, before the development of the numerical nonlinear tools analysis was carried out using the equivalent force method. Currently, many building codes use this method for structures located in seismically low regions. Furthermore, EC-8 modifies this response to account for the nonlinear material behavior using the modification factor known as "behavior factor". However, structures in a region of high seismic risk respond beyond their elastic limit during maximum earthquake (Taucer et al. 1991).

After intense research has been carried on the nonlinear beam-column models, a reasonable accuracy have been found by the models in predicting inelastic response. This leads to every countries to update their building codes. For instance, more recently in Ethiopia, the EBCS-1995 have been updated to a new version and several parameters that may affect the response of existing building have been changed.

The study aims to assess the performance of the existing non-linear models in beam-column analysis subjected to seismic loading. In frame analysis, modeling of material nonlinearities classified into two main categories: lumped and distributed plasticity models.

The earliest lumped plasticity approach is through introducing zero-length nonlinear spring at member's end. The most commonly used lumped plasticity are the two-component model (Clough et al. 1965) and one-component model (Giberson 1967). The lumped plasticity approach is characterized by inserting discrete nonlinear hysteretic backbone cure at the ends of otherwise linear elements. These models are primarily based on the phenomenological and allow for efficient modeling of bending and shear failures based on empirically calibrated hysteretic backbone curve, But, the models fail to capture the interaction between bending moment and axial force.

Research has also been carried out to improve concentrated fiber models to overcome the problem of localization due to strain concentration in a single integration section. Improvement of distributed fiber models to avoid problems of localization in distributed force-based elements briefly discussed by Scott and Fenves (2006). This formulation uses a minimum number of integration sections by preserving all the advantages of force-based elements and addressing the issues of localization in distributed force-based beam-column formulations (Scott and Fenves 2006).

Distributed plasticity beam-column elements allow the formation of plastic hinges at any location along the length of the structural members. The axial-moment interaction can be captured automatically by integrating force-deformation in the section along the length of the element. The most common distributed plasticity models used in earthquake engineering are classical displacement-based and force-based beam-column elements.

The displacement-based formulation was the first distributed based beam-column element, which follows the standard finite element approach using cubic polynomials displacement function to describe the nodal displacements (Taucer et al. 1991). The shape function contains constant axial strain and linear curvature along the length of beam-column elements. Since the displacement field is approximate and equilibrium is weak, an increasing number of integrations cannot improve accuracy, so members should be divided into several elements to describe inelastic deformations in a plastic hinge region (Neuenhofer and Filippou 2007).

In the field of structural engineering practice, the force-based beam-column models (Taucer et al. 1991; Spacone et al. 1996a) gained acceptance since they provide optimal performance in terms of both numerical accuracy and computational efficiency (Feng and Ren 2017). The force-based beam-column formulations are based on the force interpolation functions that assume linear moment and constant axial along the length of the beam-column element. Force-based elements enforce the exact equilibrium between the nodal forces and section forces along the beam-column members. In force-based formulations, determining element-resisting forces is a very complicated issue, this comes from the impossibility of obtaining element-resistant forces directly from section resisting forces (Taucer et al. 1991).

In the field of fracture mechanics, the term "localization" is well established, and various researches are available regarding this topic. Experiment tests of compressive strength of different specimen sizes have shown that the pot-peak stress-strain behavior of concrete is size-dependent. Jansen and Shah (1997) conducted compressive tests for specimens with different slender length, and they found that, the longer the specimen, the steeper the curves become. In the field of computational mechanics, studies have shown that localization issues affect numerical models too. Therefore, the numerical models provide a non-objective response, which results from the concentration of strain over a small finite element length or a single integration point.

In the displacement-based elements, deformations localize over a single displacement-based beam-column element. Therefore, the response of a single displacement-based element showing a strain-softening behavior governs the overall response of the member (Scott and Fenves 2006).

In the force-based elements, deformations localize over a single integration section. The characteristic length equal to the integration weight associated with the section exhibiting strain-softening behavior governs the overall response of the member (Scott and Fenves 2006). For section exhibiting strain-softening behavior, as the number of integration points increases the response does not converge into the same solution. This is known as a non-objective response.

Coleman and Spacone (2001) suggest regularization techniques for the concrete material; however, for the section exhibiting strain-softening behavior, steel localizes at a critical section to confirm compatibility condition (Ashtari 2018). Softening in the section is comes from both fiber materials; therefore, the regularization of concrete and steel materials should be included (Pugh 2012). Scott and Fenves (2006) suggest regularization techniques based on the concentrated force-based fiber models.

1.2 Motivation of the study

To accurately predict the nonlinear behavior of reinforced concrete structures subjected to lateral loading assessing the performance of the existing inelastic fiber beam-column models is essential. These numerical models can offer valuable information on several engineering parameters, which are important in the performance-based engineering design. The existing fiber beam-column models are numerically robust and can provide an excellent response prediction for flexure dominated structures.

The fiber beam-column models may produce a nonobjective result for structures exhibiting strain-softening behavior.

To address the localization most of the Previous works were based on the regularization of only concrete. However, experimental cyclic tests have shown that, due to cyclic degradation of the reinforcement bar, members with relatively small axial load ratio also exhibit softening response. Therefore, the regularization of the steel material is required from the fact that for fiber section softening is always results from both concrete and longitudinal bar (Pugh 2012). The regularization of steel material is more recent. Therefore, the study makes the issues related to partial and full material regularization techniques more clear, and recommend the best way to overcome the localization issue in distributed plasticity.

Finally, and what is considered to be important of conducting such a study is that the old Ethiopian Building Codes Standard (EBSC-1995) is updated to a new version, and several parameters that may affect the behavior of existing structures are also changed. Therefore, such research can serve as a guideline for the design offices, structural engineers and parishioners to assess the behavior of new and existing structures using nonlinear analysis tools.

1.3 Objective of the study

1.3.1 General objective

The MSc Thesis aims to assess performance of the existing numerical non-linear analysis models used in earthquake engineering to simulate the nonlinear response of RC structures.

1.3.2 Specific objectives

The general objective achieved through the following specific objectives

- Review the state of art of existing nonlinear numerical beam-column models. This study focusses on the most widely used component-based models based on discrete mechanics which are concentrated and distributed plasticity.
- Mesh refinement study for section exhibiting strain-hardening and strain-softening response.
- Evaluation of models performance by applying material regularization only to concrete materials for section showing strain-softening response.
- Evaluation of models performance by applying material regularization only to steel materials for section exhibiting softening response.
- Assessing performance of the numerical models and application of material regularization to multistory RC frame.

1.4 Outline of the research

The current research focuses on the evaluation of current component-based nonlinear models used in seismic analysis. The thesis work is structured in the following chapters:

Chapter 1 discusses background of the numerical nonlinear modeling and objective of the study.

In chapter 2 a detailed review of the state of art of the numerical nonlinear model has been presented. The first historical background on how the numerical modeling technique improved to the existing state of art presented briefly. Damage localization on distributed fiber beam-column models also discussed briefly. Finally, the regularization technique to overcome mesh dependent results discussed briefly.

Chapter 3 presents numerical analysis using different numerical nonlinear models of cantilever bridge columns that exhibit hardening and softening under monotonic loading. an experimentally tested cantilever bridge column was taken to assess the performance of the models and detail comparative analysis has been presented. Furthermore, the existing regularization techniques evaluated on simulating the monotonic response of the bridge column.

In chapter 4 the contents are similar to chapter 3, however, in this chapter cyclic analysis has been used to evaluate the model's performance. And furthermore how members with low axial load but high cyclic load can exhibit softening behavior also presented briefly by comparing simulated results with experiments.

In Chapter 5 an experimentally tested two-story and three-story reinforced concrete frames taken as benchmark for evaluating the performance of the models.

2 Literature Review

2.1 General

An analysis of structural system simulating applied loads or ground motion excitation to determine deformations and forces in structures is an important step in the design of structures to resist seismic loading (Filippou and Fenves 2004). An essential choice in structural analysis is to consider whether the relationship between forces and displacements is linear or nonlinear. Designing buildings to withstand seismic action using elastic analysis is most common, but under maximum earthquakes, buildings experience significant inelastic deformations. Modern performance-based guidelines and building standards require ways of representing actual nonlinear behavior. Nonlinear analysis is a way of computing structural response beyond the elastic limit, including the degradation of strength and stiffness associated with nonlinear material response and large displacements (NIST 2010).

There are two main sources of nonlinear behavior: material and geometric nonlinear. Material nonlinear is a nonlinear relationship between force and deformation that arises in the material behaviors such as ductile yielding, stiffness and strength degradation. Geometric nonlinear behavior comes from the consideration of large displacements in the compatibility and equilibrium relationships (Filippou and Fenves 2004).

2.2 Numerical nonlinear beam-column models for beams and columns

The advancement in computing technologies and application of the performance-based engineering design requires accurate and efficient computational nonlinear beam-column models. Based on their efficient and computational cost the nonlinear models used in seismic analysis can be classified into (a) global model, (b) discrete finite element model and (c) microscopic finite element models (Taucer et al. 1991).

In the global model, at selected degrees of freedom, the inelastic response of a system is lumped in the global models. For example, a multi-story building's response represented on each floor as a structural system with only one lateral degree of freedom (Taucer et al. 1991). Each degree of freedom requires a hysteretic curve with shear-lateral drift properties.

In discrete finite element models, to describe the hysteretic behavior of reinforced concrete members structures are modeled by assembling the discrete elements. In this case, two types of inelastic beam-column models are mostly adapted in the discrete mechanics: (a) lumped plasticity, and, (b) distributed plasticity models. In microscopic finite element models members and joints are discretized into a large number of finite elements (Taucer et al. 1991). Because the microscopic finite element models are based on the continuum mechanics, the models are accurate and can capture a more complexes failure phenomenon. However, the models are more complicated and require a high computational cost, therefore their application in the field of earthquake engineering is limited.

The study focusses on investigating the second class of models, which are based on the discrete finite element models. Since these models are numerically robust, accurate and their simplicity to be applied in the field of earthquake engineering, their capacity in simulating nonlinear response of structures subjected to high axial and lateral loading should be investigated.

2.1.1 Lumped plasticity beam-column models

When structures subjected to lateral loading, the inelastic deformations concentrate at the end of the structural beam-column elements (Taucer et al. 1991). The early approach to model such behavior is through introducing zero-length nonlinear springs at both ends of the member. In these models, a hysteresis backbone curve is required to define the properties of the hinge. The hysteresis backbone curve in the plastic hinge varies from a very simple to a more complicated model. These are based on the phenomenological model and allow for efficient modeling of bending and shear failures based on an empirically calibrated hysteretic backbone curve. Nevertheless, the models unable to capture the interaction between bending moment and axial force.

The first lumped plasticity was proposed by Clough et al. (1965). It is based on the parallel component model, shown in Figure 2-1. The element has two parallel elements: elastic-perfectly plastic and perfectly elastic. The elastic-perfectly plastic represents the yielding; the perfectly elastic represents strain-hardening respectively. The stiffness matrix of the member is the summation of the individual elements. The models are also known as the "two-component model". The elastic modulus of the linear component is equal to the strain hardening modulus p.K of the moment-curvature relation, where K is the elastic section stiffness.

The elastic modulus of the elasto-plastic component is equal to q · K where q = 1− p. This model has the advantage that the element formulation is the independence of the moment diagram, however assuming bilinear moment-curvature makes the model incapable of capturing strength and stiffness degradation, which is common in structures subjected to high seismic action.

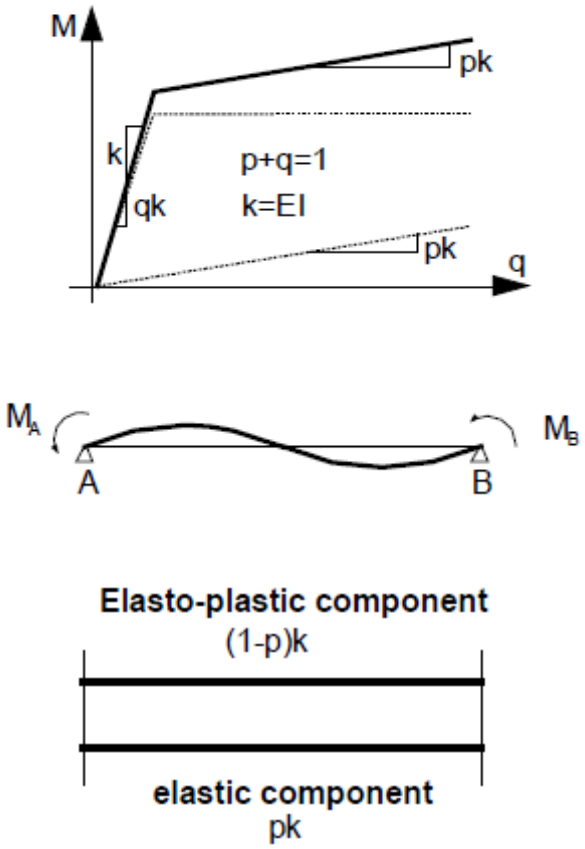

Figure 2-1 Illustration of the two-component model (Taucer et al. 1991)**.**

Giberson (1967) introduced a series model to address the problem in the two-component model. Its original form, shown in Figure 2-2, consists of a linear elastic element with one equivalent nonlinear rotational spring attached to each end. The member's inelastic deformations were assumed to be at the end of the member springs. This model is more robust than the original Clough model because it can describe a more complex hysteretic behavior by selecting the right moment-rotation relationships for the end springs (Taucer et al. 1991)**.**

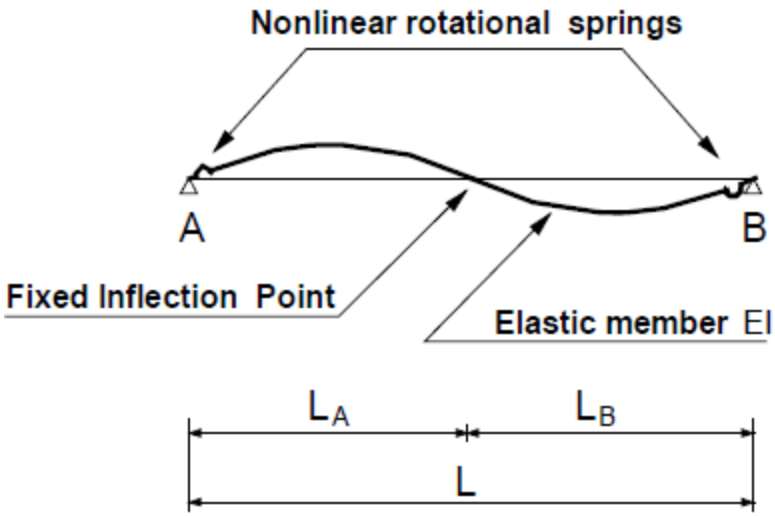

Figure 2-2 Illustration of the one-component model (Taucer et al. 1991).

Clough et al. (1965) proposed the first hysteresis model to describe the properties of the spring. Later on, Takeda et.al (1970) developed a more advanced model than the original Clough model. To capture axial-moment interaction, Lai et al. (1984) proposed a fiber hinge model that constituted by a central elastic element and a series of axial springs at the end zones. In performance-based engineering design, the concentrated plasticity models gained acceptance widely; these models recommended by several US guidelines. FEMA-440 (2005) guideline adopts a simplified backbone curve for describing the hysteresis behavior of the nonlinear hinge properties, as shown in Figure 2-3.

The lumped plasticity models proposed by Takada have been widely used by the earthquake engineering community for the past decades, due to their limitation, more recently Ibarra et al. (2005) established more advanced models that are capable of describing a more complex and damage phenomenon. To include deterioration properties that are used in seismic demand evaluation, the authors modified three of the basic hysteretic models such as, bilinear, peak-oriented, and pinching. Detail of the model can be found in the paper by Ibarra et al. (2005).

Alternatively, and which is more recent concentrated plasticity models are based on the fiber hinge models. Meaning, the nonlinear response is governed by the stress-strain of the fiber material used to define the section. Because sectional deformation integrated consistently at the section level these models successfully capture the interaction between axial force and moment.

The models are capable of capturing degradation and softening after yielding, nevertheless, fail to capture pinching, bond-slip, pullout, and nonlinear shear deformations. Some commercial analysis tools such as CSI SAP2000 provides an option for the user either to use concentrated plasticity with plastic hinge or fiber hinge models.

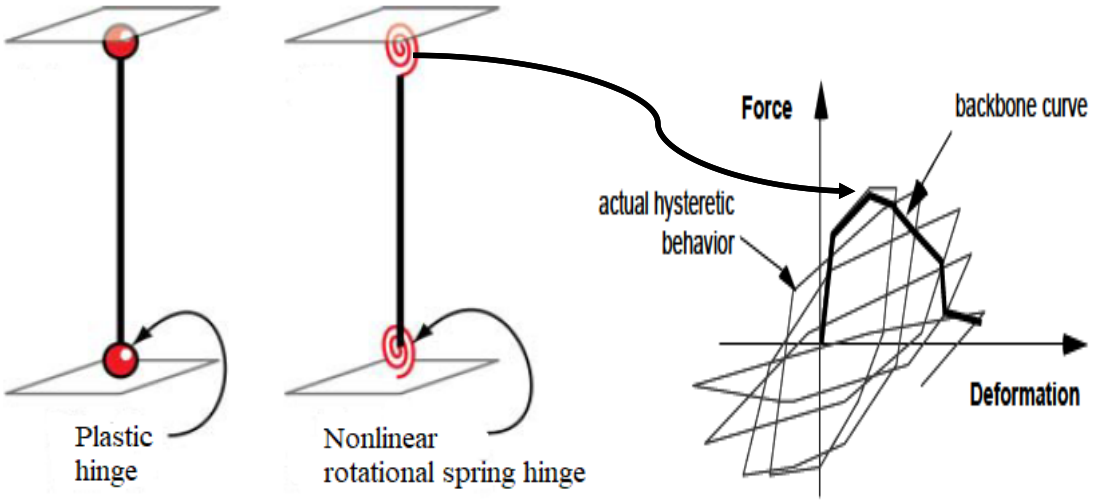

Figure 2-3 Idealized force-deformation relationships (a) concentrated plasticity nonlinear spring (b) backbone representation of hysteretic behavior (FEMA 440).

2.1.2 Distributed plasticity beam-column models

Distributed plasticity beam-column elements provide a more accurate description of the inelastic response for members subjected to lateral nodal and element load. The models allow inelastic deformation to occur anywhere along the length of the beam-column elements. Calculations are carried out numerically; the strains are evaluated at the monitored integration sections using the gauss quadrature integration method. Therefore, to be more general it is convenient to define the distributed plasticity beam-column elements as a way of integrating nonlinear sectional deformations consistently. In the distributed beam-column element, the primary unknowns are either the deformations or forces that can be obtained from displacement or force interpolation functions of the global element respectively.

Soleimani et al. (1979) were probably the first who introduced a distributed plasticity element based on the gradual spread of inelastic deformation from the beam-column interface to the member as a function of loading history. The rest of the beam remains elastic. The point hinge is inserted at the ends of the member to model the fixe-end rotation. These are related to the curvature at the corresponding end section through an "effective length" factor that remains constant during the entire response history. Meyer et al. (1983) further improved the model of Soleimani by proposing a slightly different way of calculating the stiffness of the plastic zone during reloading. Takeda's law was used to define the hysteretic behavior. In the analysis, fixed-end rotations are not considered. Later on, to include the effect of shear and axial forces on flexural hysteretic behavior, Roufaiel and Meyer (1987) mad an improvement to the original model.

Filippou and Issa (1988) proposed other approaches; by dividing the element into a finite number of short sub-elements. Each sub-element describes a single effect, such as inelastic behavior due to bending, shear behavior at the interface, or bond-slip behavior at the beam-column joints.

Nowadays, the distributed plasticity has gained a wide range of acceptance; the models provide a more accurate inelastic description for beam-column elements. Currently, those models successfully implemented in the commercial and academic finite element analysis tools. For instance, Open Sess and Siesmostruct software allow for the users to use either lumped plasticity or distributed plasticity models. The two most common distributed beam-column formulations are displacement-based and the force-based.

Distributed displacement-based beam-column model (DDB)

The DDB elements are the first distributed plasticity based on the classical stiffness method; thus, the models satisfy compatibility and equilibrium in an exact and weak form, respectively. To describe the nodal displacements, the models use a displacement interpolation function that assumes linear curvature and constant average axial strain. The element deformations are obtained directly from the shape function; hence iteration is required only at the structural level (Taucer et al. 1991). An increase in the number of gauss integration sections does not improve the accuracy; hence several elements per member are required to represent the actual inelastic response (Neuenhofer and Filippou 2007). The DDB elements cannot capture the behavior of members near their ultimate resistance and onset of strain-softening (Taucer et al. 1991).

Distributed force-based beam-column model (DFB)

The DFB elements use the flexibility method; thus, the models satisfy compatibility and equilibrium in a weak and exact form, respectively. The models enforce the exact equilibrium between nodal forces and section forces using the force shape function contain constant axial force and linear bending moment. Determining element resisting forces in the DFB formulations is a complicated issue; this arises from the impossibility of obtaining element resisting forces directly from section resisting forces (Taucer et al. 1991). For highly nonlinear systems, especially in the estimation of the inelastic flexural response of frame elements at plastic hinges, the DDB elements cannot predict such response; for such case, the DFB elements take the advantage (Ashtari 2018).

2.2 Fiber section models

The constitutive behavior of the cross-section can either be formulated by the direct relationship between the resultant stresses (such as axial force and bending moments) and generalized strains (such as a reference axial strain and curvature) or by the discretization of the cross-section into fibers, as is the case with the spread plasticity fiber model, This thesis focuses on the later models, which are indeed the most powerful, today also known as “fiber models”. The inelastic responses of the elements are obtained through integration of the responses over the monitored cross-sections as shown in Figure 2-4b. Each cross-section is discretized into a finite number of fibers, each of which following the stress-strain constitutive law of a particular material, for instance, the fiber materials in reinforced concrete section are steel reinforcement, unconfined and confined concrete Figure 2-4a.

The plane sections assumption is considered through adopting an Euler-Bernoulli beam theory, such that the strains are linearly distributed over the cross-section (Taucer et al.1991). The fiber models are capable of accounting the interaction between the axial force and bending moment, plus the coupling effect of biaxial bending moments.

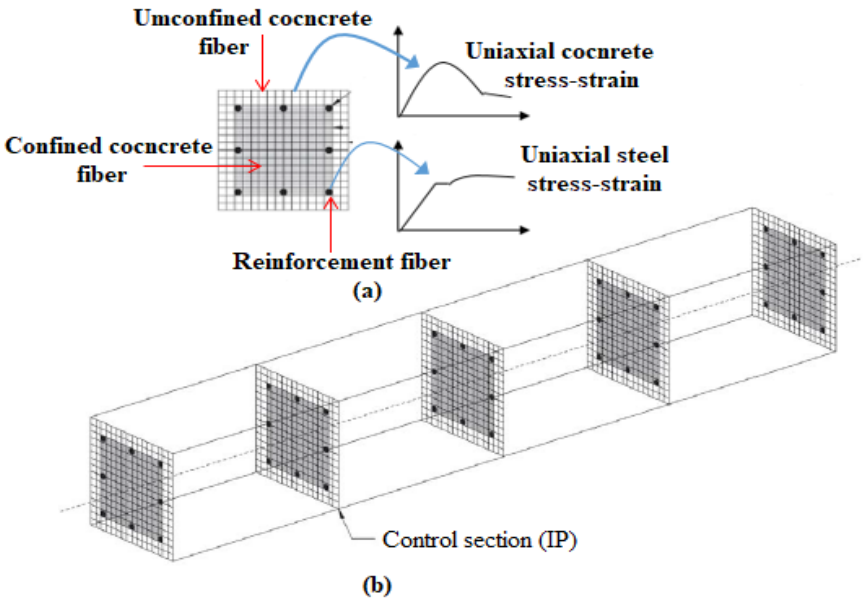

Figure 2-4 Distributed plasticity fiber based beam-column element.

Kaba and Mahin (1984) were probably the first who formulate a flexibility based fiber beam-column element. The element formulation is uses the force interpolation function b(x) in Equation 2-27 in the determination of the element flexibility matrix. By specifying slice locations are along the length of the element, the slice is further discretized into steel and/or concrete fibers.

The model of Kaba and Mahin (1984) is cable of giving fairly accurate results, but has convergence problems and is unable to describe element softening (Taucer et al. 1991). Zeris and Mahin (1988 and 1991) discuss the improvement of the original Kaba-Mahin model and extend the formulation to the biaxial. As shown in Figure 2-5, for the cantilever beam subject to constant axial load and linearly increasing horizontal displacement Zeris and Mahin (1988) reported an interesting softening behavior. When the cantilever beam loaded beyond the ultimate capacity, the member loses its load carrying capacity in the bottom section, which is section 1. To satisfy internal equilibrium section 2 through section 5 unload elastically. With the assumption of a linear curvature distribution, the displacement-based elements cannot capture the member's real behavior. Significant deviation between the assumed and actual curvature distribution is observed during element softening, as the sharp jump in the curvature value near the fixed end, indicates in Figure 2-5. Despite the satisfactory performance of the element proposed by Zeris and

Mahin, the element state determination procedure is not very clear and lacks a general theory (Taucer et al. 1991).

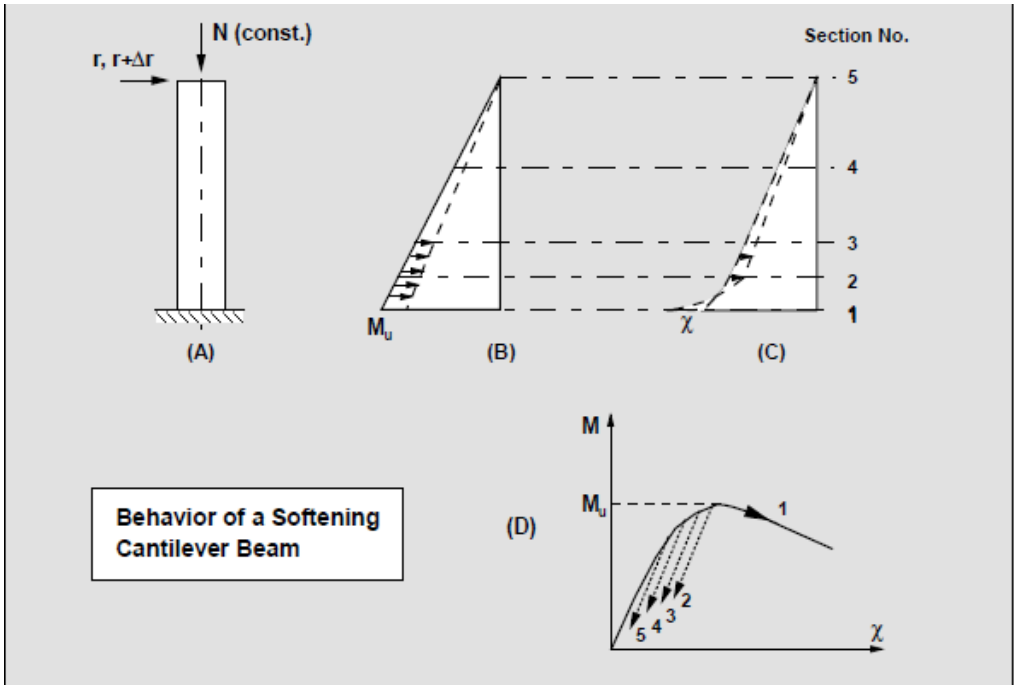

Figure 2-5 Softening behavior for cantilever beam, (a) member and loading, (b) Moment distribution, (c) Curvature distribution, (d) Moment-Curvature relation (reproduced by Taucer et al. (1991)).

Taucer et al. (1991) proposed a model that is mixed and more general, in which nodal resisting forces can be calculated for each element through an iterative procedure. At each iteration, the residual nodal displacements associated with the unbalance section forces along the element are calculated.

The main features of this model is that during the element iterations for the assumed force and deformation interpolation functions, exact equilibrium and the compatibility is always enforced along the element. The proposed model is computationally stable and robust. Using this model, complex hysteretic behavior of RC members such as, strain hardening, "pinching" and softening can be captured accurately under cyclic nodal and element loads.

2.2.1 Formulation of fiber section models

In section 2.5, the general concepts of fiber model with its background were discussed briefly. In this section, the formulation of the fiber model is presented and the models are based on the plane section remain plane.

The strain and stress are functions of the position **x** along the element axis and the position within the cross-section specified in local coordinates y and z.

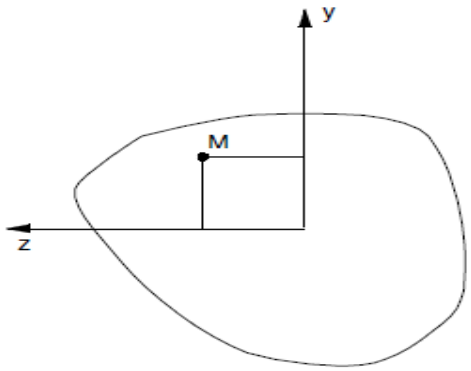

Figure 2-6 Cross section with coordinate axes (Filippou and Fenves 2004).

The axial strain at point M in Figure 2-6 can be written as the product of two functions

$$\varepsilon_i=\varepsilon_a-y\kappa_z+z\kappa_y=\begin{bmatrix}1 & -y & z\end{bmatrix}\begin{bmatrix}\varepsilon_a\\ \kappa_z\\ \kappa_y\end{bmatrix} \qquad 2\text{-}1$$

Where ε_a is the normal strain at the of reference axis, κ_z curvature along the z-axis and κ_y curvature along the y-axis. The generalized sectional deformation can written in a matrix form as

$$e(x)=\begin{bmatrix}\varepsilon_a & \kappa_z & \kappa_y\end{bmatrix}^T \qquad 2\text{-}2$$

$$a_s(y,z)e(x)=\begin{bmatrix}1 & -y & z\end{bmatrix} \qquad 2\text{-}3$$

Finally the strain distribution can be written in general form as

$$\varepsilon_m(y,z)=a_s(y,z)e(x) \qquad 2\text{-}4$$

$a_s(y,z)$ Is known as section kinematic matrix and usually it is a row vector.

The sectional vector force are axial force bending moment about z-axis M_z bending moment about y-axis M_y written as:

$$s=\int_A \left[a_s(y,z)\right]^T \sigma_m dA=\int_A \begin{bmatrix}1\\-y\\z\end{bmatrix}\sigma_m dA \qquad 2\text{-}5$$

By differentiating the above equation section tangent stiffness can be obtained

$$k_s=\frac{\partial s}{\partial e}=\int_A \left[a_s(y,z)\right]^T \frac{\partial \sigma_m}{\partial \varepsilon_m}\frac{\partial \varepsilon}{\partial e}dA=\int_A \left[a_s(y,z)\right]^T \frac{\partial \sigma_m}{\partial \varepsilon_m}\left[a_s(y,z)\right]dA \qquad 2\text{-}6$$

$$k_s=\int_A \frac{\partial \sigma_m}{\partial \varepsilon_m}\begin{bmatrix}1 & -y_i & z_i\\ -y_i & y_i^2 & y_i z_i\\ z_i & y_i z_i & z_i^2\end{bmatrix}dA \qquad 2\text{-}7$$

$$E_m=\frac{\partial \sigma_m}{\partial \varepsilon_m} \qquad 2\text{-}8$$

Equation 2-8 is Tangent material modulus at point m

For nonlinear material response the most convenient way of evaluating the integral for the resultant force s in the above equation and the section stiffness is numerical integration. Numerical integration converts the integral to sums of the forms

$$s=\begin{bmatrix}N\\M_z\\M_y\end{bmatrix}=\sum_{i=1}^{N_{IPs}}\begin{bmatrix}1\\-y\\z\end{bmatrix}\sigma_i w_i \qquad 2\text{-}9$$

$$k_s=\sum_{i=1}^{N_{IPs}}\begin{bmatrix}1 & -y_i & z_i\\ -y_i & y_i^2 & y_i z_i\\ z_i & y_i z_i & z_i^2\end{bmatrix}E_i w_i \qquad 2\text{-}10$$

Where i is an integer counting from 1 to the number of integration points or (fibers) N_{IPs} And w_i is the weight of the integration scheme at i.

$$\sigma=\sigma(\varepsilon_i) \qquad 2\text{-}11$$

$$E_i=\frac{d\sigma}{d\varepsilon}(\varepsilon_i) \qquad 2\text{-}12$$

$$\varepsilon_i=\varepsilon_a-z\kappa_y+y\kappa_z \qquad 2\text{-}13$$

2.2.2 Formulation of distributed displacement-based fiber models (DDB)

The first distributed inelasticity was formulated based on the classical stiffness method using cubic polynomials to approximate the deformations along the element (Taucer et al. 1991). For the line beam-column element in Figure 2-7, the basic element forces in the basic system without rigid body modes are denoted with q and basic element deformations are denoted with **v**.

Figure 2-7 Basic forces of 2D beam-column element

$$\mathbf{u}(x)=\mathbf{N}(x)\mathbf{v} \qquad 2\text{-}14$$

Where N(x) is a matrix containing the shape functions for the axial and transverse displacements, N1(x), N_2(x) and N_3(x).The shape functions can be written in matrix form as:

$$N(x)=\begin{bmatrix} N_1(x) & 0 & 0 \\ 0 & N_2(x) & N_3(x) \end{bmatrix} \qquad 2\text{-}15$$

The displacement shape functions are:

$$N_1(x)=\frac{x}{L} \qquad 2\text{-}16$$

$$N_2(x)=x-\frac{2x^2}{L}+\frac{x^3}{L^2} \qquad 2\text{-}17$$

$$N_3(x)=-\frac{x^2}{L}+\frac{x^3}{L^2} \qquad 2\text{-}18$$

And the generalized displacements in the basic system are:

$$v=\begin{bmatrix} u & \theta_1 & \theta_2 \end{bmatrix}^T \qquad 2\text{-}19$$

The expression for the deformation fields can be written as:

$$e(x)=B(x)v \qquad 2\text{-}20$$

Where the strain-displacement transformation matrix B contains first and second derivatives of the derivatives of the displacement shape functions and gives constant axial strain and linear curvature as written in Equation 2-2. By using the incremental version of Equation 2-20, and the constitutive relation in Equation 2-10 the following relation for the force field increment is found:

$$\Delta s(x)=k_s(x)\Delta e(x)=k_s(x)B(x)\Delta v \qquad 2\text{-}21$$

From the principle of virtual displacement the equilibrium equation is derived as:

$$\delta v^T q=\int_0^L \delta e^T(x)s(x)dx \qquad 2\text{-}22$$

$$q=\int_0^L B^T(x)\,s(x)dx=\sum_{i=1}^{N_P} B_i^T s_i \omega_i \qquad 2\text{-}23$$

Where q is element resisting force in the basic system and L is the element length

And its linearization in the form of force-displacement relationship

$$k\Delta v=R \qquad 2\text{-}24$$

Where Δv and R are the vectors of displacement increments and residual forces, respectively. And k The element stiffness matrix is further derived by taking the derivative of q with respect to the generalized degrees of freedom in the basic system, v

$$k=\frac{\partial q}{\partial v}=\int_0^L B^T(x)\,k_s(x)B(x)dx=\sum_{i=1}^{N_p}B_i^T k_{s,i}B_i\omega_i \qquad 2\text{-}25$$

Equation 2-25 indicates weak equilibrium; and this leads to error in force boundary conditions. Therefore, internal force and element basic forces are not in equilibrium.

2.2.3 Formulation of distributed force-based fiber models (DFB)

In the force-based (flexibility-based) approach the force interpolation functions are used as a shape function. The force-based approach relies on the availability of an exact equilibrium solution within the basic system of a beam-column element. Section forces are determined from the basic forces by interpolation within the basic system as:

$$s(x)=b(x)q \qquad 2\text{-}26$$

Where b(x) is a matrix containing the force interpolation functions that provides constant axial force and linear distribution of bending moment in the absence of distributed element loads

$$b(x)=\begin{bmatrix}1 & 0 & 0\\ 0 & -(1-\frac{x}{L}) & \frac{x}{L}\end{bmatrix} \qquad 2\text{-}27$$

And q nodal force in the basic system, and can be written in matrix form as:

$$q=\begin{bmatrix}N_1 & M_2 & M_3\end{bmatrix}^T \qquad 2\text{-}28$$

The inverse form of Equation 2-10 with the incremental version of Equation 2-26 gives the following incremental deformation field:

$$\Delta e(x)=k_s^{-1}\Delta s(x)=f_s(x)\Delta s(x)=f_s(x)b(x)\Delta q \qquad 2\text{-}29$$

From the equation 2-29 it is clearly seen that, the section flexibility matrix is the inverse of the section stiffness matrix, $f_s(x) = k_s^{-1}$

After setting up the equilibrium relations the geometric compatibility of the frame element can be established with the principle of virtual forces. The relation between the element deformations in the basic system **v** and sectional deformations e(x) are obtained from the principle of virtual force. This indicates that the sectional deformation e(x*)* needs to be obtained from section forces s(x). In reality, this relation is not available, but it's inverses available (Filippou and Fenves 2004). Hence, the section deformations are obtained as the solution of the nonlinear system of equations and the element state determination is more complex than the element state determination for the displacement-based fiber element. element deformations in the basic system can be written as:

$$v=\int_0^L b^T(x)e(x)dx=\sum_{i=1}^{N_p} b_i^T e_i \omega_i \qquad 2\text{-}30$$

And its linearization in the form of displacement-force relationship

$$f\Delta q=r \qquad 2\text{-}31$$

Where **Δq** and **r** are the vectors of force increments and residual displacements, respectively. And f is flexibility matrix of the element derived by taking the derivative of **v** with respect to the generalized force in the basic system, **q**

$$f=\frac{\partial v}{\partial q}=\int_0^L b^T(x)f_s(x)b(x)dx=\sum_{i=1}^{N_p} b_i^T f_{s,i} b_i w_i \qquad 2\text{-}32$$

Note that a meaningful expression for **f**, can only be derived for a beam-element that do not have any rigid-body modes (Neuenhofer and Filippou 2007).

2.3 Limitation of fiber beam-column nonlinear modes

Currently distributed plasticity have gained acceptance widely by the earthquake engineering community for doing nonlinear analysis of structures subjected to seismic loading. However, capturing shear effect is difficult using fiber beam-column models; and several researchers have been working to include nonlinear shear effect in the fiber models. The state of art regarding to nonlinear shear effects using the fiber models did not presented in this paper, because this research is limited to structures that their failure governed by flexure. Even though the distributed plasticity provide a more accurate result for flexural dominated structures, softening is found to be critical problem in such models.

2.3.1 Damage localization in distributed fiber beam-column models

In the field of fracture mechanics, the term localization is well known and studied deeply by different researchers for the past decades. These physical phenomena of damage concentration, have been also found to affect the finite element analysis models. This is a localization of strain over a mall finite element length or integration points, which leads to a non-objective response. From a physical viewpoint, it is common that the stress-strain of concrete material depends on the concrete properties used, however, Experiment tests of compressive strength of different specimen sizes have shown that the pot-peak stress-strain behavior of concrete is size-dependent. Jansen and Shah (1997) conducted compressive tests for specimens with different slender length, and they found that, the longer the specimen, the steeper the curves become, as shown in Figure 2-8.

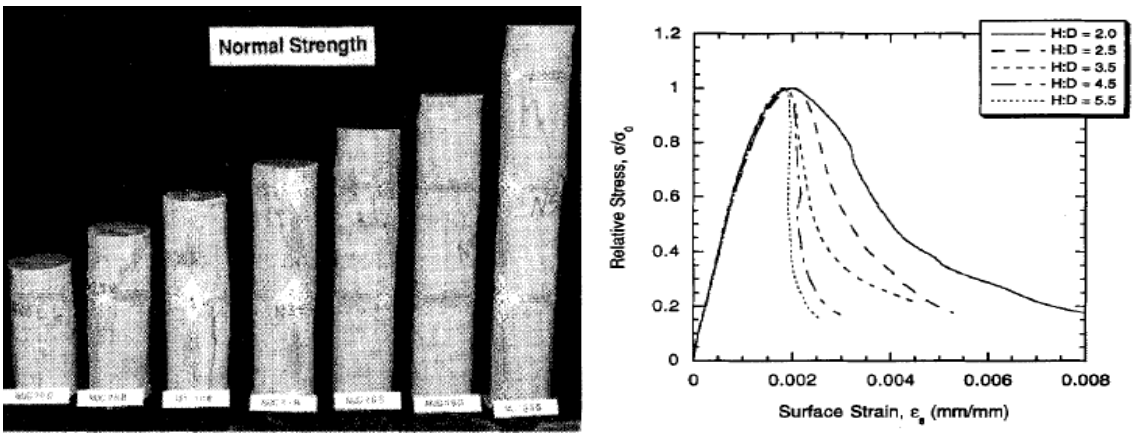

Figure 2-8 Size dependent stress-strain response of concrete in compression (Jansen and Shah 1997).

Prior to the development and application of force-based beam-column element, localization issues primarily were studied in the displacement-based elements, and still, there are several regularization techniques in literature to this model (Almeida et al. 2012). Among the earliest studies, Bazant et al. (1994) properly recognized that localization issues in displacement-based elements is sensitive to mesh size and the mean tangential bending stiffness. Zeris and Mahin (1988) were the first to schematically explain that softening in DFB elements has different features from DDB approaches.

Even though several documented researches on regularization techniques for DDB are available, the works are more recent for DFB beam-column elements. Coleman and Spacone (2001) were the first who deeply investigated localization issues in DFB beam-column model and applied the regularization techniques based on the constant fracture energy criterion to these models. This provides an objective response to the global force-displacement response.

Coleman and Spacone (2001) provide a simple demonstration for isolated cantilevered steel beam subjected to lateral load at its free end. Figure 2-9 shows the force deformation response of the beam modeled using one DFB element with different integration points. For section exhibiting strain-hardening behavior, the response is objective at the element and section levels. Using three integration points was observed in overestimating the stiffness in the strain-hardening region.

Figure 2-10 shows the response of the cantilever beam using force-based element to an imposed tip displacement with an elastic-perfectly plastic moment-curvature behavior. In this case, the global force displacement response is objective, however, the peak curvature is non-objective. The loss of objectivity in the curvature response is due to localization of the inelastic curvature at the base integration point (Coleman and Spacone, 2001). When the bottom section reaches the plastic moment, the column reaches its maximum carrying capacity.

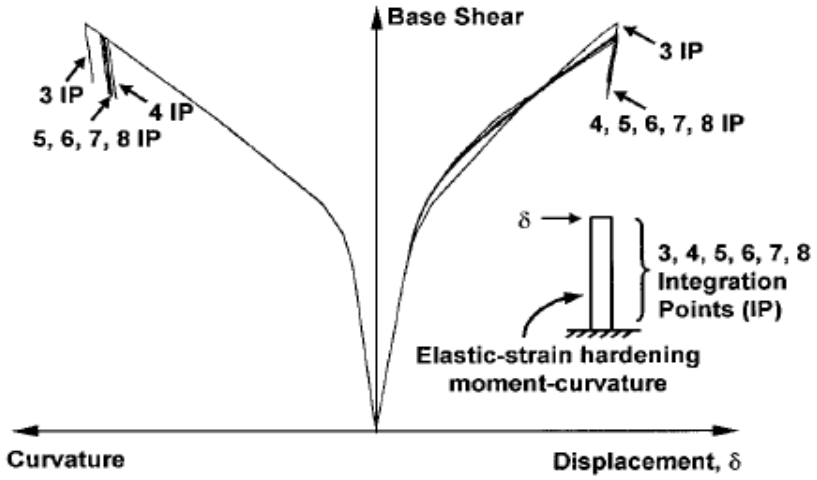

Figure 2-9 Elastic-strain-hardening section response of cantilever beam (Coleman and Spacone, 2001).

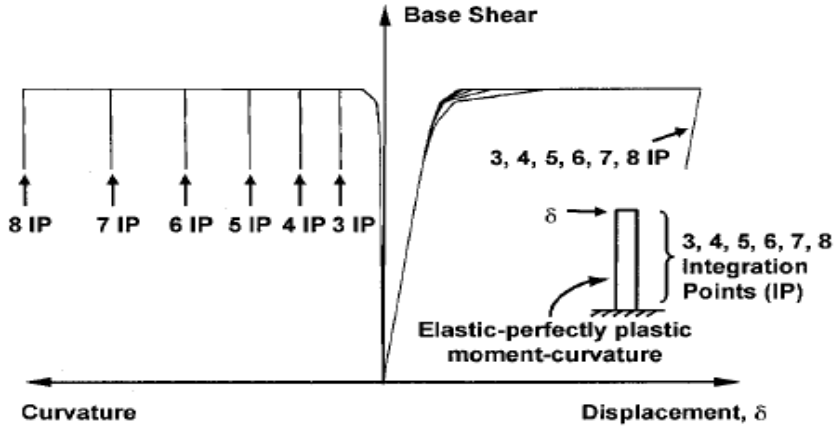

Figure 2-10 Elastic-perfectly plastic section response of cantilever beam (Coleman and Spacone, 2001).

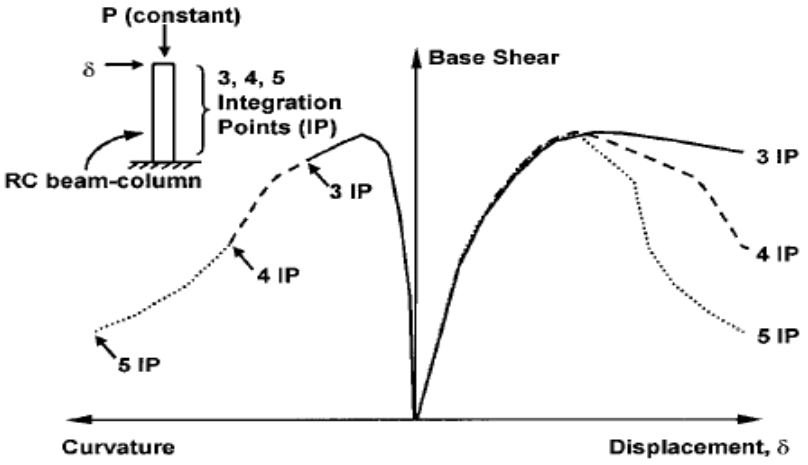

Figure 2-11 Strain-softening section response of RC beam-column (Coleman and Spacone, 2001).

Figure 2-11 shows the response of an RC column analyzed using one force-based element by varying integration sections. Both the local moment-curvature and the global base shear-displacement responses are mesh dependent. As the number of integration points increases, the length of the first integration becomes very small and inelastic deformation localizes over this length. Therefore, to achieve the same level of prescribed tip displacement the curvature should be increased. The softening of concrete comes from the reason that when the fiber compressive strains in the hinge region quickly increase, the material stiffness degraded rapidly (Coleman and Spacone 2001).

2.3.2 Material regularization to overcome localization issues

2.3.2.1 Regularization for concrete material

To tackle mesh-dependent response, Coleman and Spacone (2001) proposed a material regularization technique for the DFB models using the constant fracture energy criterion concepts. The authors modified the Kent-Park concrete model shown in Figure 2-12. The ultimate strain is modified at the quadrature integration points to maintain a constant release of energy after that the strain-softening initiates. The shaded area is proportional to the energy that is released after the softening of the pressure. The idea is that the concrete material models assigned to distributed-plasticity fiber sections are modified to have constant dissipated material energy during crushing.

$$G_f^c = \int \sigma du_i \qquad 2\text{-}33$$

Where σ is the concrete stress and u_i the inelastic displacement. The integral represents the area of the compressive stress-displacement curve under the post-peak portion. Adapting the concept of fracture energy to the general use, Equation 2-33 may be cast in terms of stress and strain:

$$G_f^c = h\int \sigma d\varepsilon_i = L_{IP}\int \sigma d\varepsilon_i \qquad 2\text{-}34$$

Where ε_i indicates inelastic strain and h is a length scale. For smeared crack elements, h represents the size of a single element in the crack band. For force-based frame elements, h becomes the length of the softening integration point L_{IP}.

Even though the proposed procedure is general, Coleman and Spacone applied to the Kent and Park (1971) concrete model to define the fibers sections. Because the Kent–Park concrete models describe the softening in concrete, in this study this concrete model is used to define concrete fiber materials.

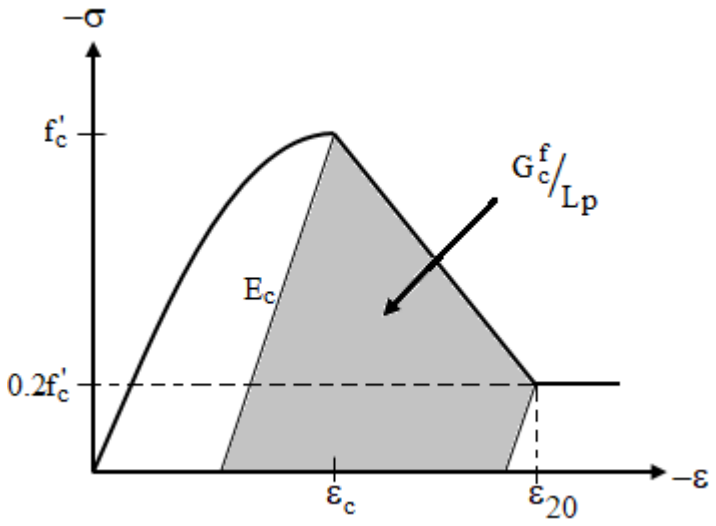

Figure 2-12 Kent–Park concrete stress–strain model with fracture energy in compression as shaded area (Coleman and Spacone 2001).

As shown in Figure 2-12 the pre peak behavior is represented by a parabola and the post-peak given by a linear softening branch until a stress of $20\%f_c'$ (residual strength) is reached at a prescribed strain labeled by ε_{20}. From the peak stress f_c' until the end of the softening branch is considered to be the fracture energy. Therefore, to maintain a constant energy release ε_{20} must be calibrated. For known value of G_c^f from the experimental tests (Jansen and Shah 1997), together with the definition of G_c^f from Figure 2-12, leads to the following expression for ε_{20}:

$$\varepsilon_{20}=\frac{G_f^c}{0.6f_c^{'}l_p}-\frac{0.8f_c^{'}}{E_c}+\varepsilon_c \qquad 2\text{-}35$$

The parameters for the Kent-Park concrete model are f_c' concrete compressive strength; ε_c peak compressive strain $E_c$elastic modulus; and ε_{20}strain corresponding to 20% of the compressive strength.

The parameter G_c^f concrete fracture energy in compression, and L_p plastic hinge length, which acts as the characteristic length for the purpose of providing objective response.

Coleman and Spacone (2001) employed the G_c^f value recommended by Jansen and Shah for unconfined concrete and recommend a value of $G_{cc}^f = \mathbf{6}G_c^f$ for confined concrete; however, these values are not verified through comparison of simulated and measured response for typical reinforced concrete component (Pugh 2012).

Curvature Post processing

The regularization techniques based on the constant fracture energy concept tackles localization issues only at the global level and at local response yet the response is mesh-dependent. The reason is that the length of the first integration section is not always the same as the actual plastic hinge length. Therefore, to address mesh-dependent result, Coleman and Spacone suggested curvature post-processing. The total curvature can be separated into elastic and inelastic curvature components in the plastic hinge region as $\phi = \phi_e + \phi_i$. Considering the geometry of Figure 2-13, the inelastic hinge rotation is $\theta_i = \phi_i L_{iP}$. Neglecting the elastic curvature in the other integration points, and using a small angle approximation for u_i, the inelastic curvature can be approximated as:

$$\phi_i^{model} = \frac{\delta_i}{L_{ip}\left(L/2 - L_{ip}/2\right)} \qquad 2\text{-}36$$

Where ϕ^{model} indicates the inelastic curvature that results from the analysis.

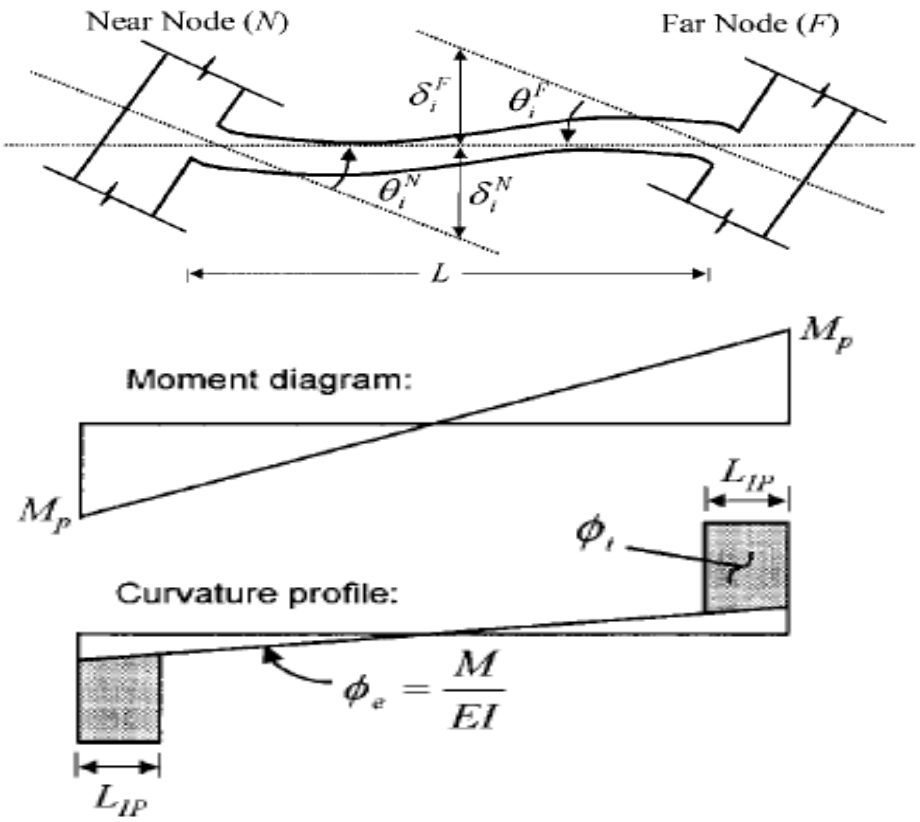

Figure 2-13 Plastic hinges at both ends forming in the interior beam

Substituting the actual length of the plastic hinge L_p for L_{ip} yields a similar approximation for the true curvature demand.

$$\phi_i^{predicted} \cong \frac{\delta_i}{L_p\left(L/2-L_p/2\right)} \qquad 2\text{-}37$$

Where $\phi^{Predicted}$ indicates the inelastic curvature demand based ϕ_i on the assumed plastic hinge length L_p. Finally, the model output can be scaled according to:

$$\phi=\phi_e-\left(scalefactor\right)\phi_i^{model} \qquad 2\text{-}38$$

Where the scale factor is computed according to:

$$Scalefactor=\frac{w_{ip}L^2\left(1-w_{ip}\right)}{L_p\left(L-L_p\right)} \qquad 2\text{-}39$$

The double-curvature case shown in Figure 2-13 prevails in the analyses of buildings under lateral loads. On the other hand, some structural components such as cantilevers have a single curvature, and the plastic hinge only forms at one end. Therefore, in terms of single curvature, the scale factor written in Equation 2-39 can be written by replacing the full length of the L/2 term. This approach results in:

$$Scalefactor=\frac{w_{ip}L^2\left(2-w_{ip}\right)}{L_p\left(2L-L_p\right)} \qquad 2\text{-}40$$

Coleman and Spacone (2001) were applied the regularization of material only for distributed force-based beam-column models, however, most recently Pugh (2012) extended the work to include displacement-based fiber models. Coleman and Spacone suggested using a value of 20 N/mm for the crushing energy of unconfined concrete based on the recommendation made by Jansen and Shah (1997), up to a value of 30 N/mm. The confined concrete crushing energy a value up to six times of the crushing energy for the unconfined concrete (150-180 N/mm) was suggested by Coleman and Spacone. Pugh expressed the crushing energies value in terms of the specified strength of unconfined and Confined concrete. Pugh (2012) recommeded to use defferent value of crussing energies for force-based and displacement-based fiber beam column model.

$$G_{fc}=2f_c^{'}\left(N/mm\right)\left(DBF\right) \qquad 2\text{-}41$$

It has been assumed that the concrete crushing energies developed to be used for the force-based beam-column element also appropriate to be applied for the displacement-based element. Nevertheless, using Equations 2-41 for he displacement-based element produces an over prediction of drift capacity. Therefore, for the DDB element te unconfined crusing enrgies is:

$$G_{fc}=0.56f_c^{'}\left(N/mm\right)\left(DDB\right) \qquad 2\text{-}42$$

And the confined concrete crushing energy for both DFB and DDE can be estimated as:

$$G_{fcc}=1.7G_{fc} \qquad 2\text{-}43$$

Then Equation 2-35 can be written for the confined concrete properties as:

$$\varepsilon_{20c}=\frac{G_{fcc}}{0.6f_{cc}^{'}L_{IP}}-\frac{0.8f_{cc}^{'}}{E_{cc}}+\varepsilon_{oc} \qquad 2\text{-}44$$

The crushing energies suggested to be applied in displacement based fiber models are significantly lower than distributed force based fiber models and detail of this issue discussed briefly on the literature by (Pugh 2012).

2.3.2.2 Steel material regularization

Coleman and Spacone (2001) recommended to apply material regularization techniques to the concrete material only. However, this technique can be valuable only for sections subjected to high axial load and if failure is only due to crushing of concrete material. If member with widely spaced stirrups subjected to high axial and cyclic load, the section face softening of concrete and localization of reinforcement bar.

It is clear that for reinforced concrete members at the critical section post peak behavior of steel shows strain hardening, whereas concrete exhibits strain softening. Even though steel shows hardening behavior, for section exhibit softening steel response also localize at a critical section to confirm compatibility condition (Ashtari 2018). Therefore, because softening in the section is comes from both fiber materials regularization of concrete and steel materials should be included (Pugh 2012).

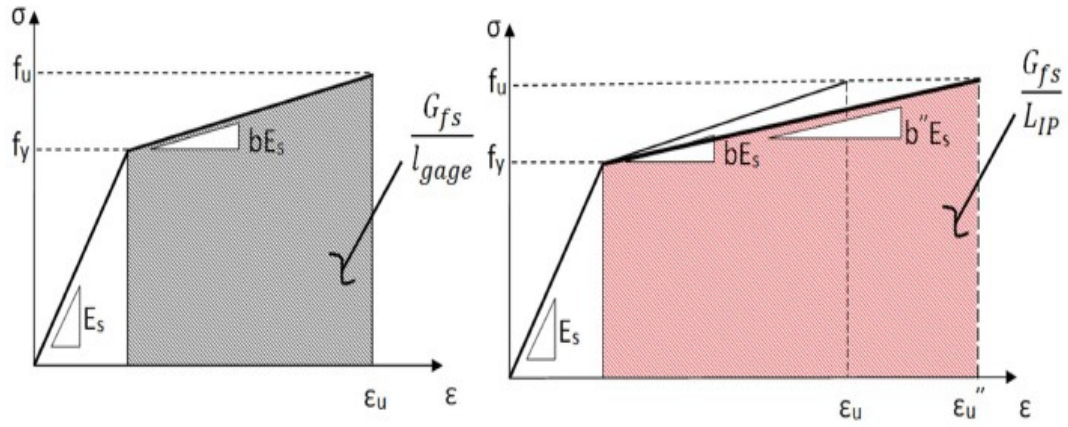

(a) Measured steel response (b) Regularized steel model

Figure 2-14 Stress-strain response histories for steel material (Pugh 2012).

The post-yield energy of steel is a hardening energy defined by the area under the experimentally determined post-yield stress-strain envelope Figure 2-14 (a) multiplied by the length over which inelastic deformation localizes, which was assumed equal to the gage length, L_{gage}, used in the laboratory. For the simplified bi-linear steel stress-strain shown in Figure 2-15b the hardening energy, G_s, can be defined by

$$G_s = \frac{1}{2}\left(\varepsilon_{u,exp} - \varepsilon_y\right)\left(f_u - f_y\right)L_{gage} \qquad 2\text{-}45$$

Where $\boldsymbol{\varepsilon_{su,exp}}$ **i**s the expected rupture strain, $\boldsymbol{\varepsilon_y}$ is the yield strain, and $\mathbf{f_u}$ and $\mathbf{f_y}$ are the ultimate tensile strength and yield strength, respectively. For regularizing the steel material, the ultimate rupture strain assigned to the steel material model in the analysis should be modified based on the length associated to the critical section or element

By using Equation 2-45 and Figure 2-14b, the strain at ultimate strength, εu, used in defining the regularized model can be calculated as:

$$\varepsilon_u'' = \varepsilon_y + \left(\varepsilon_{u,exp} - \varepsilon_y\right)\frac{L_{gage}}{L_{IP}} \qquad 2\text{-}46$$

Thus, as the mesh becomes more highly refined and LIP is reduced, the hardening modulus for the reinforcing steel is also reduced and larger strains are required to achieve a given post-yield stress level. It should be noted that these definitions ignore the curved transition defined by the Menegotto-Pinto model between the initial and post-yielding hardening slopes; however, this is a minor simplification and was determined to have minimal impact on numerical results.

Gage length has been taken as 0.203 m as suggested by ASTM A370 (Pugh 2012). Ones after the ultimate strain is modified according to the gage length and length of the first integration section or element length, the post-yield hardening modulus should be changed based on the value calculated for the ultimate rupture strain of the regularized material (Ashtari 2018).

2.3.3 Regularization based on plastic hinge integration methods

In the previous section regularization techniques based on material regularization were presented, now the second method based on the plastic hinge integration method is presented. By keeping all the advantage of force-based fiber models Scott and Fenves (2006) presented a force-based plastic hinge integration methods in which the, L_P (length of plastic hinge) is specified as part of the element integration rule and it becomes a free parameter. In this case, a plastic hinge length that maintains a constant energy release without modification to the concrete stress-strain relationship can be obtained by using the Equation 2-35

$$l_p = \frac{G_f^c}{0.6f_c^{'}\left(\varepsilon_{20}-\varepsilon_c+\frac{0.8f_c^{'}}{E_c}\right)} \qquad 2\text{-}47$$

As an Alternative way, one can define the plastic hinge length that experimentally validated empirical formula that takes into account the effects of bar pullout and strain penetration, can be used such as the Paulay and Priestley (1992) equation for reinforced concrete members

$$L_p = 0.08L + 0.022f_y d_b \qquad 2\text{-}48$$

The plastic hinge integration methods assumes that nonlinear constitutive behavior is confined to regions of length L_{PI} and L_{PJ} at the element ends. Such assumptions are valuable for columns or beams that carry small member loads. The model developed by Scott and Fenves (2006) is a force-based concentrated fiber beam-column element that is based on modification on the original two-point Gauss–Radau integration rule. The model implemented in OpenSees and known as “BeamWithHinge” model. In Seismostruct known as “Concentrated force-based plastic hinge” method. The model is based on using integration weights at the element ends equal to $l_{pI}/4$ and $l_{pJ}/4$ instead of l_{pI} and l_{pJ}. Meaning, the two-point Gauss-Radau integration rule is applied over lengths of $4l_{pI}$ and

4*lpJ* as shown in Figure 2-15. The locations and weights of the integration points are as follows:

$$\xi=\left\{0,\frac{8l_{pI}}{3},L-\frac{8l_{pJ}}{3},L\right\}$$
$$\omega=\left\{l_{pI},3l_{pI},3l_{pJ},l_{pJ}\right\} \qquad 2\text{-}49$$

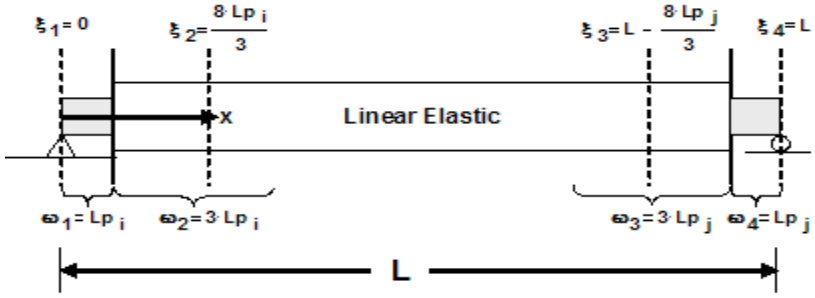

Figure 2-15 Modified of Two-Point Gauss–Radau Integration (Scott and Fenves, 2006).

3 Comparison of the Numerical Non-Linear Models under Monotonic Loading

3.1 Introduction

This section investigates performance of four nonlinear modeling strategies that are commonly used in the field of earthquake engineering: distributed force-based fiber models (DFB) shown in Figure 3-1a, distributed displacement-based fiber model (DDB) shown in Figure 3-1b, concentrated force fiber model with finite hinge length (Beamwithhinge) shown in Figure 3-1c And lumped plasticity with zero-length at the ends of the member (Lumped plasticity with zero-hinge length) shown in Figure 3-1d.

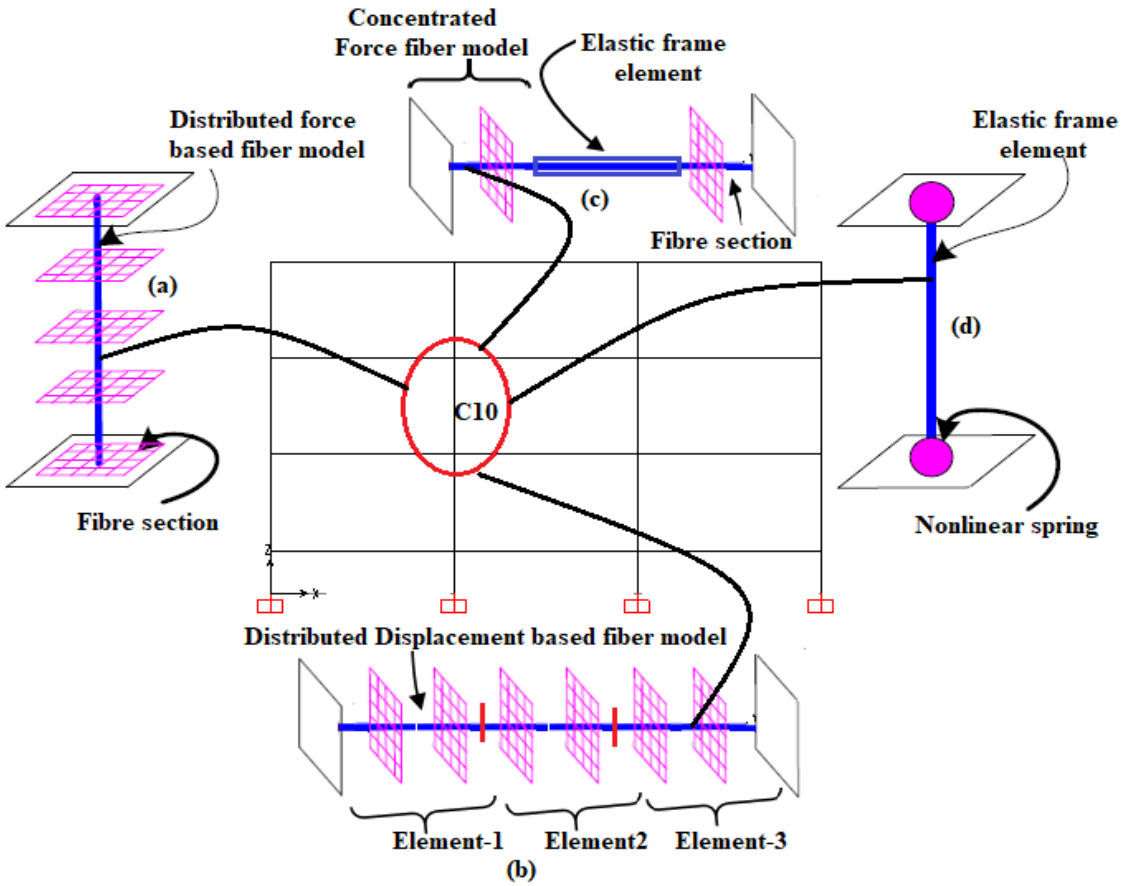

Figure 3-1 Nonlinear modeling strategies for selected column C10 in RC frame: a) distributed force-based fiber model; b) distributed displacement-based fiber model; c) concentrated force-based fiber model; and d) lumped plasticity with zero length hinge.

3.1.1 Uniaxial materials

Material stress-strain relationships that describe the concrete and steel fibers should be defined properly to capture the inelastic response of structures subjected to axial and lateral loading. For OpenSees modeling of column specimens, the material object used for confined and unconfined concrete is Concrete02. The concrete Kent-Park model (Kent and Park 1971) is adopted to describe the stress-strain relation of concrete fibers.

$$f_c = f_c'\left[\frac{2\varepsilon_c}{\varepsilon_o} - \left(\frac{\varepsilon_c}{\varepsilon_o}\right)^2\right] \qquad \text{For} \quad \varepsilon_c \le \varepsilon_0 \qquad 3\text{-}1$$

$$f_c = f_c'\left[1 - z\left(\varepsilon_c - \varepsilon_o\right)\right] \ge 0.2f_c' \qquad \text{For} \ \boldsymbol{\varepsilon_c \ge \varepsilon_0} \qquad 3\text{-}2$$

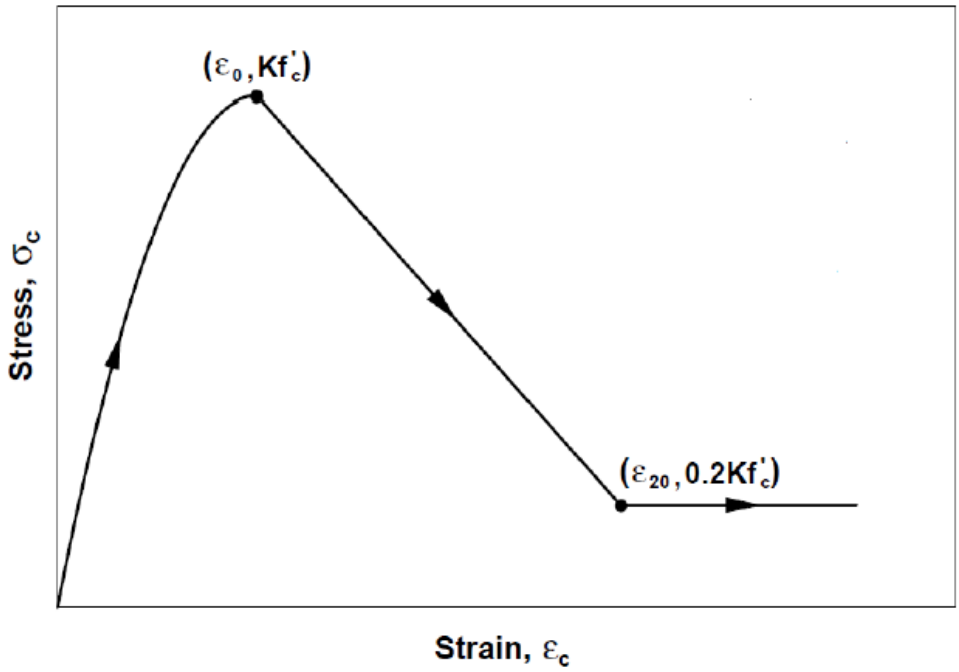

Figure 3-2 Modified Park-Kent monotonic envelope.

The monotonic compression envelope shown in Figure 3-2 has an initial parabolic envelope, a linear softening envelope, and an ultimate stress plateau. The confinement effect factor, K can be determined by using the formula proposed by Mander et al. (1988). For unconfined concrete fibers, the strain associated with 80% strength loss, f_{20u} was assumed to be 0.008. The ultimate strain capacity of the confined concrete can be calculated using Priestley et al (1996) expression as follows:

$$\varepsilon_{ccu}=0.004+1.4\frac{\rho_s f_{yh}\varepsilon_{fs}}{f'_{cc}} \qquad 3\text{-}3$$

For cyclic implementation, as shown in Figure 3-3, Yassin assigned bilinear unloading and linear reloading branches to unload and reload to the monotonic compression envelope (Pugh 2012). These hysteretic rules account for degradation of stiffness in both unloading and reloading and assume that tensile response occurs immediately after complete compression unloading. Sudden crack closure is assumed; this can be realized by the sudden change in stiffness when compression is reloaded (Figure 3-3). The tensile strength and post cracking softening can be controlled.

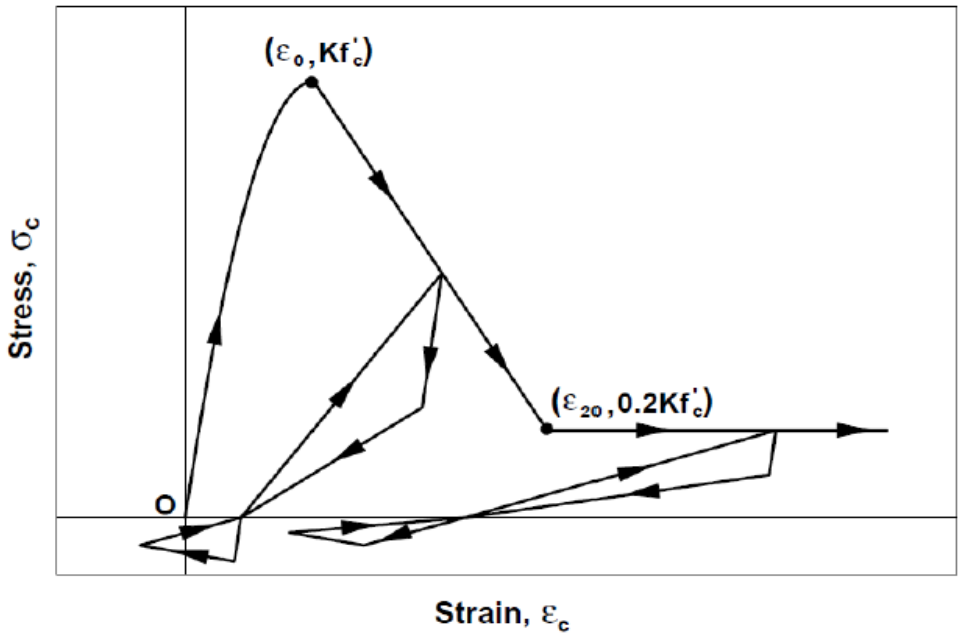

Figure 3-3 Yassin/Modified Park-Kent cyclic response.

Steel-02 which is a bilinear steel envelope used to define the reinforcement bar. Cyclic reinforcing steel behavior is commonly modeled using the Menegotto-Pinto-Filippou (1983) which includes isotropic strain hardening as shown in Figure 3-4. This model represents steel behavior as a series of curved transitions between asymptotes defined by linear elastic and strain hardening properties. The curved transition allows for the representation of the Bauschinger effect. Model input parameters allow for control of cyclic stiffness deterioration.

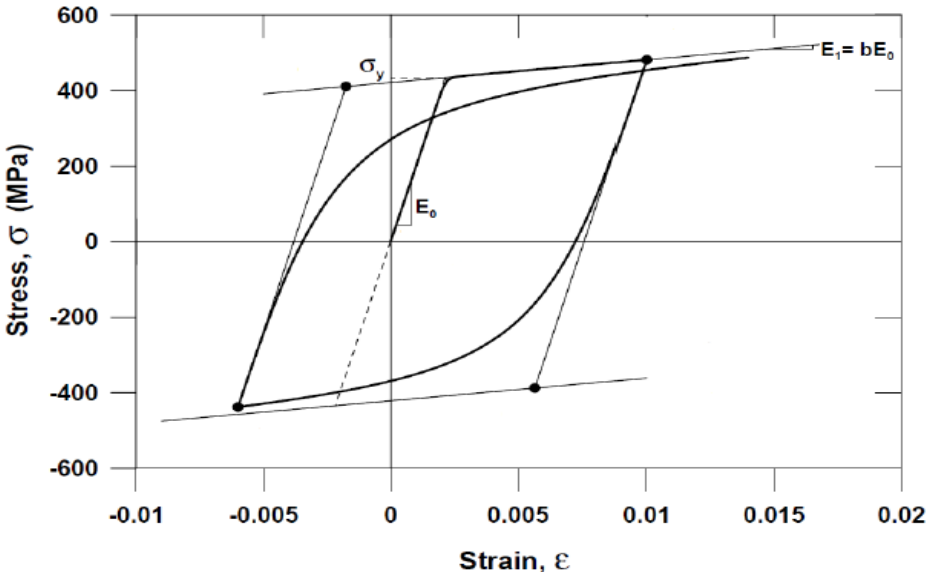

Figure 3-4 Menegotto-Pinto-Filippou model.

3.2 Pushover analysis of RC bridge column (hardening)

Pushover analysis is a powerful nonlinear analysis tool, and several engineers and researchers use this method of analysis in performance-based design. Pushover analysis provides important information about a structural system's capacity. Using this method of analysis one can easily identify a critical region in a structural system (Fragiadakis and Papadrakakis 2008).

The reinforced concrete column downloaded from the peer structural performance database and modeled in the Open System for Earthquake Engineering Simulation, abbreviated as OpenSees, finite element software. The software developed by the Pacific Earthquake Engineering Research Center, which is located at the University of California, Berkeley. Specimen A2 that tested by Kunnath et al. (1997) taken as a case study for a strain-hardening behavior. Strain-hardening behavior was considered from the perspective that the column was subjected to a relatively low axial load. Furthermore, the hysteresis response obtained from the experiment hasn't shown any softening or degradation in strength. The uniaxial materials discussed in the previous section have been used to define the fiber section. The loading strategies were done first by applying a constant axial load of 200 kN in a downward direction through the force control loading, and then an increasing lateral load is applied through the displacement control. The detail of the specimen is found in Appendix A1.

Table 3-1 Material properties of specimen A2 **(**Kunnath et al. 1997, A2).

Unconfined concrete 02	
Maximum Concrete strength (f_c')	29 Mpa
Peak strain (ε_{c0})	$\frac{2 \cdot f_c'}{E_c}$
Crushing stress f_{c20}')	$0.2 \cdot f_c'$
Crushing strain (ε_{cu})	0.008
confined concrete 02	
Confinement factor (k)	(1.62 Mander 1988 Equation)
compressive strength (f_{cc})	$k \cdot f_c$
Peak strain (ε_{cc0})	$\frac{2 \cdot f_{cc}'}{E_{cc}}$
Crushing stress(f_{cc20}')	$0.2 \cdot f_{cc}'$
Crushing strain (ε_{ccu})	Equation 3.1
Reinforcement bar steel 02	
yield strength(f_y)	448 (mpa)
Modulus of elasticity (E_s)	200000 (mpa)
Strain Hardening	1%

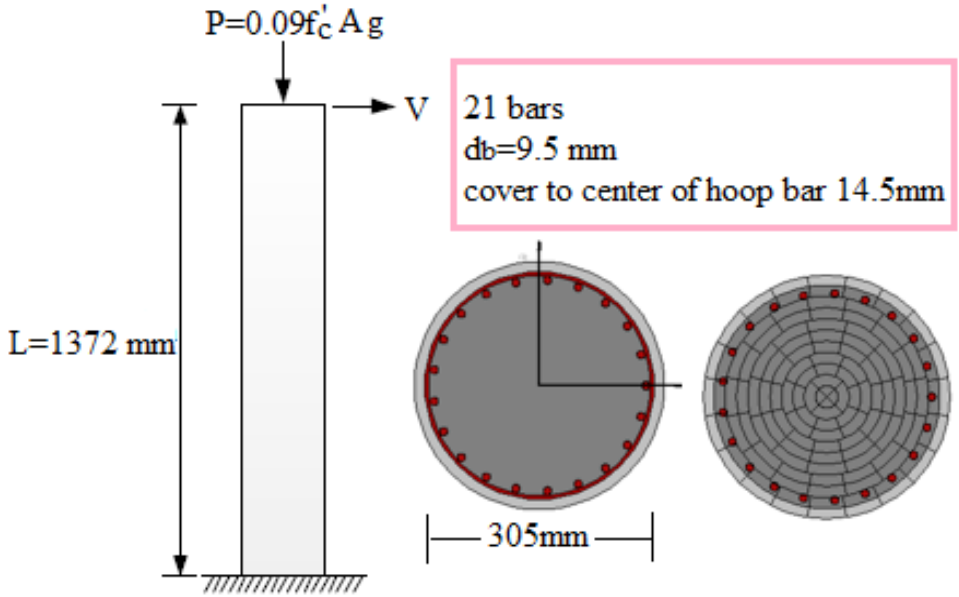

Figure 3-5 Geometry, axial load and sectional properties of the specimen **(**Kunnath et al. 1997, A2) .

3.2.1 Hardening pushover analysis using DDB

The member analyzed using DDB elements with two Gauss-Legendre integration points. For the DDB elements, Neuenhofer and Filippou (2007) suggest that an increasing number of integration does not improve accuracy. The analysis shows that when the member divided into several elements, the moment-curvature response does not converge to the same solution, As shown in Figure 3-6. Such an issue does not represent the term localization exactly but a weakness in the DDB elements in capturing highly nonlinear sectional deformation.

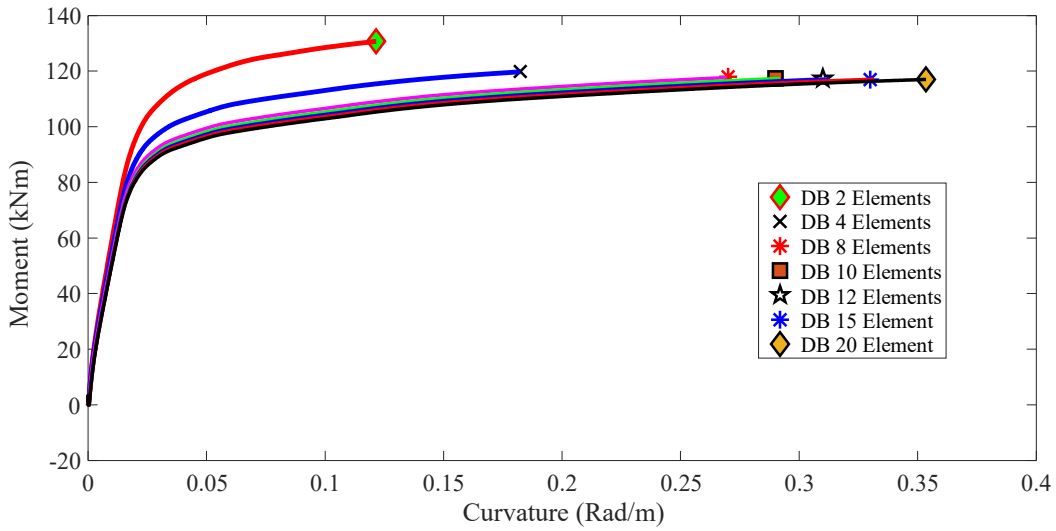

Figure 3-6 Hardening moment-curvature response using DDB (Specimen A2).

The global force deformation response obtained using four elements per member approximately captured the cyclic envelope of the experimental response, as shown in Figure 3-7. The force deformation response obtained using the DDB models overestimates the real strength and stiffness. Since the force equilibrium is not satisfied in the exact sense, the rate of convergence in the global force deformation response is fast compared to the local response. In the work of Calabrese et al. (2010) and Gharakhanloo (2014), a similar issue was also recognized in this formulation.

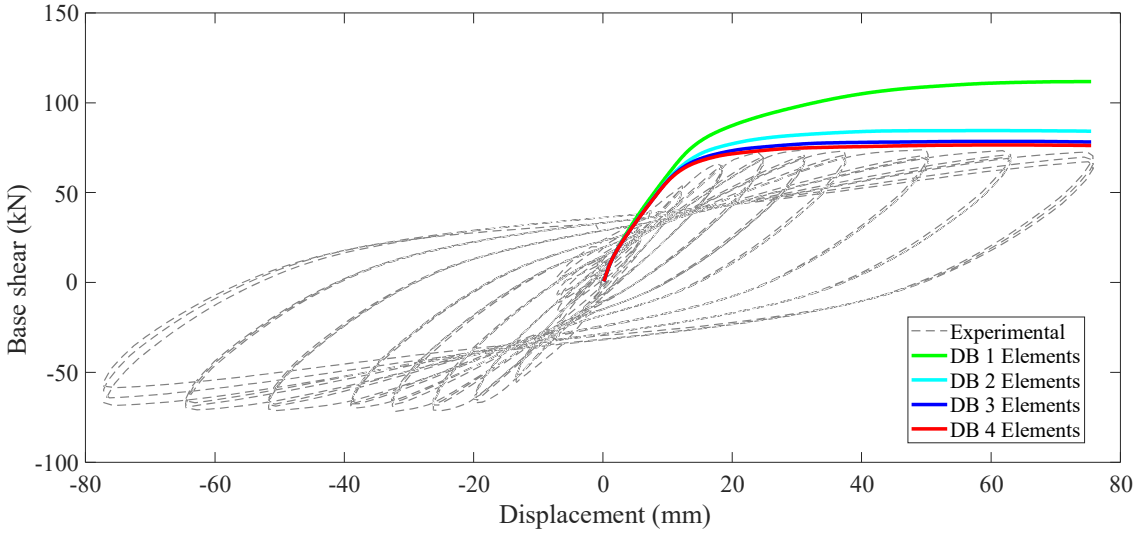

Figure 3-7 Hardening force-displacement response using DDB.

3.2.2 Hardening pushover analysis using DFB

The column modeled using only one force-based element, and by varying the integration points. The analysis shows that both global and local responses are objective. As the number of integration section increases, the response converges into the same result. For section exhibiting hardening behavior, the force-based elements provide accurate results at the global and local levels. In DFB formulation, the Local response converges fast with an increasing integration section, as shown in Figure 3-8.

Using DFB formulation, the global pushover results are very close to the experimental cyclic envelope, as shown in Figure 3-9. The analysis result captures the maximum base shear capacity and stiffness satisfactory.

Figure 3-10 shows the comparison of force deformation response of both the DFB and DDB elements. The analysis shows the inelastic response using one DFB element with 4 IPs is accurate, whereas, the DDB with 4 elements slightly overestimates the capacity, as shown in Figure 3-10.

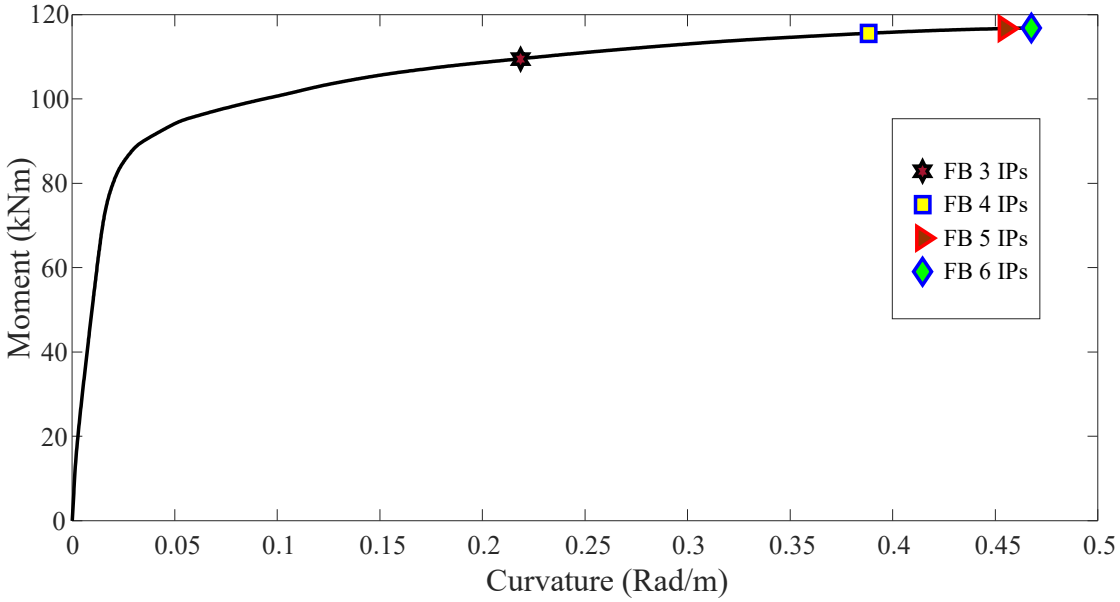

Figure 3-8 Hardening moment-curvature response using DFB.

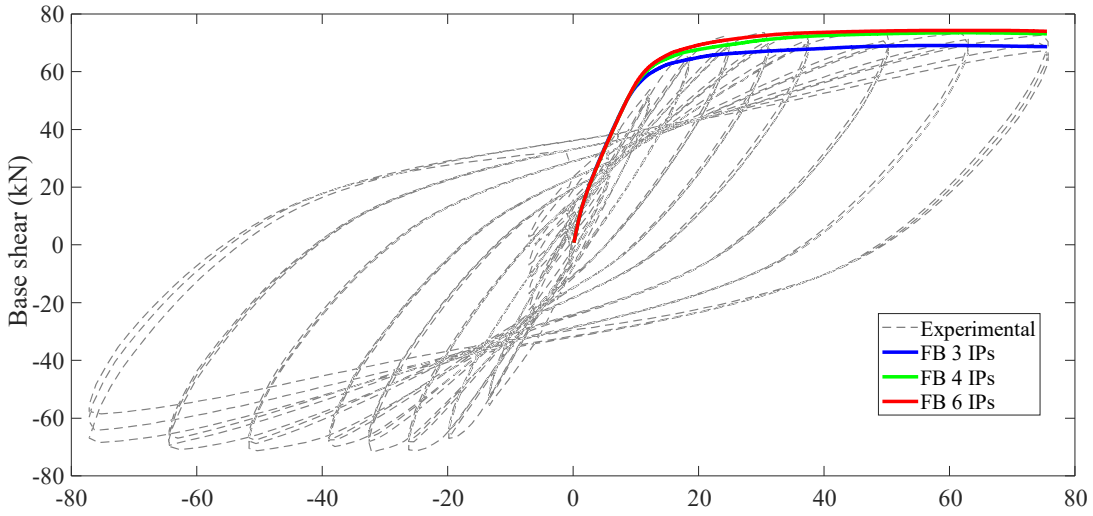

Figure 3-9 Hardening force-displacement response using DFB.

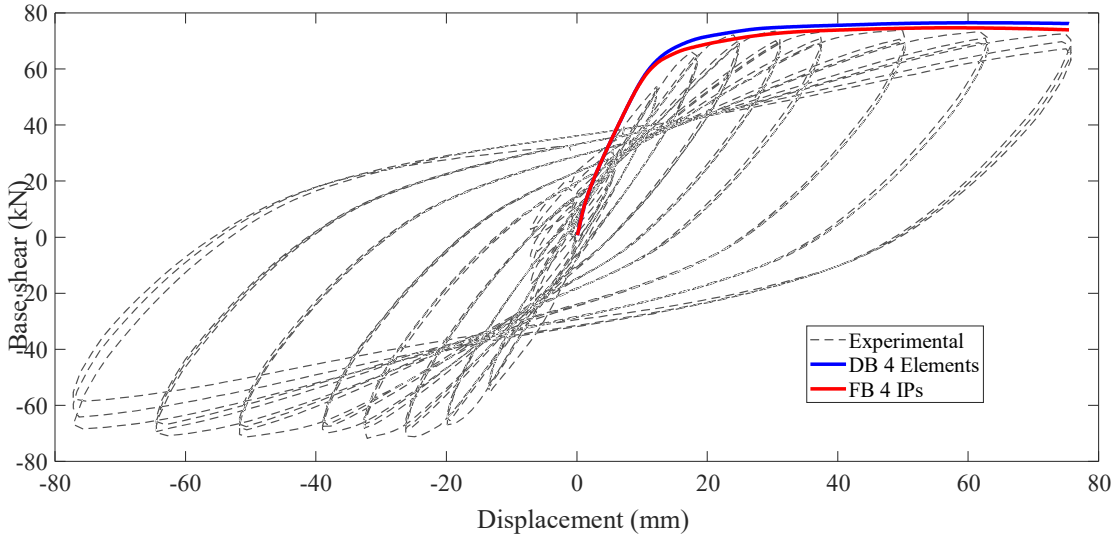

Figure 3-10 Comparative hardening force-displacement response between DDB and DFB.

3.2.3 Hardening pushover analysis using beamwithhinge fiber models

This section presents a comparison between forces based concentrated fiber models that have different integration methods for integrating nonlinear response in the plastic hinge region. As shown in Figure 3-11, the yield moment and maximum moment capacity computed with the midpoint integration method is greater than of the other three integration methods because the bending moment is sampled at the center of the plastic hinge regions. The maximum sectional curvature obtained using the two-point Gauss-Radau integration method is large, as shown in Figure 3-11; however, this is the best representation of the curvature of the four integration methods. The curvature is approximately the same maximum curvature with distributed force-based response obtained in Section 3.2.2, Figure 3-8. The reason is that in the Two-point Gauss-Radau integration method, hardening spreads across two integration points in the plastic hinge regions. When Scott and Fenves (2006) was comparing the four integration methods, the yielding moment obtained using the Two-point Gauss-Radau integration method was the same as the closed-form solution.

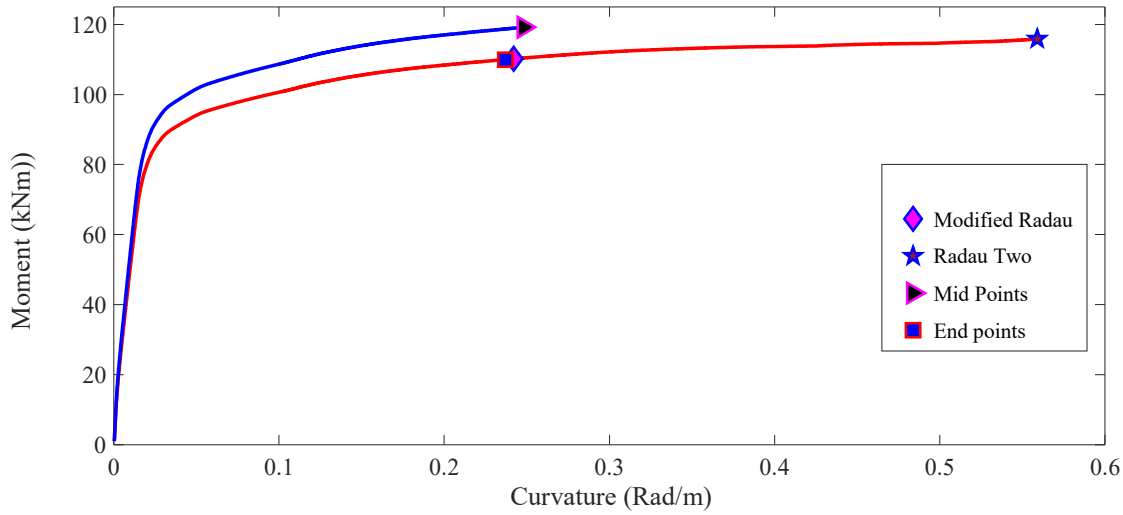

Figure 3-11 Hardening moment curvature response using Beamwithhinge (Specimen A2).

As shown in Figure 3-12, the endpoint and modified Gauss-Radau integration methods unable to predict the post-yield response of the force deformation because nonlinear behavior is restricted to a single integration point at both ends of the element. For endpoint integration, the elastic response method is too flexible because of the large integration error.

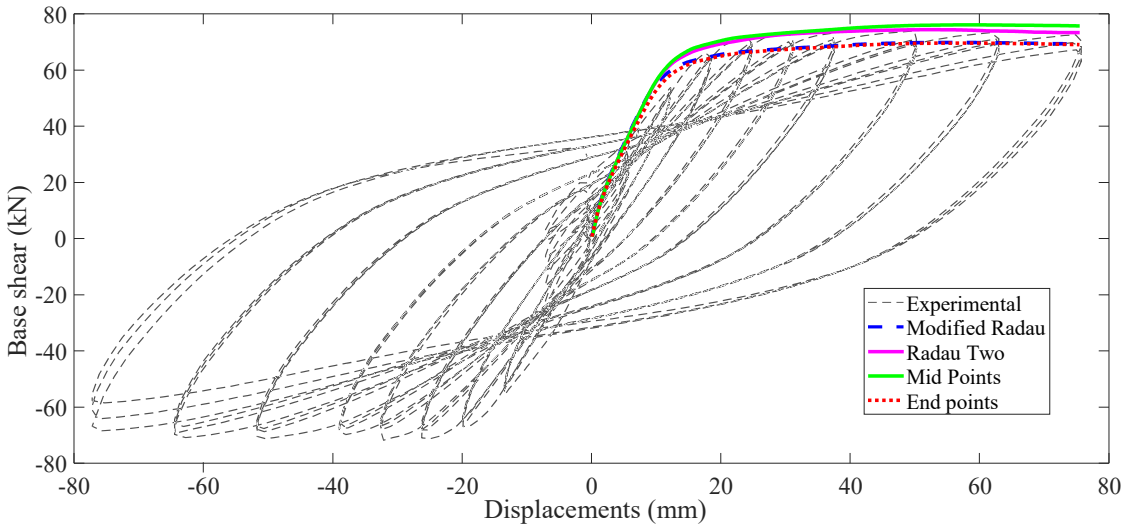

Figure 3-12 Hardening force deformation response using beamwithhinge (Specimen A2).

3.2.4 Lumped plasticity with zero hinge length

The column modeled in Siesmostruct software using Lumped plasticity with zero hinge length. The cross-sections associated with non-linear behavior (plastic-hinges) calculated according to a global modified Takeda type model Takeda et al. (1970). As shown in Figure 3-13, because of the assumption of fixed plastic hinge length and the constant elastic stiffness, the models capture the initial stiffness satisfactorily; but unable to predict the cracking and onset of yielding. The models do not allow the soft transition of the progressive spreading of cracks from the elastic zone to the yielding. Furthermore, the models underestimate the maximum base shear capacity because the assumptions made in the plastic hinges are conservative.

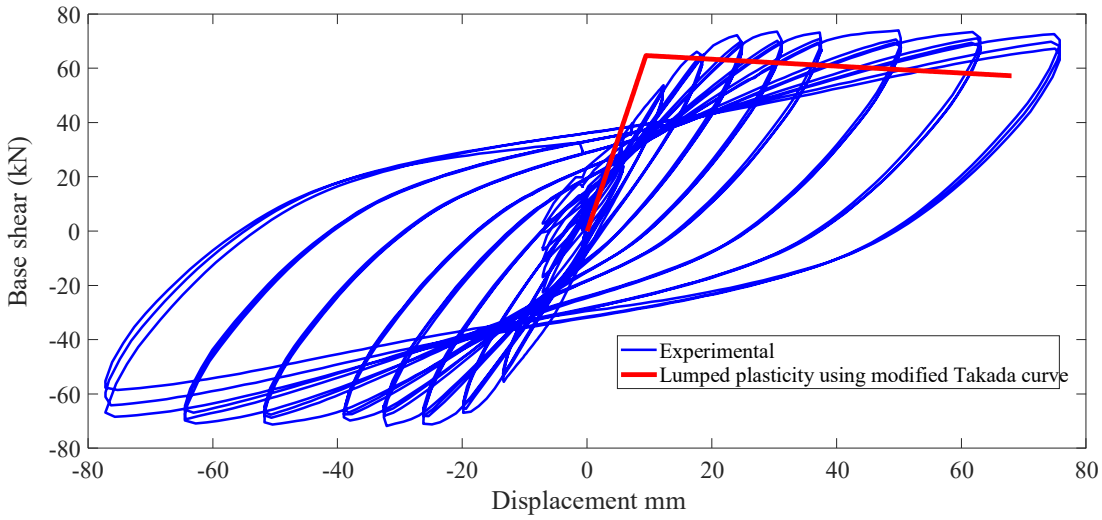

Figure 3-13 Hardening moment-curvature response using beamwithhinge (Specimen A2).

3.3 Pushover analysis of RC bridge column (Simulated softening)

To show localization due to high axial load and verify the proposed regularization for compression-controlled members by Coleman and Spacone (2001), specimen A2 analyzed by increasing the axial load up to 50%; and other parameters kept constant. On the other hand, the section is assumed to fail in compression, and only concrete material regularization is required.

3.3.1 Softening pushover analysis using DDB

The column subjected to an increased axial load up to 50% was analyzed using the DDB elements. As seen in Figure 3-14, the local response does not converge to the same solution for a different level of mesh refinement. Furthermore, the global response in the post-peak region localizes over a small length of the single DB element; and provides mesh dependent responses, as shown in Figure 3-15. In the post-peak region, the numerical model showed degradation of capacity, but for 15 and 20 DB elements, the response hardened because the failure is only due to the crushing of concrete, as shown in Figure 3-15. When only the ultimate strain in the concrete reaches, the force deformation loss the strength linearly, and the steel starts hardening up to reaching the ultimate strain. After the steel fracture strain reaches, the section suddenly drops its strength.

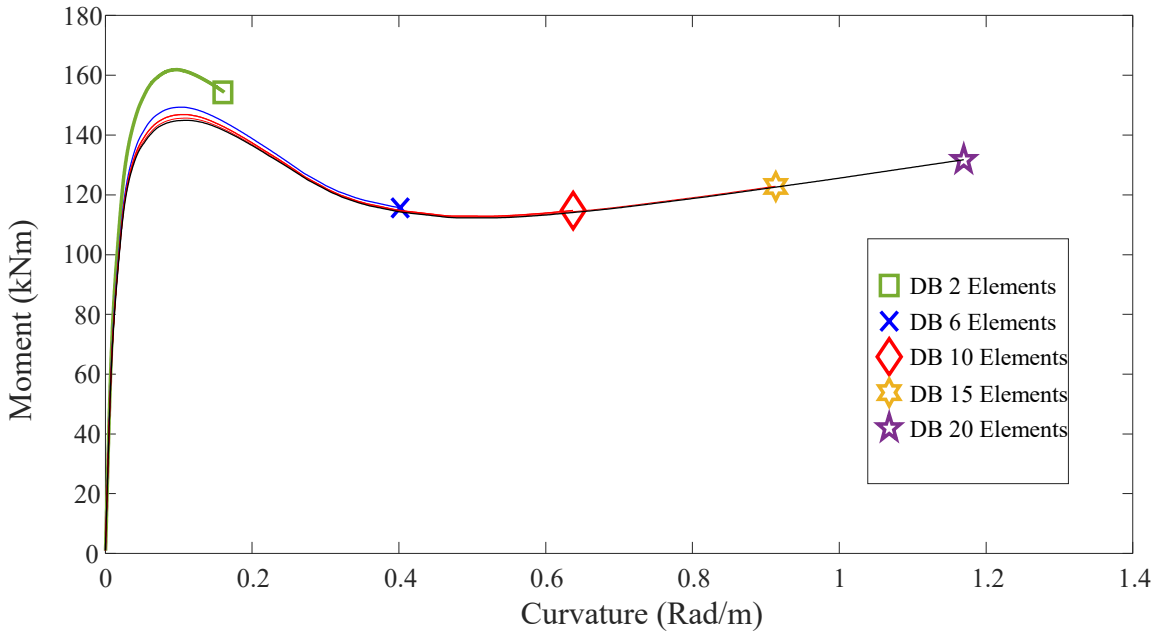

Figure 3-14 Softening moment-curvature response using DDB (Specimen A2).

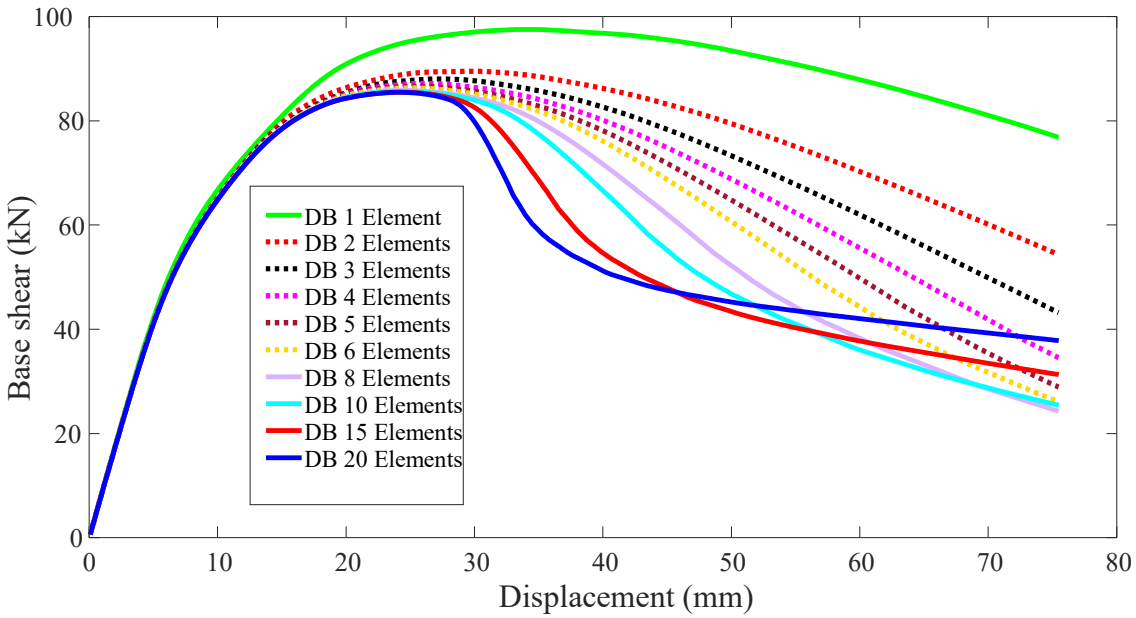

Figure 3-15 Hardening force-displacement response using DDB (Specimen A2).

3.3.2 Softening pushover analysis using DFB

Figure 3-16 shows the moment-curvature curve for different integration points; the maximum curvature does not have a unique solution. The same localization issue in the global response also detected, as seen in Figure 3-17. In the DFB model, the rate of softening is fast because the inelastic deformation localizes of single integration point instead of a single element.

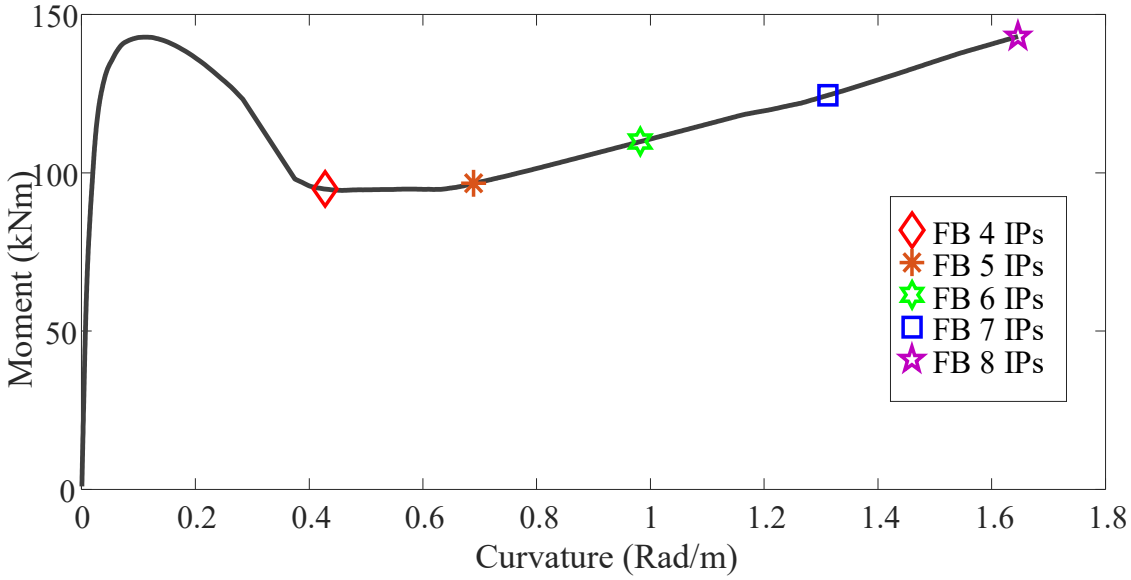

Figure 3-16 Softening moment-curvature response using DFB (Specimen A2)

.

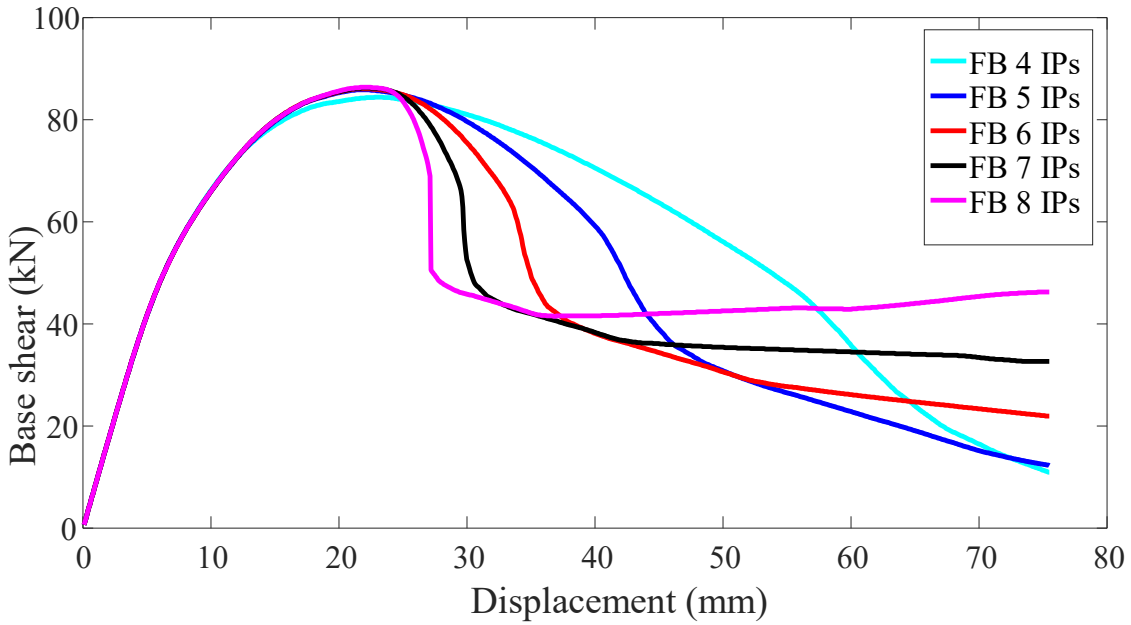

Figure 3-17 Hardening force-displacement response using DFB (Specimen A2)

3.3.3 Softening pushover analysis using Beamwithhinge fiber models

The sectional curvature estimated using the Radau-Two integration method is extremely large compared with the other models, as shown in Figure 3-18. The Radau-Two integration method utilizes two integration points in a single plastic hinge region; hence, the response localized over a single section at both the global and local levels. As seen in Figure 3-18, the modified Gauss-Radau method is valuable in the case where deformations localize due to softening behavior. The midpoint and endpoint models use one integration point; hence, the response does not localize over a single section..

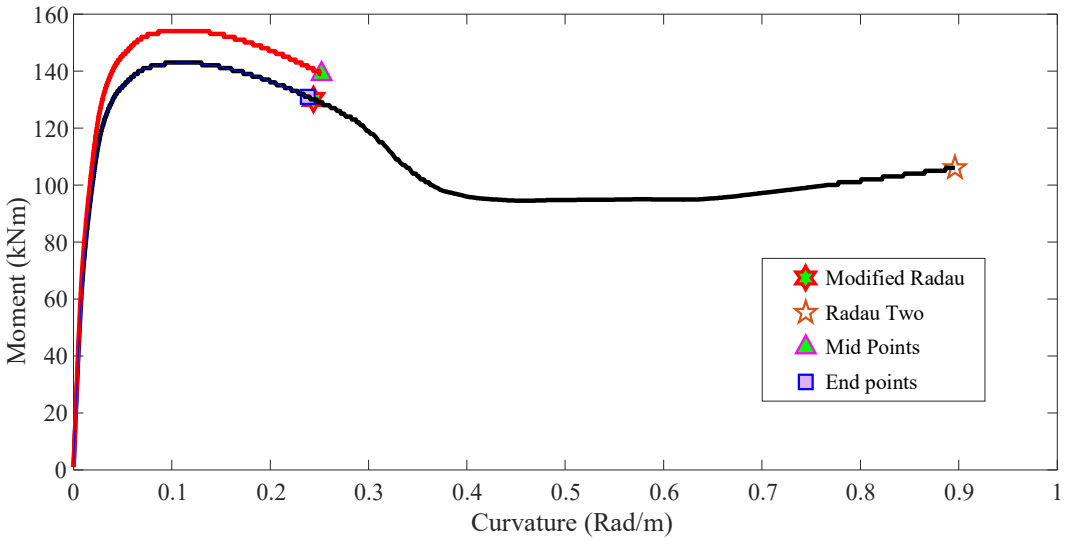

Figure 3-18 softening moment curvature response using Beamwithhinge (Specimen A2).

The maximum curvature obtained using the endpoint and the modified Gauss-Radau methods are almost the same because for both the characteristic length used to integrate localized deformation at the element ends is LP. In the original two-Point Gauss-Radau method, the characteristic length used to integrate localized deformation at the element ends is LP /4. The characteristics length of the two-Point Gauss-Radau is four times lesser than the endpoint and modified Gauss-Radau; hence, the curvature obtained using the two-Point Gauss-Radau is four times greater, as shown in Figure 3-18.

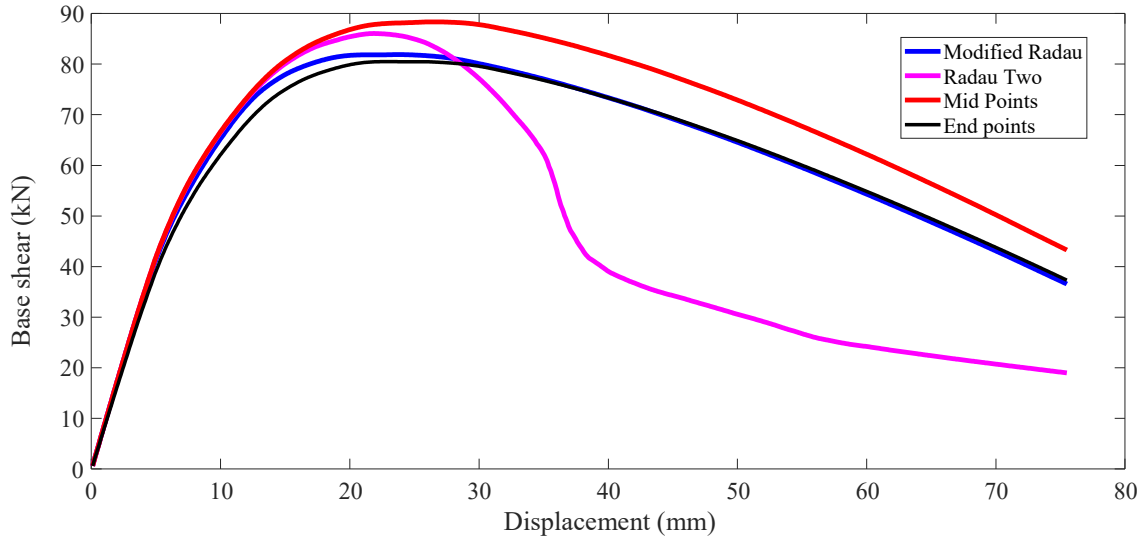

Figure 3-19 Softening force-deformation response using BeamwithHinge (Specimen A2).

3.4 Regularization methods to overcome mesh dependent results

Coleman and Spacone (2001) proposed regularization techniques for force-based elements based on the concept of constant fracture energy. The constant fracture energy criterion enforced to adjusting the softening slope of the stress-strain law for concrete; the ultimate strain e20 for each integration point is estimated and summarized in Table 3-2.

It should be noted that steel regularization is not done in this section because the member is assumed to be subjected to high axial load and only concrete will be affected by strain softening. Sensitivity analysis was carried out and regularizing the steel has an insignificant effect on producing objective response there for this case was neglected. The regularization of both steel material has been presented in detail and compared with experimental in Section 3.5. Figure-3-20 shows the global response of DFB formulation using regularized and non-regularized concrete material. The force deformation response is objective; therefore, the proposed regularization technique is effective. Furthermore, a comparative between regularization techniques based on the concentrated plastic hinge method and material regularization have been plotted in the same graph as shown in Figure 3-21. Both methods are able to overcome mesh dependent results.

Table 3-2 Weight and length of Gauss-Lobatto integration points and regularized crushing strain of confined concrete.

Number of integration points N_{IP}	Weight of the first Integration point w_{IP}	Length of the first integration pint $L_{IP} = w_{IP} \cdot \frac{L}{2}$	Crushing strain $\varepsilon_{20} = \frac{G_f^c}{0.6f_c' L_p} - \frac{0.8f_c'}{E_c} + \varepsilon_c$
5	$1/10$	68.6	0.09369
6	$1/15$	45.73	0.1402
7	0.047619	32.67	0.1960
8	0.035714	24.50	0.2612

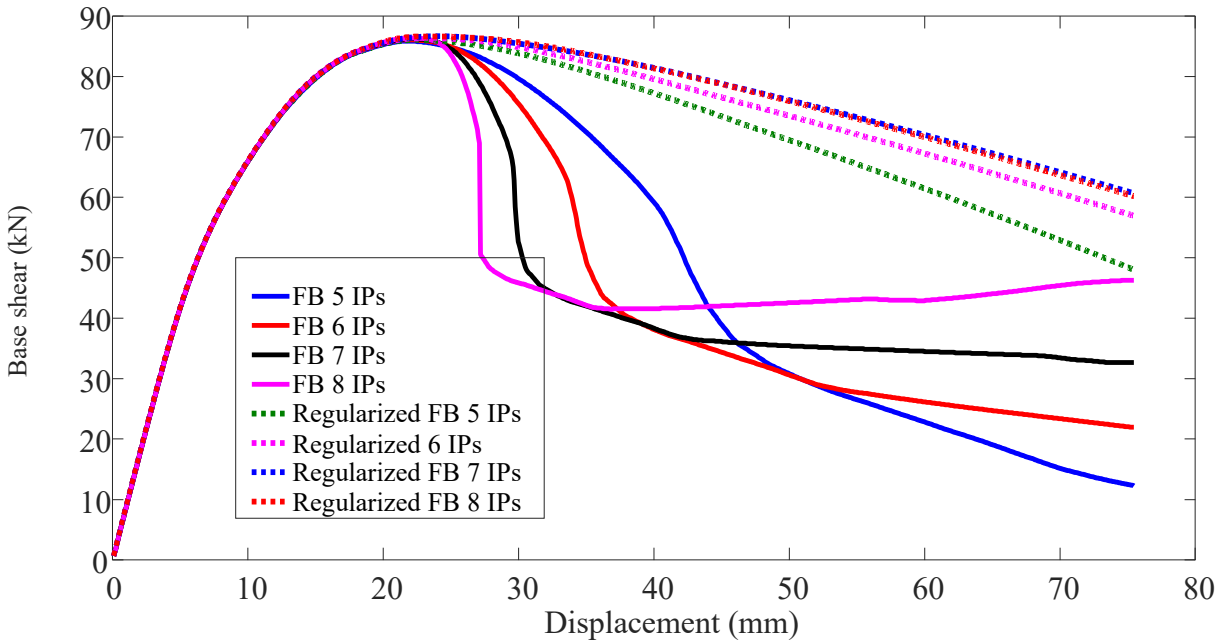

Figure 3-20 Monotonic response using DFB before and after applying material regularization (Specimen A2).

Curvature post processing for regularization of local response

Coleman and Specone (2001) suggested a post-processing of curvature after analysis is carried out. To regularize the local response, the curvature output for a typical beam hinge is scaled according to Equation 2-41. Because the column is cantilever a single curvature approach has been used to calculate the curvature scale. For the six, seven and eight the curvature scale factor are 0.225, 0.184 and 0.1389, respectively**.** after post-processing has been applied the moment-curvature becomes mesh independent result, as shown in Figure 3-21.

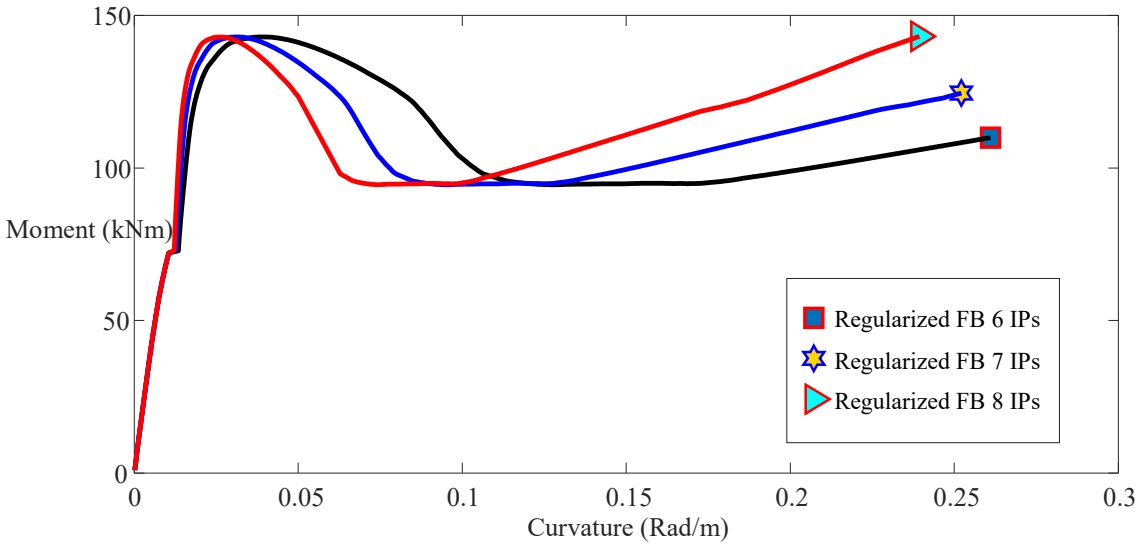

Figure 3-21 Moment-curvature after applying post-processing (Specimen A2).

3.5 Pushover analysis of RC bridge column (experimentally soften column)

This section briefly discusses partial and full material regularization techniques for fiber beam-column elements. Coleman and Specone (2001) suggested material regularization only for the concrete section that fails due to the crushing of concrete. Later on, Pugh (2012) suggested to include the regularization of steel material. To verify the proposed regularization techniques, a reinforced concrete column that exhibit strain-softening behavior from both fiber materials, specimen No.3 in the tests by Wong et al. 1993, is modeled in OpenSees. Detail of the specimen geometry and material properties is found in Appendix A.2. The specimen is subjected to a high axial load which is 1813 kN ($\mathbf{0.39f'_cA_c}$), as shown in Figure 3-22. From the experiment observation, the significant

concrete spalling and longitudinal bar buckling was observed at a drift of 1.21% (9.7 mm) and 3.23% (25.9 mm) respectively. Table 3-3 shows the material properties used for modeling the specimen before regularization was applied.

Table 3-3 Material properties of specimen (Wong et al. 1993, A3).

Unconfined Concrete 02	
Maximum Concrete strength (f_c')	37 Mpa
Peak strain (ε_{c0})	0.002
Crushing stress f_{c20}')	$0.2 \cdot f_c'$
Crushing strain (ε_{cu})	0.008
Confined Concrete 02	
Confinement factor (k)	1.348 (Mander et al. 1988)
Compressive strength (f_{cc})	49.9 ($k \cdot f_c$)
Peak strain (ε_{cc0})	0.00549
Crushing stress(f_{cc20}')	$0.2 \cdot f_{cc}'$
Crushing strain (ε_{ccu})	0.0205
Reinforcement bar Steel 02	
Yield strength(f_y)	475 Mpa
Modulus of elasticity (E_s)	200000 Mpa
Strain Hardening (b_s)	1%

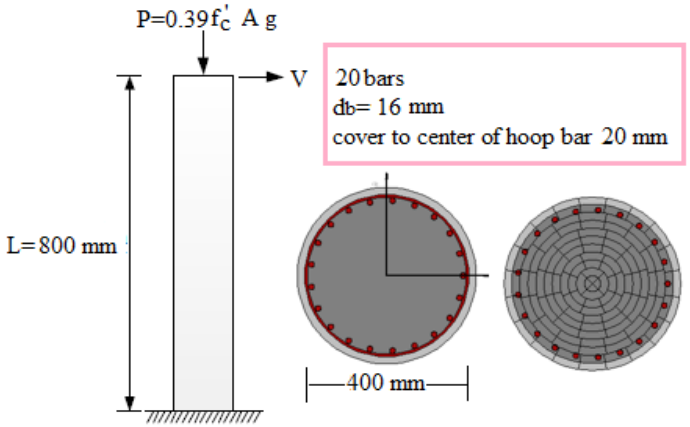

Figure 3-22 Reinforced concrete column with softening behavior (Wong et al. 1993, Specimun No. 3).

3.5.1 Regularized and non-regularized pushover response using DFB

Figure 3-23 shows the monotonic response of the member without applying material regularization. The response showed two types of localization, one is linearly softening, which is the softening of concrete material that occurs from the crushing of concrete; second is a sudden drop in strength, which comes from localization of the steel material (see Figure 3-23). It should be noted that the stress-strain of steel material always exhibits a hardening behavior after the post-peak response; however, the strain in the steel localizes to confirm compatibility. The mesh dependent result underestimated the ultimate strength and drift capacity of the column.

To regularize concrete material modification on the ultimate strain for unconfined and confined concrete carried out according to Equation 2-43. Adjusted fracture strain for steel material calculated according to Equation 2-47. Gauge length was assumed to be 203 mm, as recommended by ASTM A370, and maximum strain taken as 0.09. For the steel a MinMax criteria have been assumed, this enforces the stiffness and strength of the steel fibers to become zero when the compressive strain is reached. The estimated properties of the regularized material summarized in Table 3-4.

Table 3-4 Regularized strains of the unconfined and confined concrete, ultimate rupture strain and strain hardening reinforcement steel Wong et al. 1993, Specimen-No.3 (for DFB model).

No IPS		G_{fc}=180 N/mm	$G_{fc}=2\cdot f_c'$	$G_{fcc}=1.7\cdot G_{fc}$		
	L_{IP}	ε_{cc20}	ε_{c20}	ε_{cc20}	ε''	b_s
3	133.3	0.0467	0.026	0.0332	0.136	0.006
5	40	0.1518	0.0844	0.1066	0.448	0.002
7	19	0.317	0.176	0.2221	0.937	0.001

Applying material regularization only to concrete failed to address the mesh-dependent response, as shown in Figure 3-24-25. The ultimate drift capacity using DFB with 7 IPs is less than of the 5 IPs; the ultimate drift capacity obtained using 5 IPs is less than of the 3 IPs. In the case study column, the onset of significant concrete sapling was observed at a drift of 1.21% (at the displacement of 9.7 mm), so regularizing only the concrete material overcomes localization issues up to this drift level**.** Furthermore, the crushing energies values suggested by Pugh showed good performance compared with that of Coleman and Specone. This is because Pugh suggested crushing energy value for both confined and unconfined concrete that depends on the compressive strength of concrete, Whereas, Coleman and Specone suggested a constant value based on the engineering judgment (recall section 2.6.2.1).

Applying material regularization only to steel material also failed to address the mesh-dependent response, as shown in Figure 3-26. However, the localization or sudden drop of strength observed in the non-regularized response **(**see Figure 3-22**)** successfully tackled.

The most recent way is based on the regularization of both steel and concrete materials for fiber beam-column models (Pugh 2012). As shown in Figure 3-27 and 3-28, the response is objective for all integration sections. Furthermore, the ultimate strength of the column obtained from experimental was 578 kN, whereas, the estimated based share using non-regularized DFB with 7 IPs was 465 kN, which has a 19.31% error. When regularization for both material applied, the ultimate strength was 508 kN, which has a 12.56% error. This shows that the localization issue underestimates the ultimate strength of the member subjected to high axial load. From the plot, the fully-regularized response does not capture the ultimate base shear obtained using the cyclic test, but still, the response is fairly accurate and conservative.

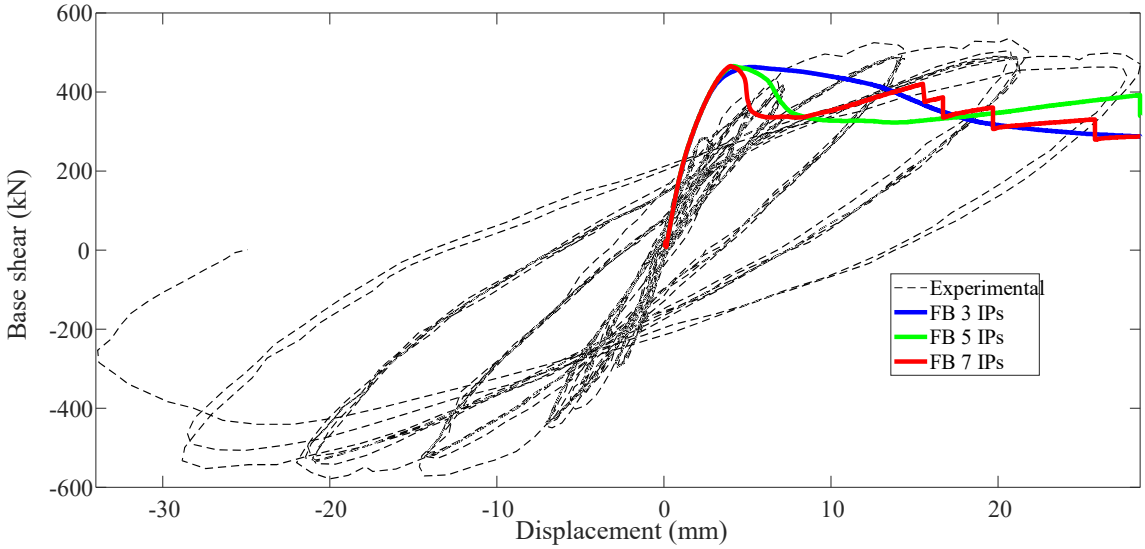

Figure 3-23 Monotonic response using DFB without applying material regularization (Specimen No. 3).

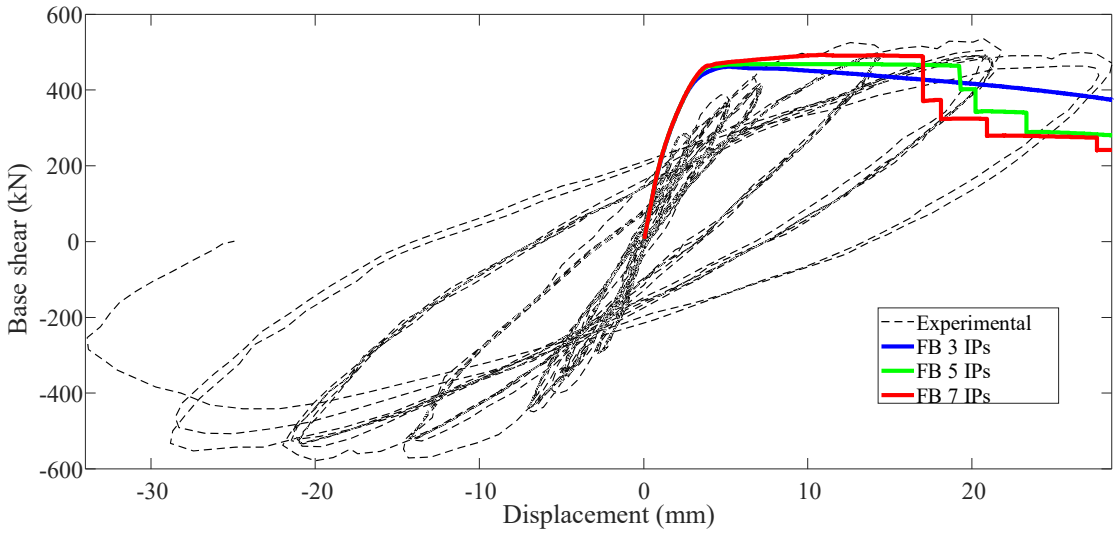

Figure 3-24 Monotonic response using DFB (Specimen No. 3) applying regularization only for concrete using Gfc value suggested by Coleman and Specone (2001).

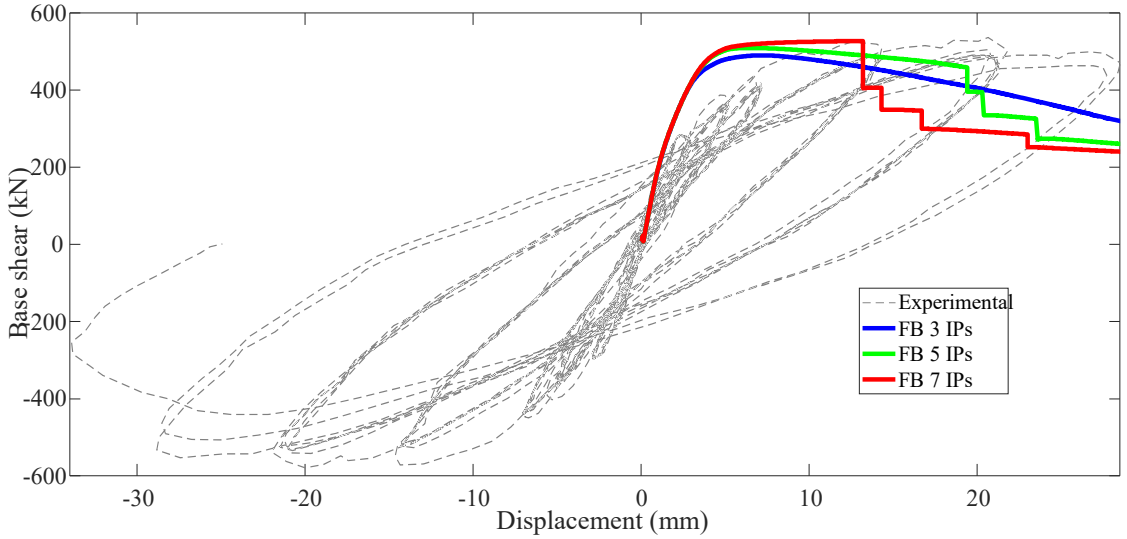

Figure 3-25 Monotonic response using DFB (Specimen No. 3) after applying material regularization only for concrete using suggested Gfc value by Pugh (2012).

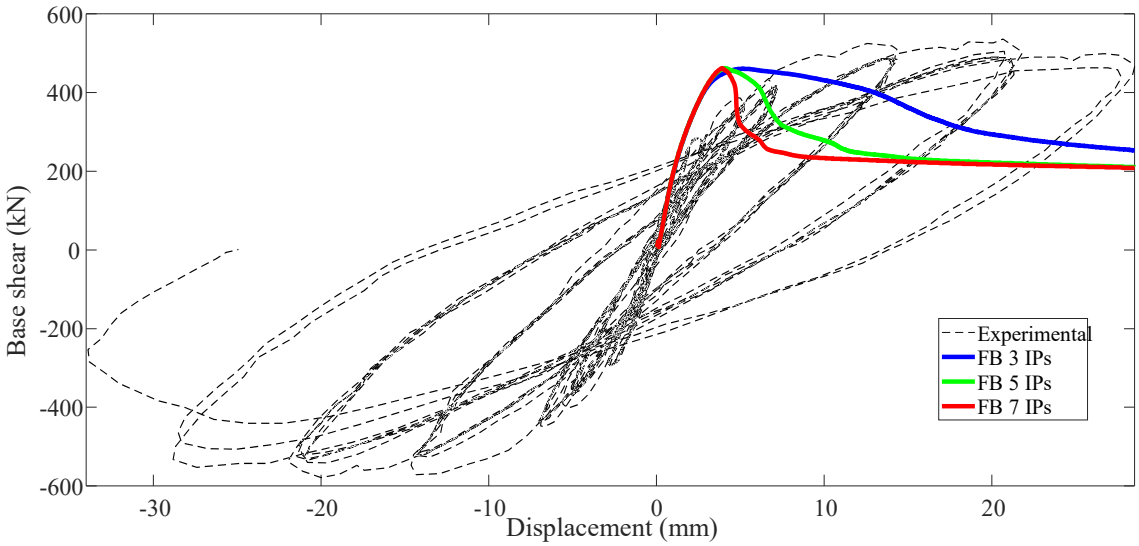

Figure 3-26 Monotonic response using DFB (Specimen No. 3) after applying material regularization only for steel material .

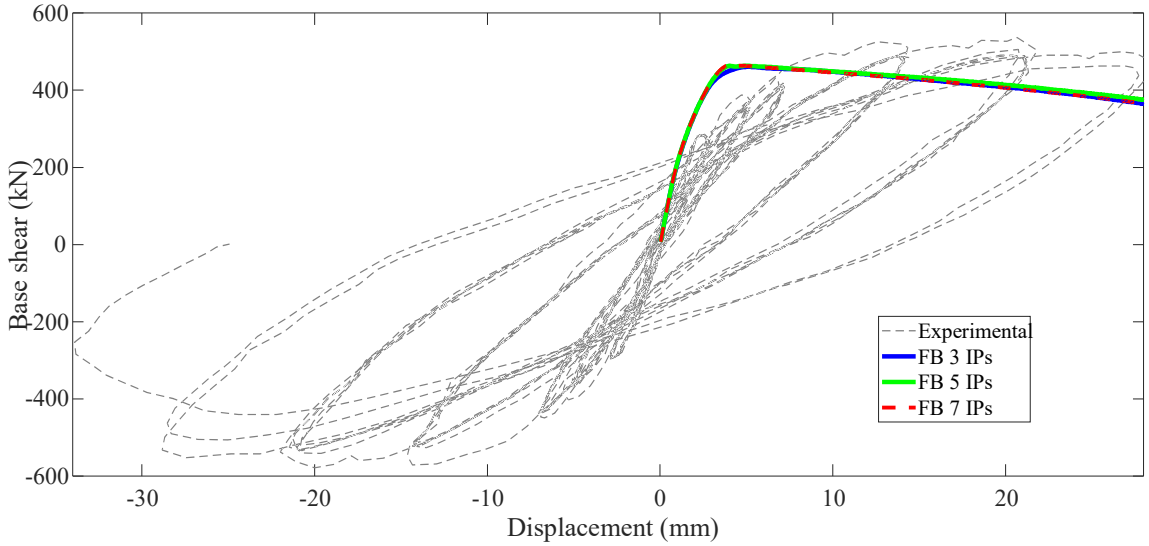

Figure 3-27 Monotonic response using DFB (Specimen No. 3) after applying material regularization for both concrete and steel sing suggested Gfc by Coleman and Specone (2001**).**

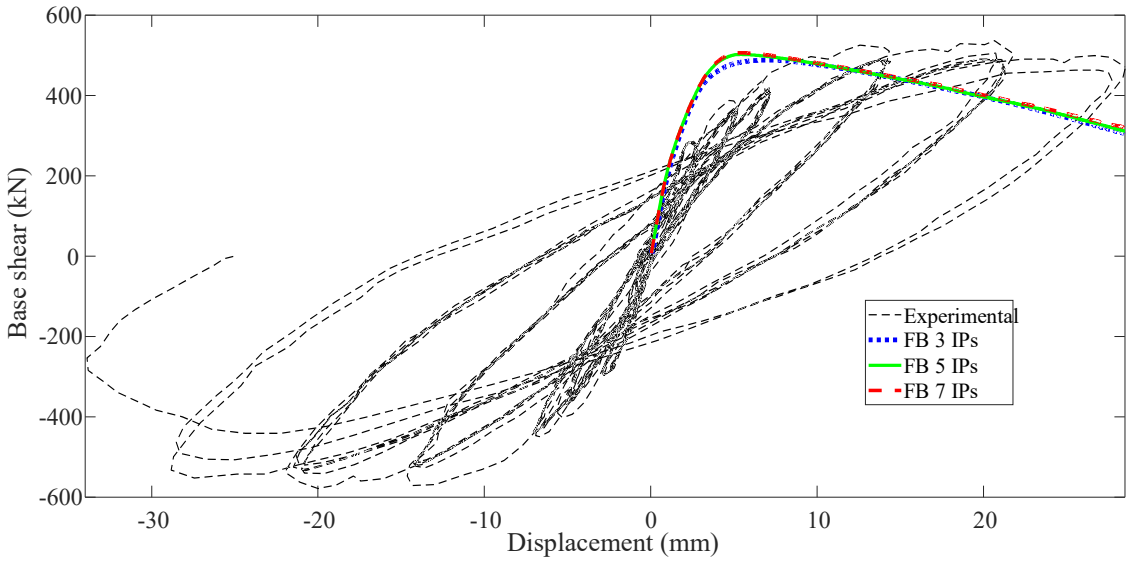

Figure 3-28 Monotonic response using DFB (Specimen No. 3) after applying material regularization for both concrete and steel sing suggested Gfc by Pugh (2012).

3.5.2 Regularized pushover response for DDB

The specimen analyzed using the DDB with two Gauss-Legendre points. The response obtained using the non-regularized model is mesh dependent, as shown in Figure 3-29. For 4, 8 and 16 elements, the force deformation after the post-peak response has different drift capacity. Using these formulations rate of softening is slow compared with the DFB elements. Two regularization techniques can be used to regularize mesh dependent responses in DDB elements. The first approach is by setting the extreme length equal to 2Lp. In this case, the remaining internal elements may be divided equally (Calabrese et al. 2010 and Gharakhanloo 2014). Using this approach overestimates the capacity of the beam-column members (Calabrese et al. 2010). Therefore this regularization technique is not covered in this paper.

The second approach is the regularization of material using constant fracture energies. For nonlinear analysis of slender reinforced concrete walls, Pugh (2012) proposed material regularization for the DDB elements using. Pugh (2012) suggests a lower value of crushing energies for the DDB elements (recall section 2.6.2). As far as the RC structure is concerned, the recommended regularization techniques implemented to the reinforced concrete bridge columns. The estimated properties of the regularized material summarized in Table 3-6. When regularization for both materials is applied, the response becomes objective, as shown in Figure 3-30. Furthermore, the ultimate strength of the column obtained from the experiment is 578.6 kN, whereas, the estimated based share using non-regularized DDB with 16 elements was 4472.612 kN, which is an 18.3 % error. When regularization for both material is applied, the ultimate strength was 501.83 kN, which is a 13.2 % error.

Table 3-5 Regularized strains of the unconfined and confined concrete, ultimate rupture strain and strain hardening reinforcement steel Wong et al. 1990, Specimen-No.3 (for DDB model).

Elements number	L_{IP}	ε_{c20}	ε_{cc20}	ε''	b
4	100	0.0108	0.0135	0.1804	0.004
8	50	0.0201	0.0252	0.3585	0.002
16	25	0.0250	0.02487	0.7146	0.001

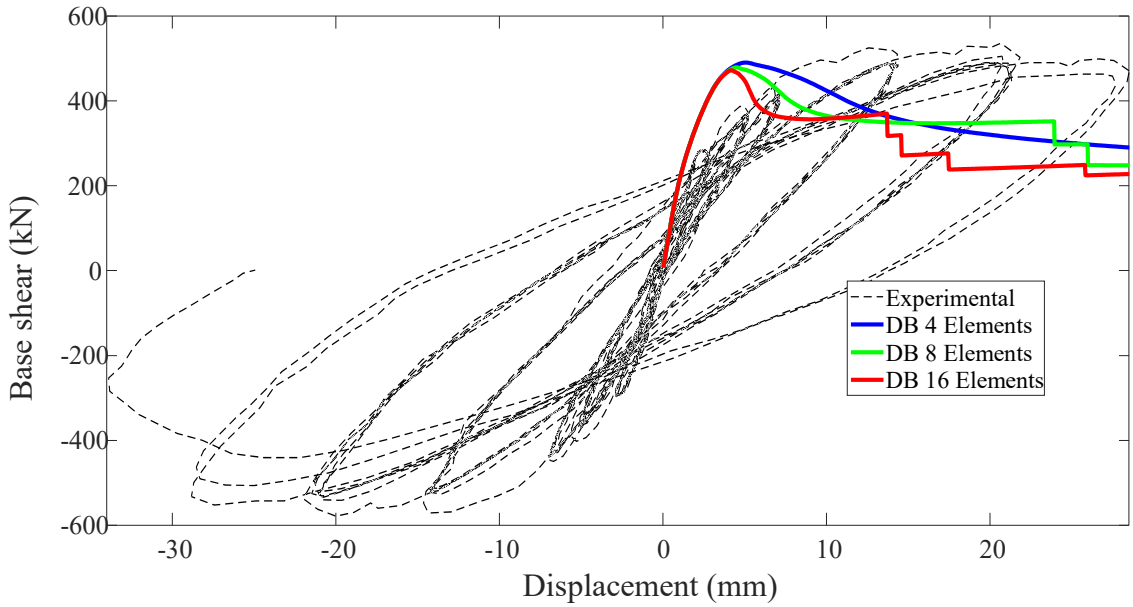

Figure 3-29 Monotonic resposnse using DDB (Specimen No. 3) with out applying material regularizatio.

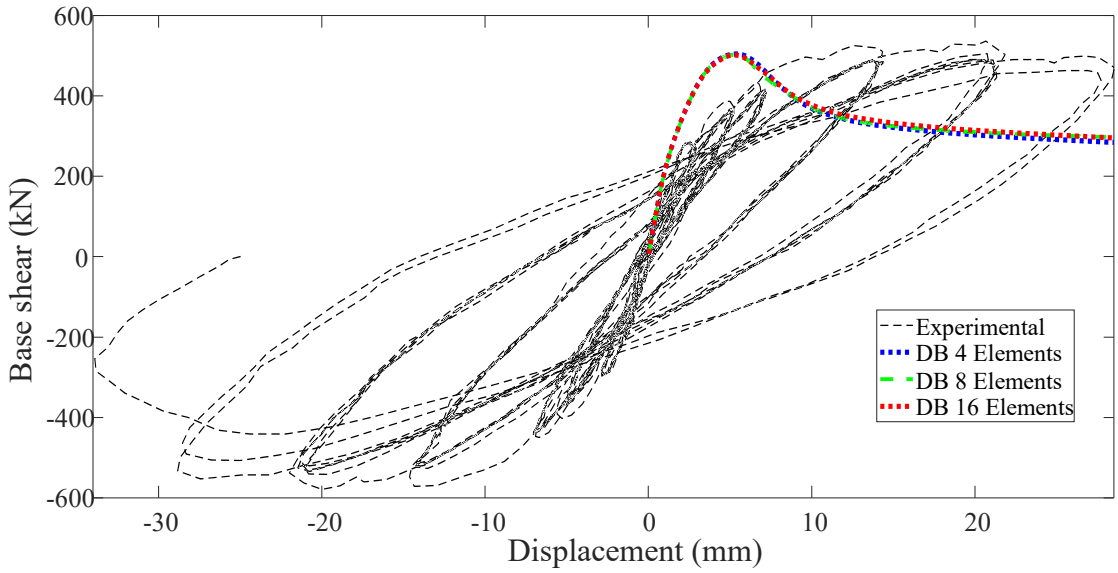

Figure 3-30 Monotonic response using DDB (Specimen No. 3) after applying material regularization for both concrete and steel using suggested Gfc by Pugh (2012).

4 Evaluation of the Numerical Non-Linear Models for Simulating Cyclic Response

4.1 Introduction

In the previous section, pushover analysis carried out to evaluate the models' performance for section exhibiting strain-hardening and strain-softening behavior. This section presents the comparison of models in simulating the cyclic response of the reinforced column bridge column. The loading strategies were done first by applying a constant axial load in the downward direction through the force control loading, and then the cyclic lateral load is applied through the displacement control. The cyclic analysis carried out using OpenSees finite element software.

4.2 Cyclic analysis of RC column under strain-hardening response

In this case, the previously investigated specimen has been taken to carry out cyclic analysis. To verify the nonlinear numerical models, a reinforced concrete column under strain-hardening behavior, specimen A2 in the tests Kunnath et al. (1997), is modeled in OpenSees.

4.2.1 Cyclic analysis using DDB (Hardening)

Cyclic analysis carried out using displacement-based beam-column elements. As shown in Figure 4-1, when mesh refinement increases, the cyclic moment-curvature does not converge into the same solution because the DDB element formulation assumes linear curvature, which is true only for elastic.

For the global response, as seen in Figure 4-2, convergence achieved fast; however, in the local response, the ultimate curvature still varies with a large magnitude. This issue with the DDB elements discussed briefly in the case of monotonic loading. To investigate how the displacement-based fiber models overestimate the capacity, DDB with one and two-element compared with the experimental results. As shown in Figure 4-3, the response with one DDB element and two DDB elements have a huge difference in terms of overestimating the capacity. The DDB with one element highly overestimates the actual response compared to two DDB elements.

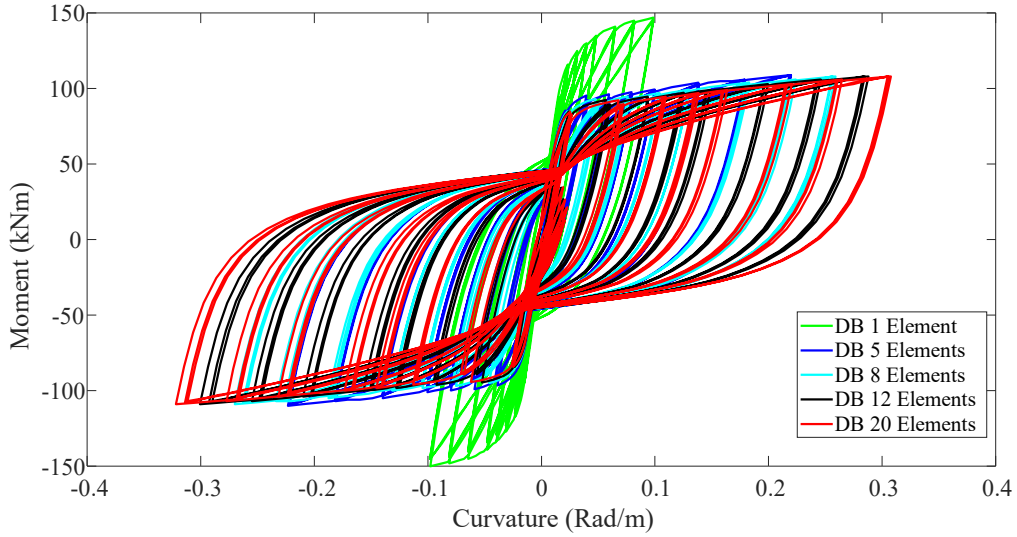

Figure 4-1 Hardening cyclic moment-curvature using DDB (Specimen A2).

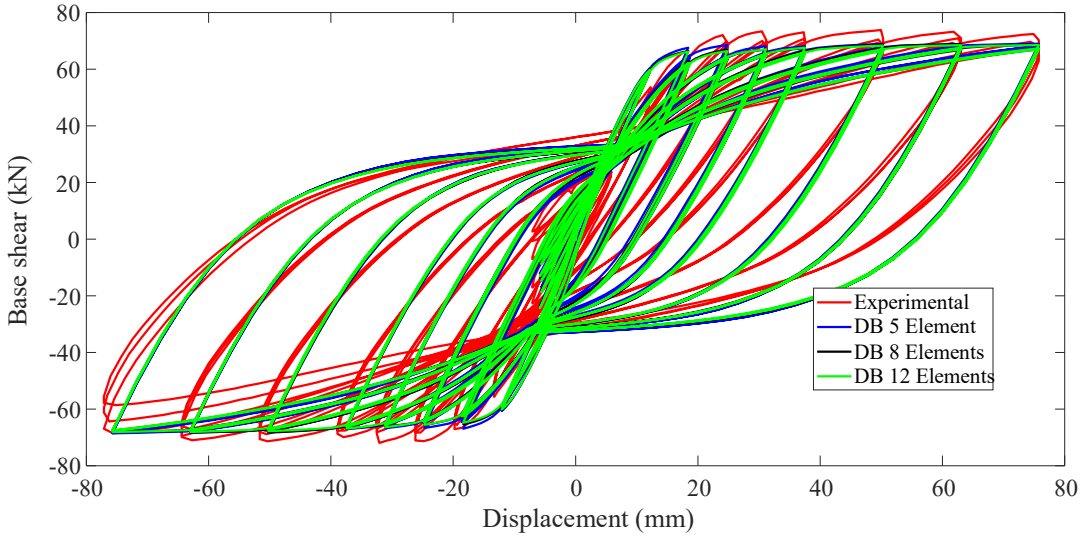

Figure 4-2 Hardening hysteresis response using DDB (Specimen A2).

4.2.2 Cyclic analysis using DFB (Hardening)

Cyclic analysis carried using force-based fiber models. As seen in Figure 4-4, for strain-hardening behavior with the increase in integration points, the maximum curvature converges into a unique solution. For the global response, the DFB models capture the shape of the hysteresis force deformation accurately without showing any premature failure in the cyclic loading, as shown in Figure 4-5.

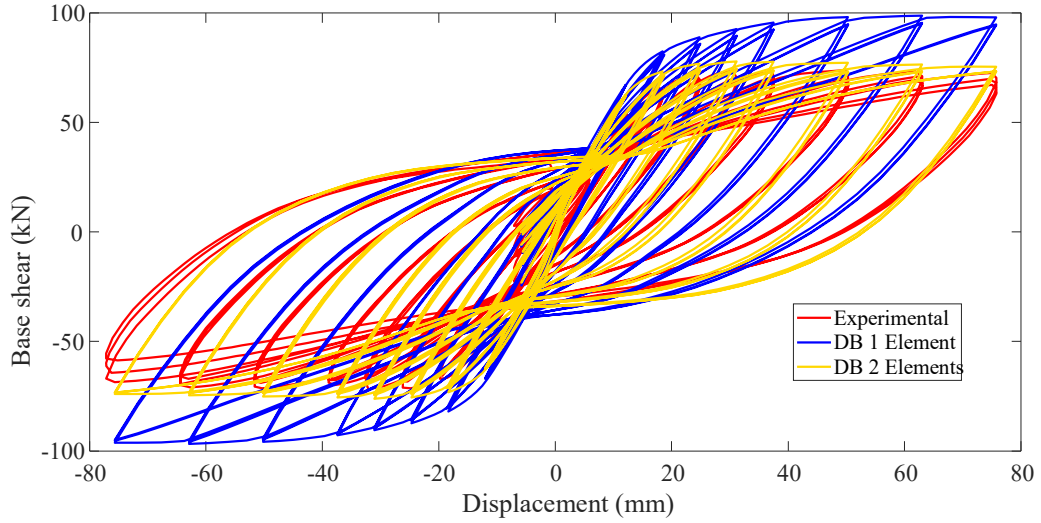

Figure 4-3 Hardening hysteresis response using 1 and 2 DDB elements (Specimen A2).

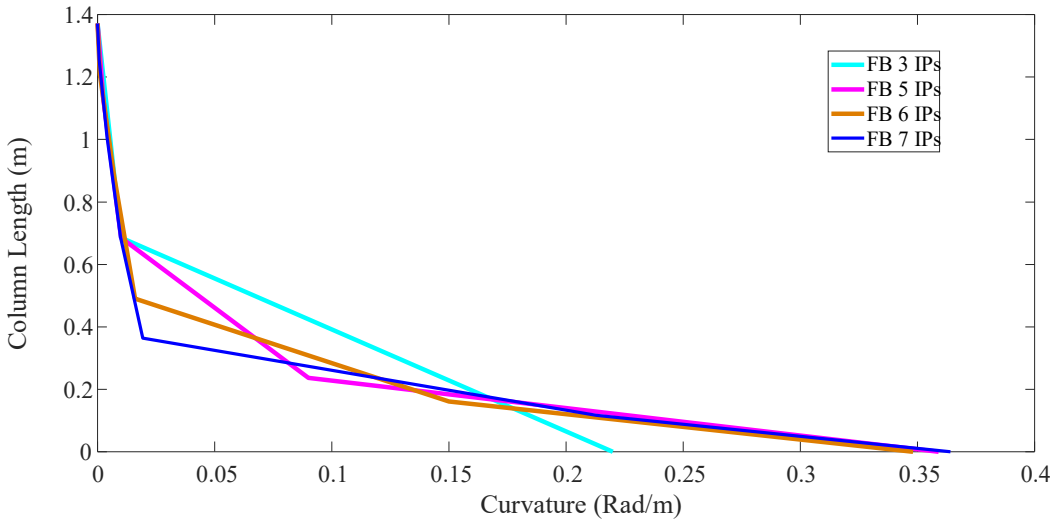

Figure 4-4 Hardening Curvature distribution using DFB (Specimen A2).

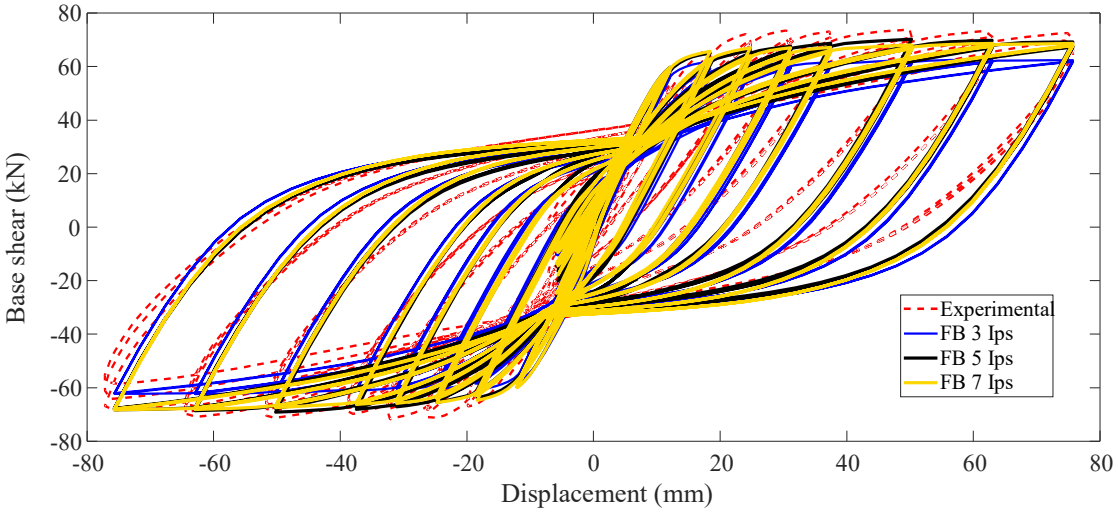

Figure 4-5 Hardening Hysteresis response using DFB (Specimen A2)

4.2.3 Cyclic analysis using Beamwithhinge fiber models (Hardening)

Cyclic analysis carried out using concentrated force-based or BeamWithHinge models with different integration methods. For the global force deformation response, as shown in Figure 4-6, the endpoint integration method and modified Gauss-Radau method, unable to predict the post-yield response of the force deformation curve because plasticity restricted to a single integration point at each end of the element.

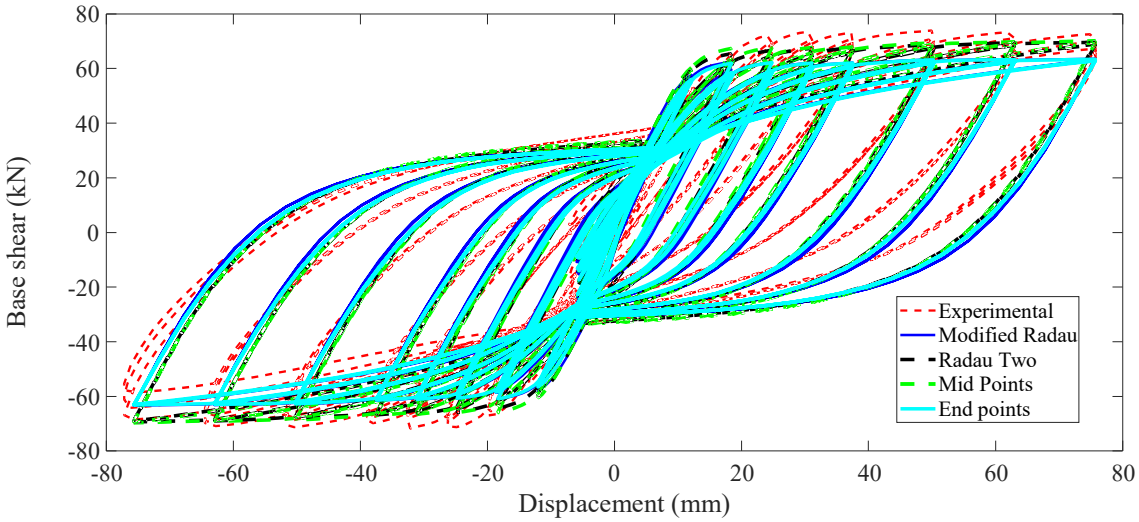

Figure 4-6 Hardening hysteresis response using Beamwithhinge (Specimen A2).

4.2.4 Cyclic analysis using lumped plasticity with zero hinge length (Hardening)

Figure 4-7 shows a cyclic response using lumped plasticity with zero hinge length. This model captures the initial slope satisfactorily; but unable to predict the cracking and onset of overall yielding. Furthermore, because of the conservative assumptions in the predefined plastic hinges, the model underestimates the maximum capacity in terms of force. Similar trends in this model observed in Chapter three for the monotonic loading case.

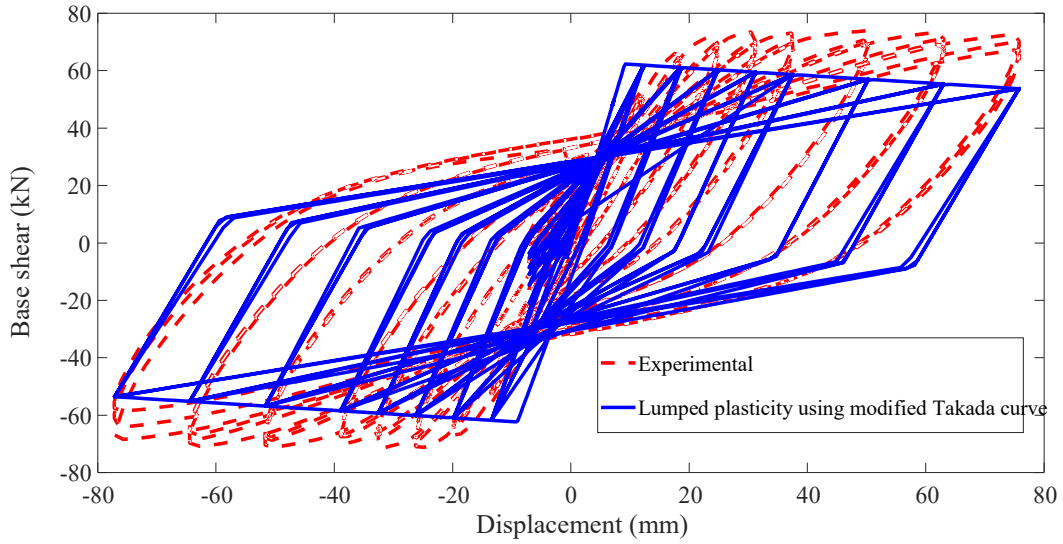

Figure 4-7 Hardening hysteresis response using lumped plasticity with zero hinge length model (Specimen A2).

4.3 Investigation cyclic softening issues in force-based fiber models

As discussed in the previous sections, the force-based elements with only one element per member give more accurate results. In chapter three, analysis has shown that the localization issue affects the post-peak response of both force-based and displacement-based elements. The column taken as a case study to investigate the localization issue is a circular cantilever bridge column tested by Lehman et al. (2000). Detail of the specimen found in Appendix A.3. Therefore, this section presents a parametric study on the localization issues in force-based models.

4.3.1 Cyclic analysis using DFB (softening)

The column under investigation failed by buckling and rapture of bar at cyclic displacement of 127 mm. At this drift level, the cyclic behavior lost strength suddenly. Figure 4-8 shows the maximum curvature for each integration section along the height of the column using distributed based fiber models. It is seen that the curvature does not converge to the same result as the integration sections increase. It should be noted that the curvature distribution is not the actual distribution; instead, it is the maximum curvature at the integration section and uses straight-line to connect the points for illustration purposes.

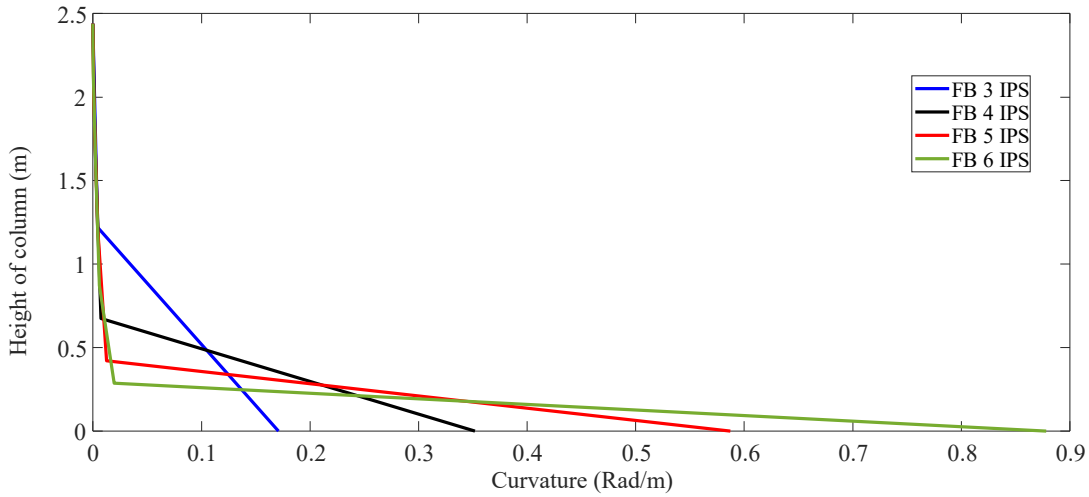

Figure 4-8 Softening curvature distribution using DFB (Specimen 415).

Localization issues affect the cyclic global response, as seen in Figure 4-9. For different integration points, the cyclic response exhibited different drift capacity. The column under investigation experienced crashing of concrete at a displacement of 38.1 mm, and buckling and rupture of longitudinal bar at a displacement of 127 mm and 178 mm, respectively. To investigate that localization is caused by the increment of cyclic displacement, the column analyzed using only cyclic displacement before the onset of concrete crushing. The response is objective at both global and local levels, as shown in Figure 4-10.

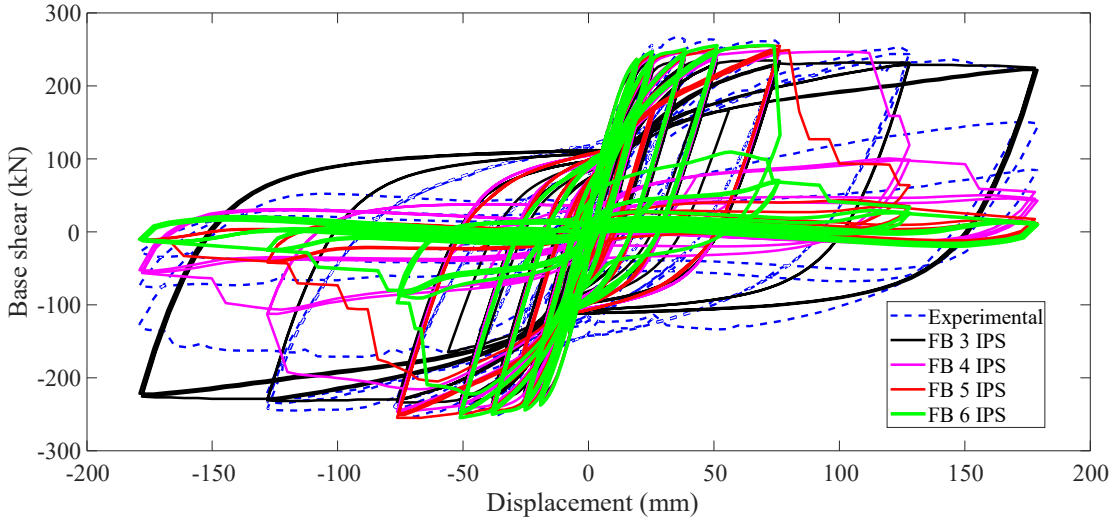

Figure 4-9 Softening hysteresis response using DFB (Specimen 415).

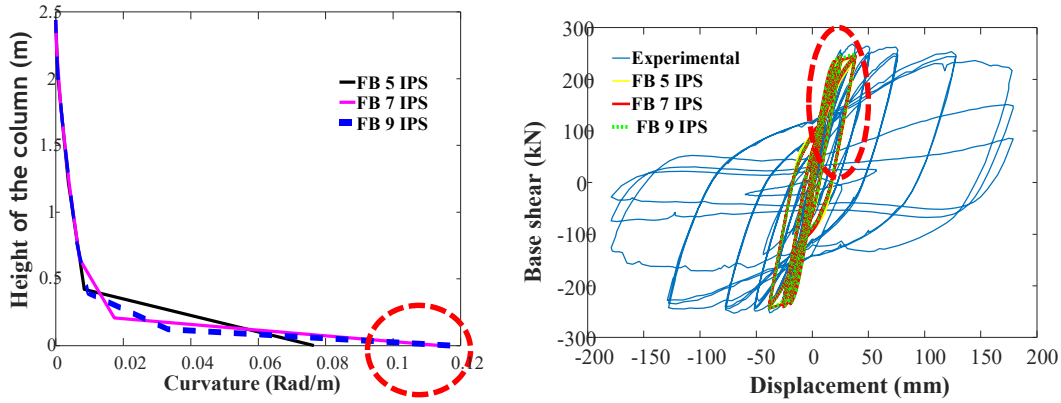

Figure 4-10 Hardening hysteresis response using DFB before softening (Specimen 415).

4.3.2 Cyclic analysis using BeamWithhinge (softening)

The modified Gauss-Radau method automatically overcomes the mesh dependent response, as shown in Figure 4-11. The localization issue affects the Radau-Two integration method. The midpoint integration method yields a higher capacity because the midpoint does not take integration point at the end, where a higher bending moment is expected to occur.

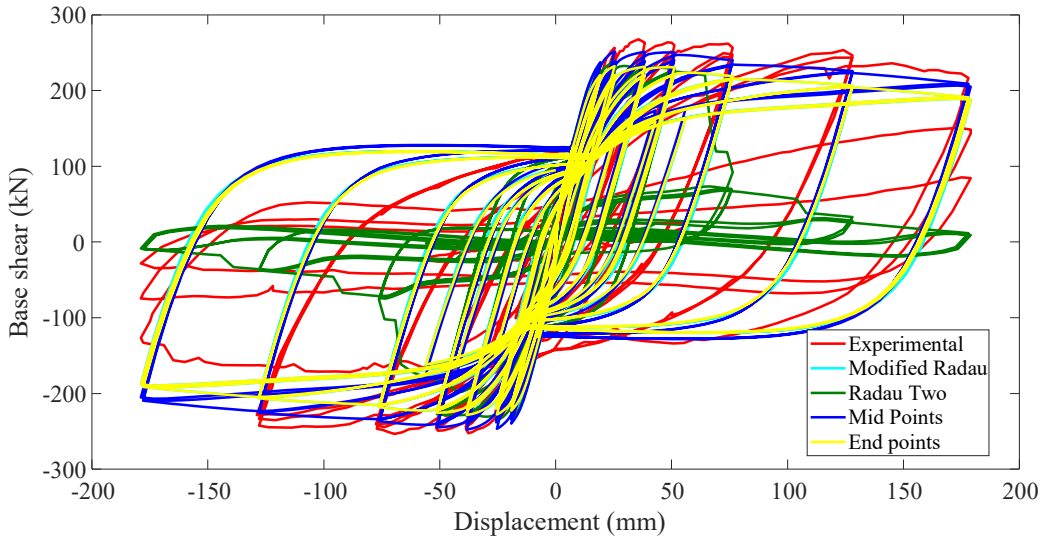

Figure 4-11 Softening hysteresis response Beamwithhinge models (Specimen 415).

4.3.3 Regularization of global force deformation response

In chapter three, the regularization techniques based on the constant energy exhibited good performance in overcoming mesh dependent response. This section applies the same procedure of material regularization, as in chapter three. The maximum crushing strain for concrete and tensile strain for steel summarized in Table 4-1.

Table 4-1 Regularized strain of the unconfined and confined concrete, ultimate rupture strain and strain hardening reinforcement steel Lehman et al. 2000,Specimun 415 .

$No\ IPs$	L_p	ε_{20c}	ε_{20cc}	ε_u''	b_s
3	406.4	0.0095	0.0114	0.0462	0.0192
5	121.9	0.0287	0.0343	0.148	0.006
7	81.28	0.0588	0.0703	0.301	0.003

The analysis carried out by using three cases of regularization strategies: only concrete, only steel, and both steel and concrete materials. For the case study column, the analysis indicates that applying regularization only to the concrete material yields mesh dependent response, as shown in Figure 4-12.

Furthermore, the specimen analyzed by applying material regularization only to steel material. As shown in Figure 4-14, the response converges better because the specimen failure is governed by buckling and rapture of the longitudinal bar, which depends on the maximum strain value of steel materials. It should be noted that even though applying regularization to steel material showed a good performance in capturing the cyclic envelope, but the response exhibited a slight mesh dependent result at the drift level of 3.13% (displacement of 76.3 mm).

Finally, which is indeed the best way for modeling members exhibiting softening response, is based on applying regularization for both material (Pugh 2012). The cyclic response simulated using this technique showed an objective response, as shown in Figure 3-14. In this case, the yield drift, maximum strength, and ultimate drift capacity predicted accurately without loss of objectivity

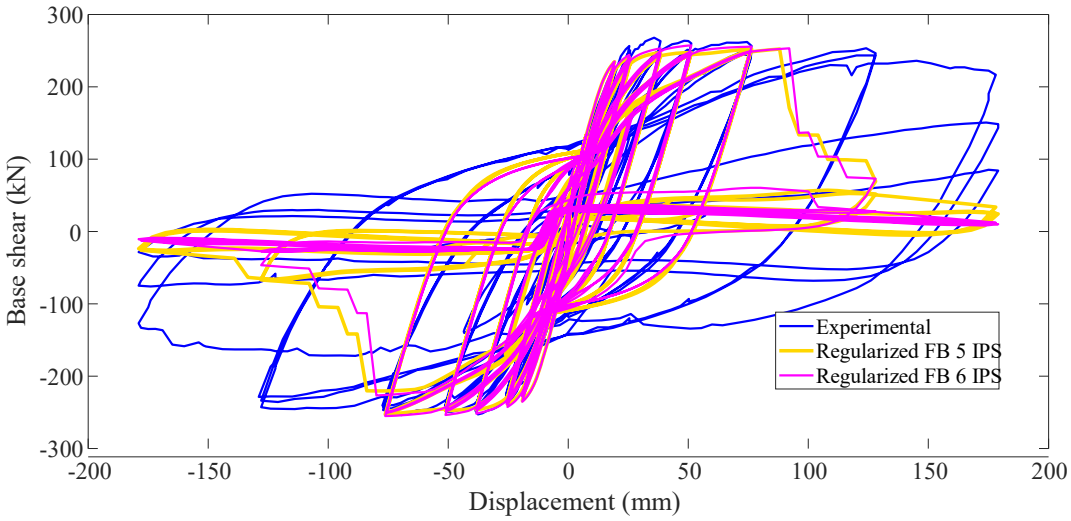

Figure 4-12 Hysteresis response using DFB applying regularization only to the concrete material (Specimen 415).

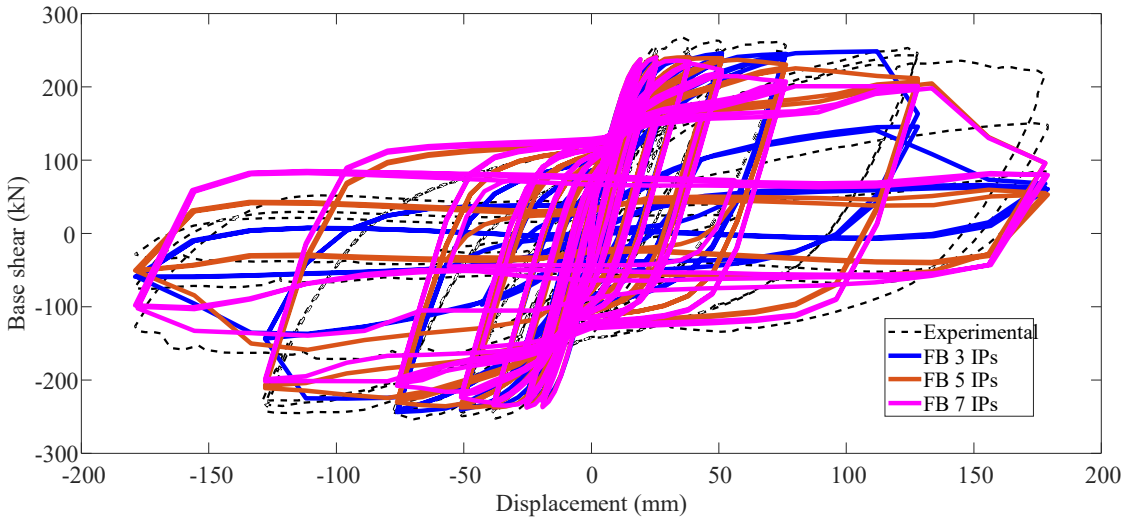

Figure 4-13 Hysteresis response using DFB applying regularization only to the steel material (Specimen 415).

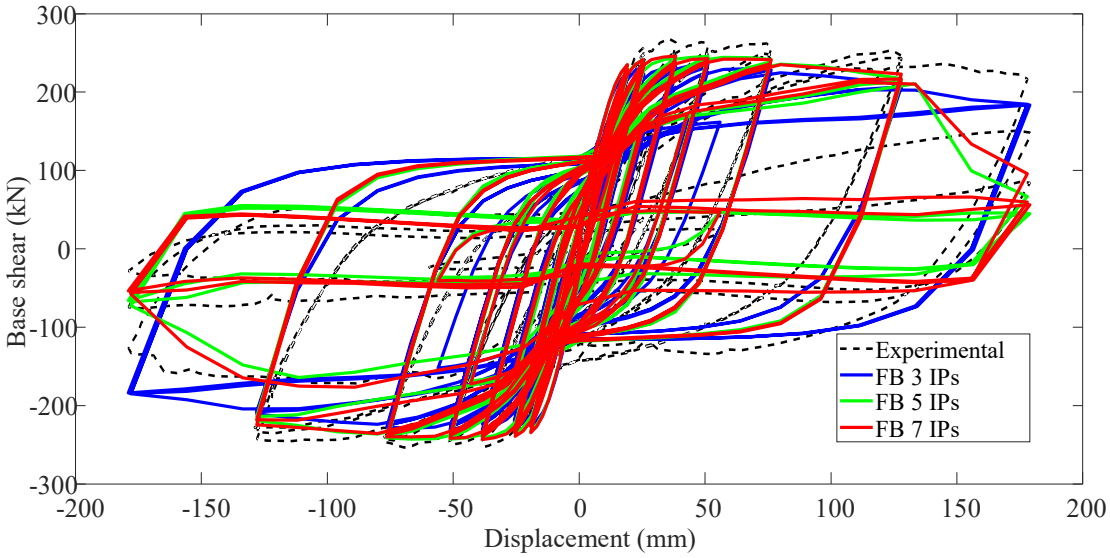

Figure 4-14 hysteresis response using DFB applying regularization to concrete and steel material (Specimen 415).

5 Nonlinear response of RC frame using different nonlinear models

5.1 Introduction

This section evaluates the performance of the numerical inelastic models in simulating the inelastic response of reinforced concrete frame structure using the OpenSees finite element software. In the previous sections, the numerical nonlinear models were evaluated by taking a bridge column as a case study. Localization issues and regularization techniques to address localization issues were discussed briefly. In the previous chapters, the lumped plasticity with zero-hinge length was observed to have several limitations compared to the other models; hence, the model will not be presented in this chapter.

5.2 Nonlinear analysis of two-story RC frame

A one-span, two-story, flexure-critical reinforced concrete frame that had been tested by Vecchio and Emara (1992) was taken as the first case study to evaluate the model's performance under monotonic loading. The frame has a story height of 2000 mm with an overall height of 4600 mm and center-to-center distance of 3500 mm as shown in Figure 5-1. The cross-sectional dimension of the beams and columns are 300 mm wide and 400 mm deep, while the base was 800 mm wide and 400 mm deep. To create an essentially fixed foundation The frame was built integral with a large, heavily reinforced concrete base. Cylinder tests and steel coupons were used to determine the concrete and steel materials properties respectively and are summarized in Table 5-1.

Table 5-1 Matrial properties of the two sory frame, Vecchio and Emara (1992)

	Reinforcement								Concrete				
	A_s (mm^2)	d_b (mm)	f_y (MPa)	f_u (MPa)	E_s (MPa)	E_{sh} (MPa)	ε_{sh} ($x10^{-3}$)	ε_u ($x10^{-3}$)	f'_c (MPa)	ε_0 ($x10^{-3}$)	E_c (MPa)	G_c (MPa)	μ
No.20	300	19.5	418	596	192500	3100	9.5	66.9	30	1.85	23674	9864*	0.2*
No.10	100	11.3	454	640	200000*	3100*	9.5*	69.5					

* estimated

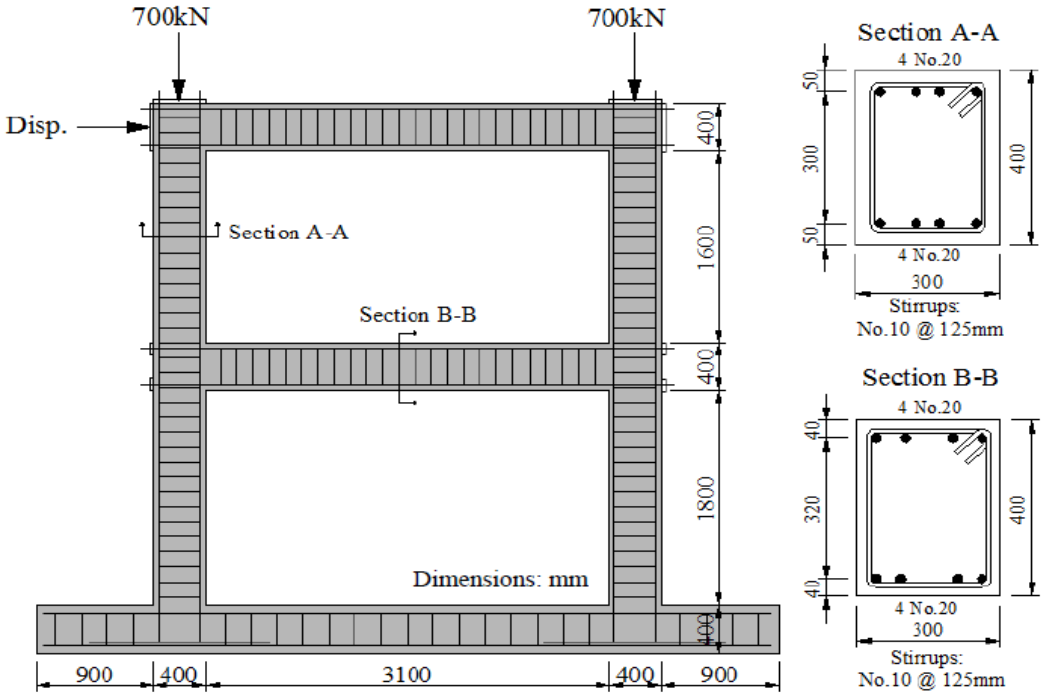

Figure 5-1 Details of Vecchio and Emara Frame

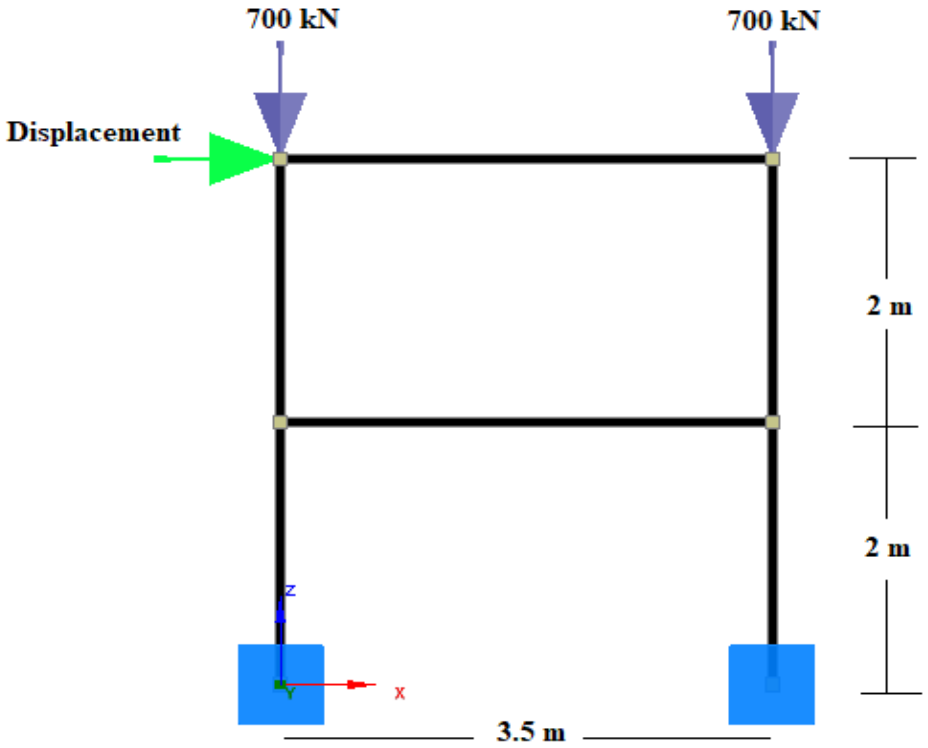

Figure 5-2 Model of the two-story RC specimen.

The loading strategies were done first by applying a constant axial load of 700 kN in the downward direction through the force control loading and the monotonic lateral load is applied through the displacement control, as shown in Figure 5-2. The pushover response obtained using distributed and concentrated fiber models compared with the experimental response, as shown in Figure 5-3. The maximum base shear determined from the experimental test is 332 kN. When equal displacement-based fiber models with 4 elements per member used, the base share is 402.2 kN; however, when the first element of the members assumed as 15% of the member's length, the base share is 368.2 kN, which is fairly accurate result. The distributed and concentrated force-based fiber models with only one element per member accurately captured the experimental result. The ultimate base shear obtained using distributed and concentrated force-based fiber models is 322.75 kN and 321.08 kN, respectively.

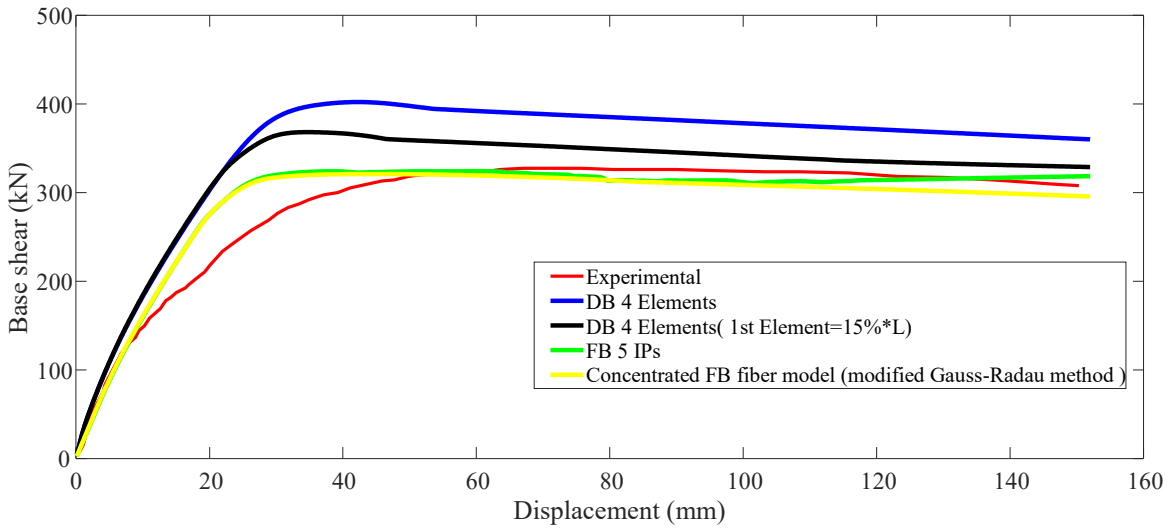

Figure 5-3 Comparison of the numerical model for the two-story RC frame.

5.2.1 Localization issues and regularization in RC frame

In the previous sections, a mesh refinement study for the different numerical models carried out using a cantilever bridge column. Furthermore, for section exhibiting softening behavior regularization techniques discussed briefly, and applied to a cantilever bridge RC columns. This section extends the concepts to a two-story RC frame. As seen in Figure 5-3, the distributed force-based model provides a more accurate result compared to the distributed displacement-based and concentrated fiber hinge models.

This section briefly discusses the performance of distributed force-based fiber models, under strain-hardening, and strain-softening behavior. As seen in Figure 5-4, as the number of integration points increases, the response converges to the same result. To simulate softening behavior the axial load has been increased up to 1400 KN, which is two times the original axial load.

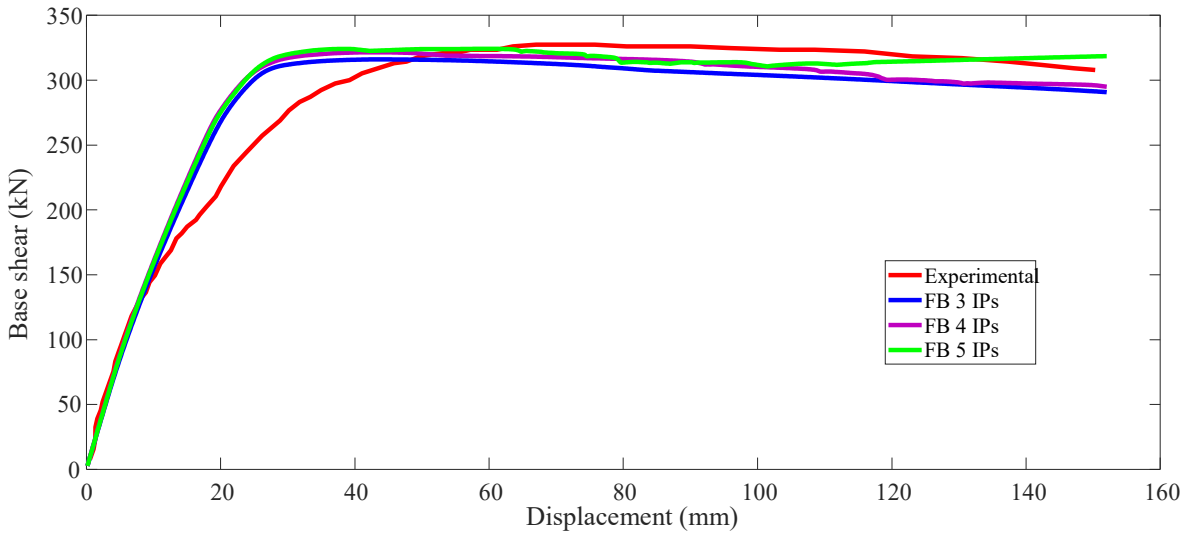

Figure 5-4 Comparison of the numerical model for the two-story RC frame

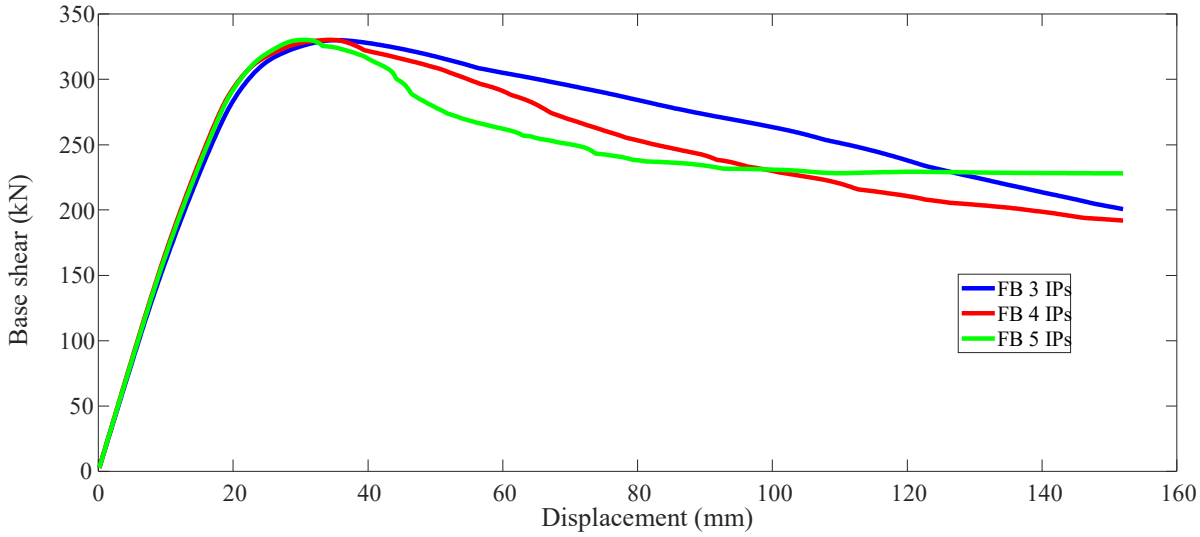

Figure 5-5 Comparison of the numerical model for the two-story RC frame (softening)

The force-deformation response using the DFB model for the RC frame subjected to an increased axial load is mesh dependent response, as shown in Figure 5-5. As the integration points increase, the response localizes over a single integration point and produces a non-objective response. In chapter three and chapter four, to overcome mesh dependent results, material regularization for both concrete and steel was suggested. To the best of the author's knowledge, the existing regularization techniques are for the RC cantilever column and walls. Therefore it essential to apply these techniques to full RC frame structures. The regularized material strain for the columns and beams summarized in Table 5-2. Figure 5-6 shows that the regularized response of the two-story frame is mesh-independent; thus, the existing material regularization successfully addresses the softening issues in the two-story RC frame.

Table 5-2 Regularized strain of the unconfined and confined concrete, ultimate rupture strain and strain hardening for steel, two-story RC frame, (Vecchio and Emara 1992)

Regularized material for columns					
$No\ IPs$	L_p	ε_{20c}	ε_{20cc}	ε_u''	b_s
3	333.3	0.0113	0.0171	0.0557	0.0166
4	166.7	0.0213	0.0328	0.1093	0.0083
5	100	0.0346	0.0538	0.1807	0.005
Regularized material for beams					
$No\ IPs$	L_p	ε_{20c}	ε_{20cc}	ε_u''	b_s
3	583.33	0.007	0.0104	0.0327	0.0297
4	291.66	0.0127	0.0194	0.0633	0.0145
5	175	0.0204	0.0313	0.1042	0.0087

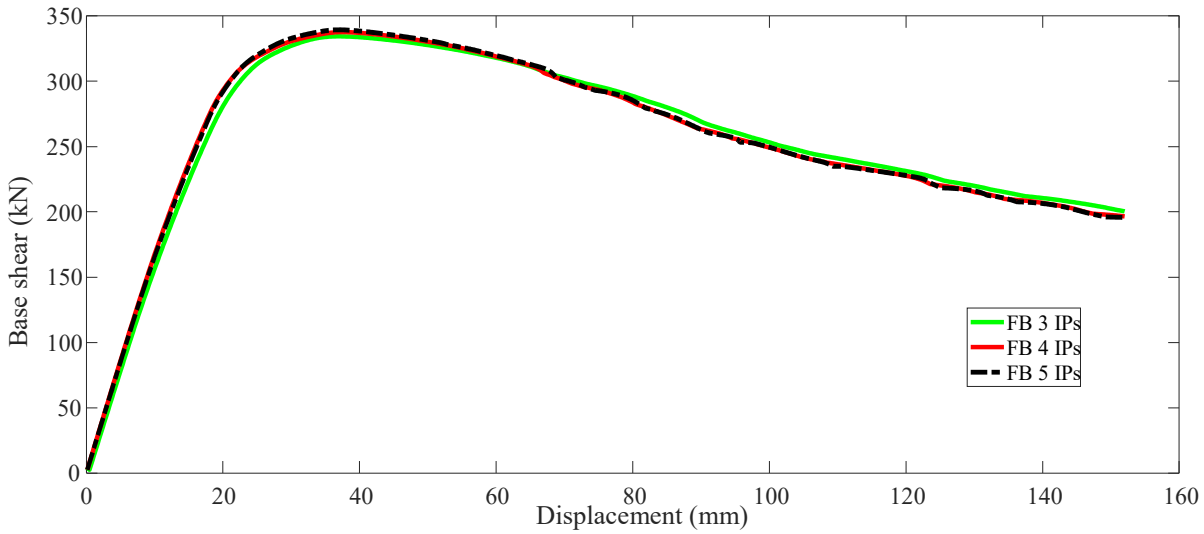

Figure 5-6 Regularized push over response for the two-story RC frame.

5.3 Nonlinear analysis of three-story RC frame

In this case, a three-story frame that tested under a pseudo-static test is investigated using different nonlinear numerical techniques. Pseudo-static collapse experiment of a three-story concrete frame structure shown in Figure 5-4b, which is sponsored by AERDP, ASC (Association of Earthquake Resistance and Disaster Prevention, Architectural Society of China), and honored excellent prize. The load pattern of the experiment is shown in Figure-5-7a, where the upper three stories are simplified into four concentrated loads applied downward by two vertical actuators and two load-distributing girders. Each actuator provides a 489 kN vertical load at the one-third point of the corresponding load-distributing girder. The dimensions and reinforcement details of the scaled model are presented in Figure 5-8.The properties of concrete and steel and steel materials summarized in Table 5-3 and Table 5-4, respectively.

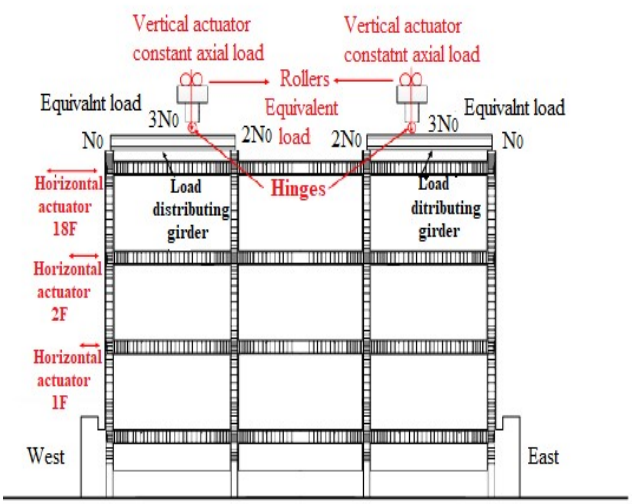

a

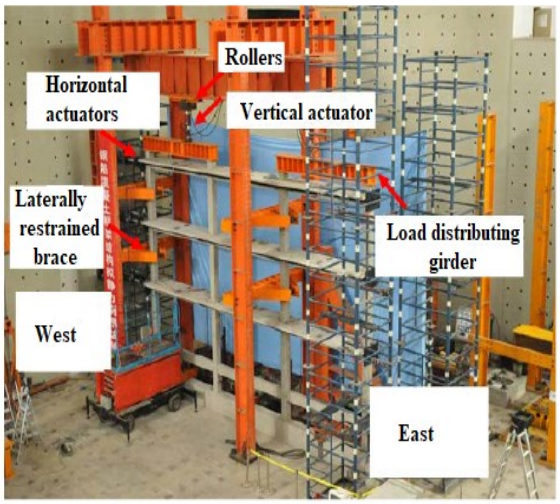

b

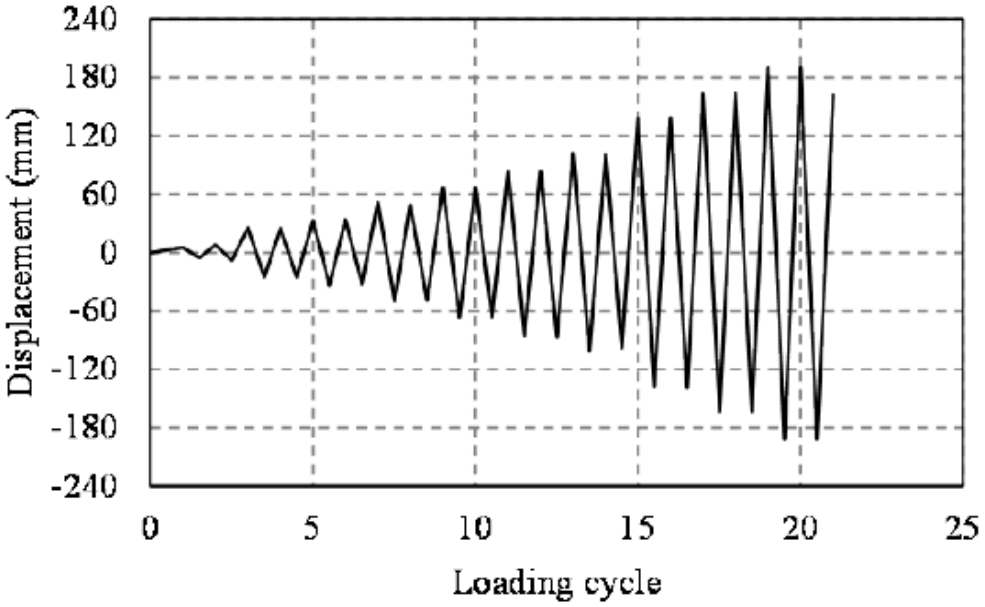

Figure 5-7 Test setup of the overall frame: (a) load pattern of the experiment, (b) experimental setup of the overall frame and (c) lateral loading protocol (Xie et al. 2015).

Table 5-3 Concrete compressive strength of the specimen.

Location	Foundation	Tie beam	1st story	2nd story	3rd story
$f_{cu,150mm}$(Mpa)	36.6	31.8	36.2	34.7	33.6

Table 5-4 Steel yield strength and fracture strain of the specimen.

Diameter(mm)	f_y (Mpa)	f_u (Mpa)	Fracture strain
10	481	745	23.6
8	582	855	28.8
6	441	592	34.2
4	390	414	26.7

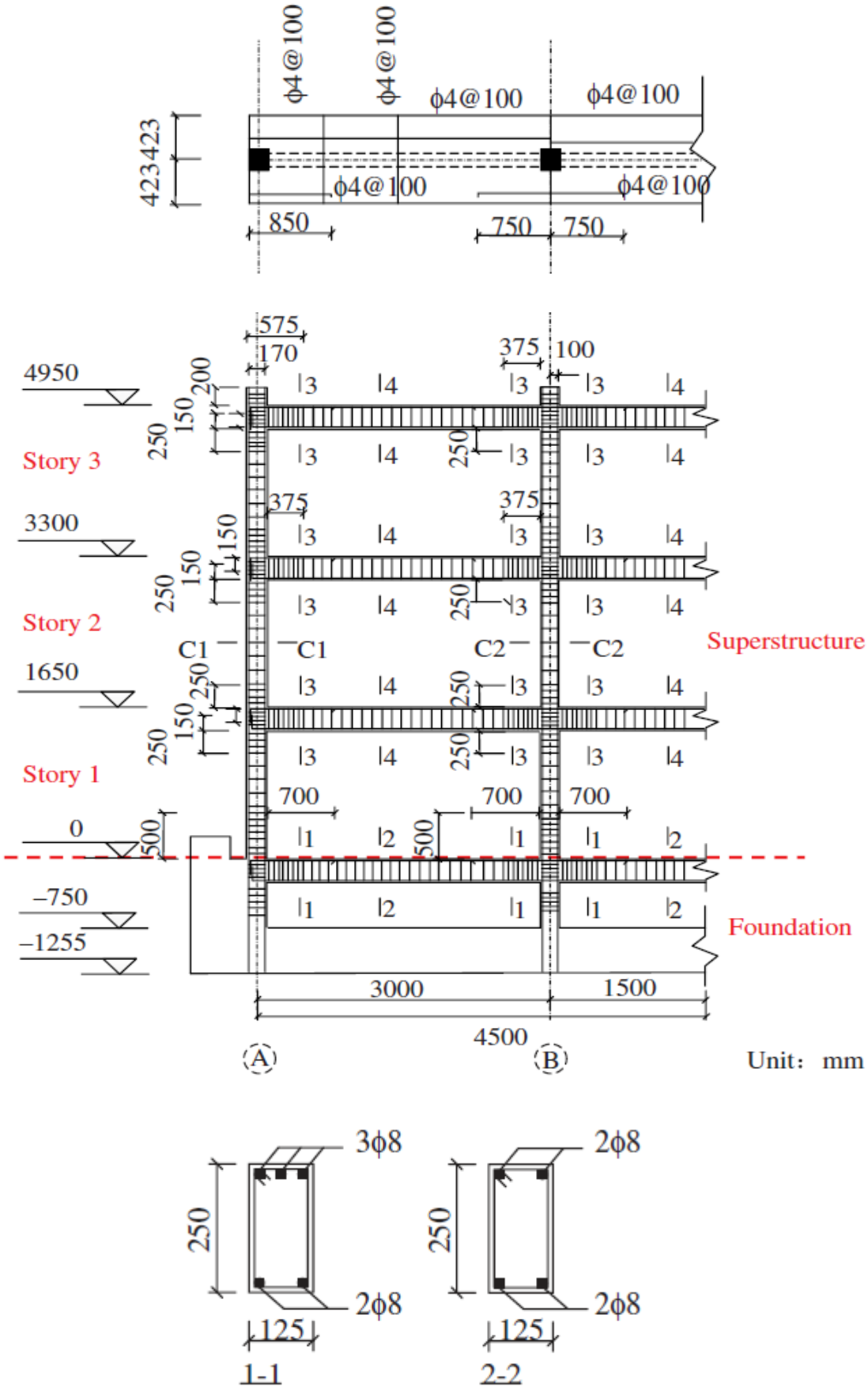
ϕ4@100
ϕ4@100
ϕ4@100
ϕ4@100
ϕ4@100
ϕ4@100
423423
850
750
750
575
170
375
100
4950
Story 3
3300
Story 2
1650
Story 1
0
–750
–1255
C1
C2
Superstructure
Foundation
700
500
3000
1500
4500
A
B
Unit: mm
3ϕ8
2ϕ8
250
125
1-1
2ϕ8
2ϕ8
250
125
2-2

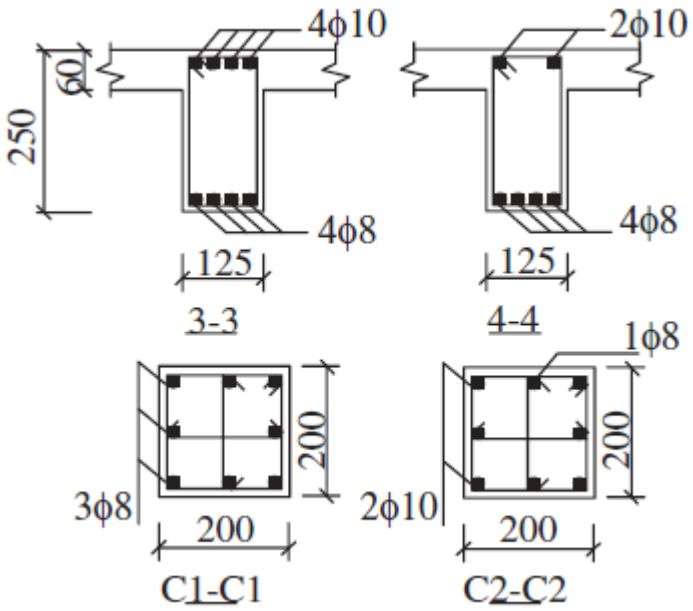

Figure 5-8 Dimensions and reinforcement details of the scaled frame: (a) frame, (b) beams-columns (Xie et al. 2015).

Table 5-5 Reinforcement detailing of the middle and side columns.

Columns	Story	Bottom stirrups	middle stirrups	Top stirrups
C1	1	ϕ6@70 (500 mm)	ϕ6@140 (825 mm)	ϕ6@70 (325 mm)
	2	ϕ4@50 (375 mm)	ϕ4@100 (900 mm)	ϕ4@50 (375 mm)
	3	ϕ4@50 (375 mm)	ϕ4@100 (900 mm)	ϕ4@50 (375 mm)
C2	1	ϕ6@70 (500 mm)	ϕ6@140 825 mm)	ϕ6@70 (325 mm)
	2	ϕ6@70 (375 mm)	ϕ6@140 (900 mm)	ϕ6@70 (375 mm)
	3	ϕ6@70 (375 mm)	ϕ6@140 (900 mm)	ϕ6@70 (375 mm)

5.3.1 Test observations and analysis of the experimental data

For the overall frame test when the displacement of the top floor reached 33 mm diagonal cracks were observed as shown in Figure 5-9 (point A). Furthermore as the displacement of the top floor reached 84 mm, concrete crushing was observed at the bottom of the side and middle columns, and concrete peeling at the joints as shown in Figure 5-9 (point B). When the frame experienced displacement of the top floor reached 139 mm, severe concrete spelling was noticed on the cover layer at the bottom of Columns 1–3 as indicated in Figure 5-9 (point C). Finally, when the peak displacement of the top floor reached 190 mm, a large vertical deformation and completely crushing of concrete at the bottom of Columns 1–3 was observed as shown in Figure 5-9 (point D). At this stage, the vertical loads applied to the top floor could no longer be maintained (Xie et al. 2015).

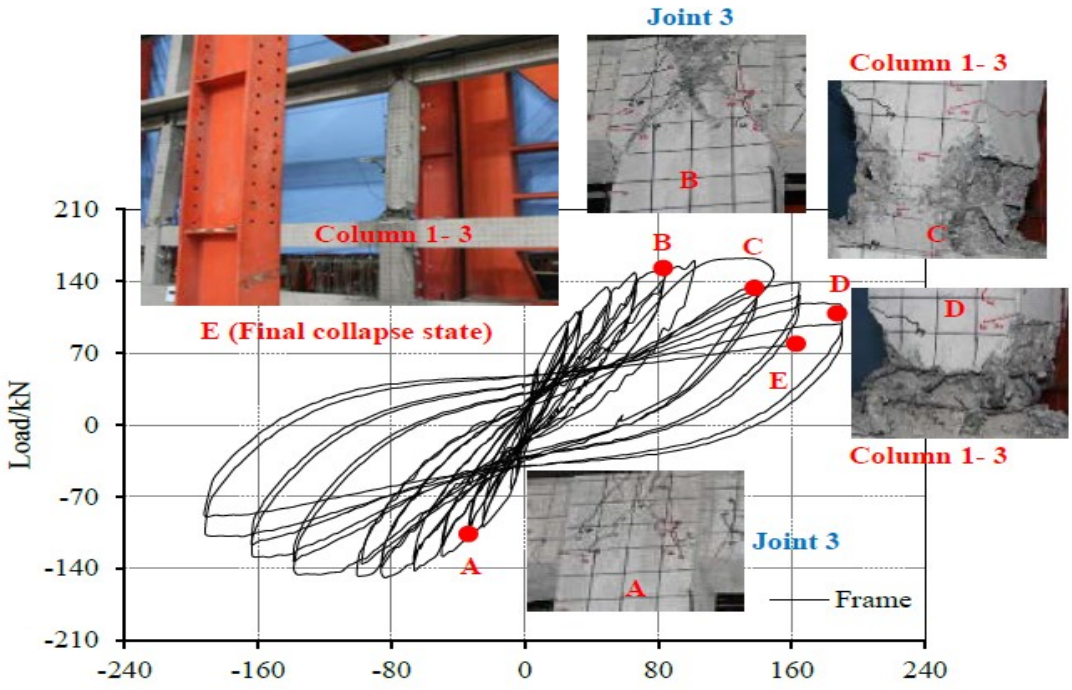

Figure 5-9 Damage observed in the tests and hysteresis response of the frame structure (Xie et al. 2015).

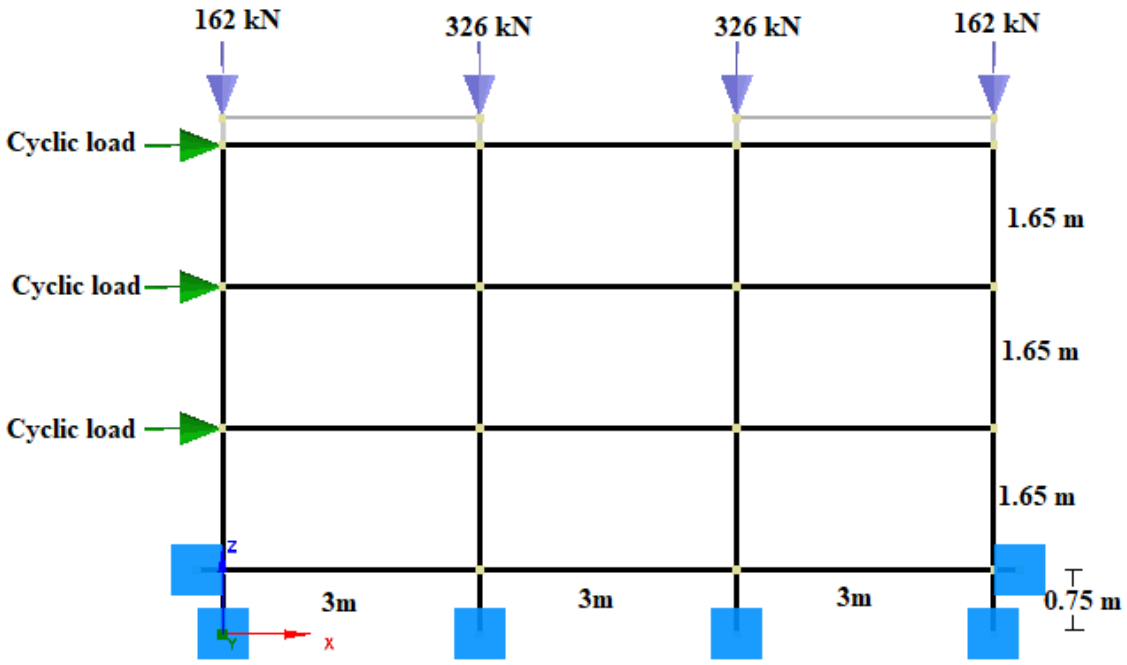

Figure 5-10 Model of the three-story RC specimen.

5.4 Numerical modeling of the three-story frame

This section presents comparison of the models in simulation cyclic and monotonic behavior of three-story RC frame. The loading strategies were done first by applying a constant axial load of 163 kN and 326 kN in the downward direction through the force control loading to the external and internal columns, respectively. The cyclic lateral load is applied through the displacement control, as shown in Figure 5-10. Pushover analysis and cyclic analysis is carried out to further asses the performance of the models in predicting the response of experimentally tested three-story reinforced concrete frames. The target displacement for pushover analysis taken as the maximum top displacement experienced during the cyclic test. The structure pushed up to 189 mm top displacement using displacement load control, which is the maximum displacement the frame experienced during the pseudo cyclic test. As sown in Figure 5-11, the distributed force-based model with one element per member accurately captures the pushover and cyclic responses. Pushover response for different integration sections have shown convergence of global response, as shown in Figure 5-11a. As seen in Figure 5-12, the displacement-based model with 4 elements per member somewhat overestimates the capacity for both monotonic and cyclic loading. The concentrated force-based fiber model underestimates the capacity, but the model capable of yielding satisfactory results, as shown in Figure 5-

13. The advantage of these models comes to picture for structures exhibiting softening responses. The accuracy of the nonlinear models in predicting the ultimate base shear is summarized in Table 5-6.

Table 5-6 Comparison of ultimate base shear obtained using the nonlinear models

Response	Experimental	DFB using one element with 4 IPs	DDB using 4 elements with 2 IPs	Force-base concentrated plasticity
Ultimate base shear (kN)	162.5	154.5	188.9	152.1
Error (%)		4.92	16.24	6.4

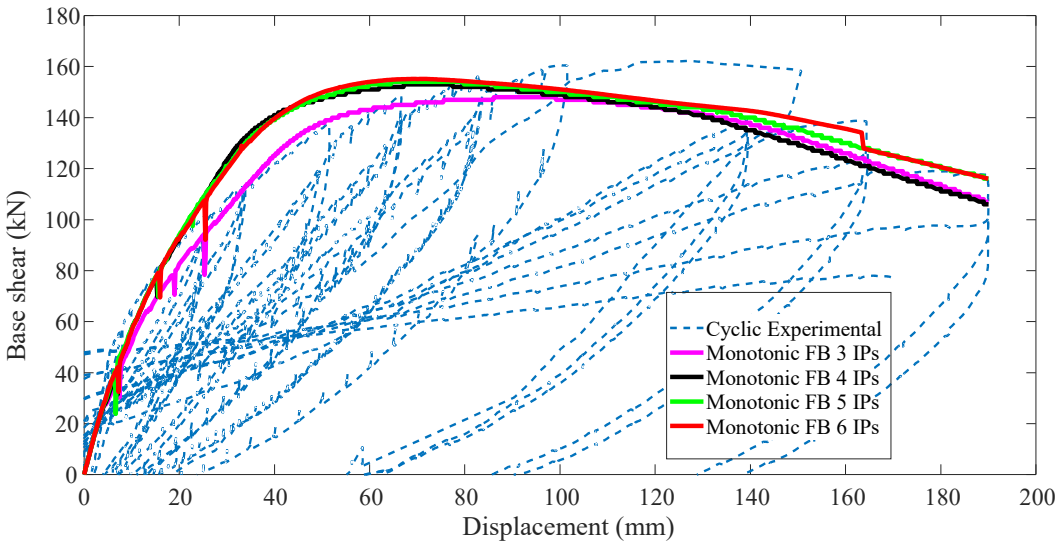

(a)

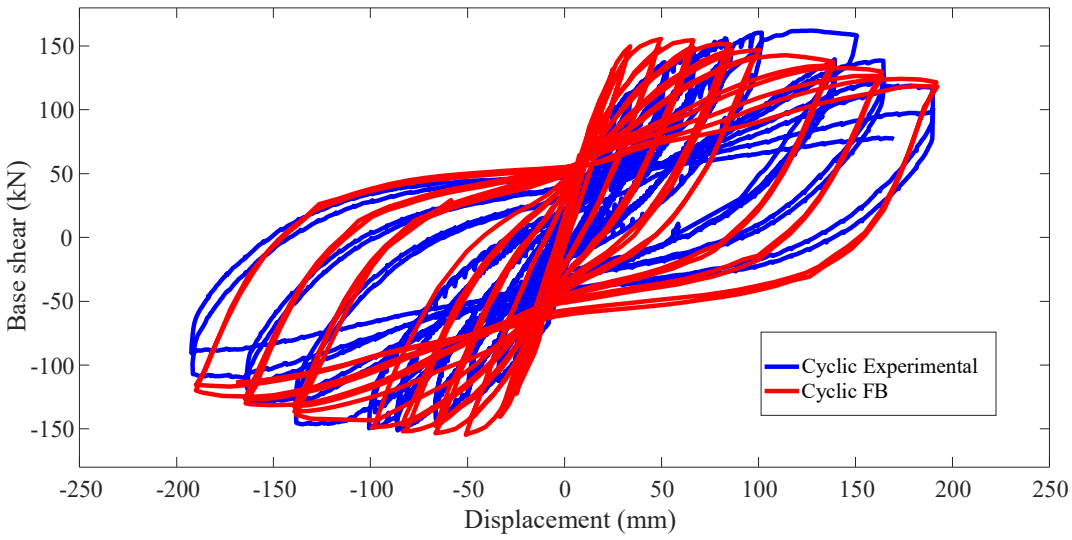

(b)

Figure 5-11 Monotonic and cyclic response of the frame using DFB models **.**

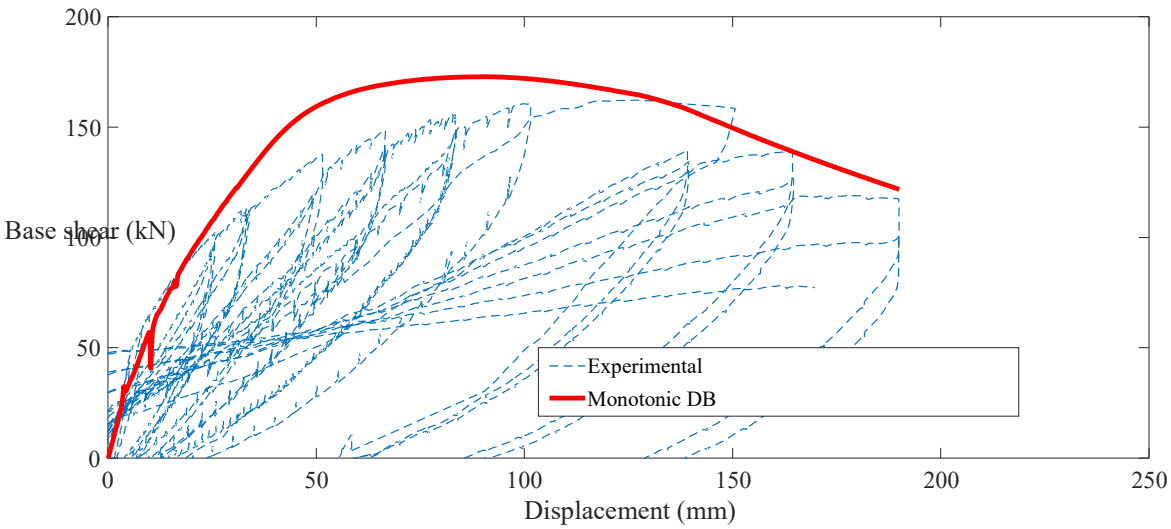

(a)

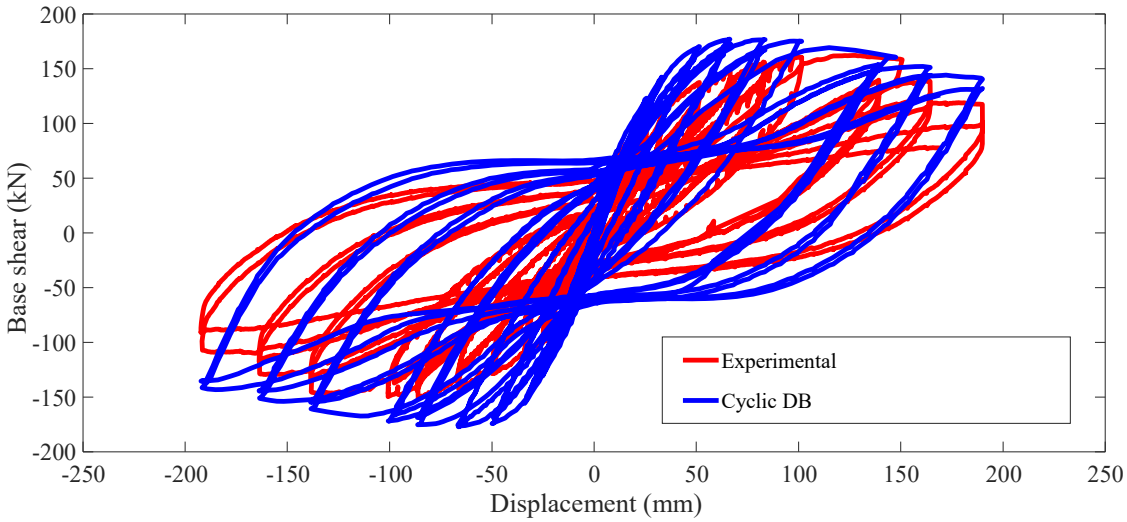

(b)

Figure 5-12 Monotonic and cyclic response using 4 DDB element.

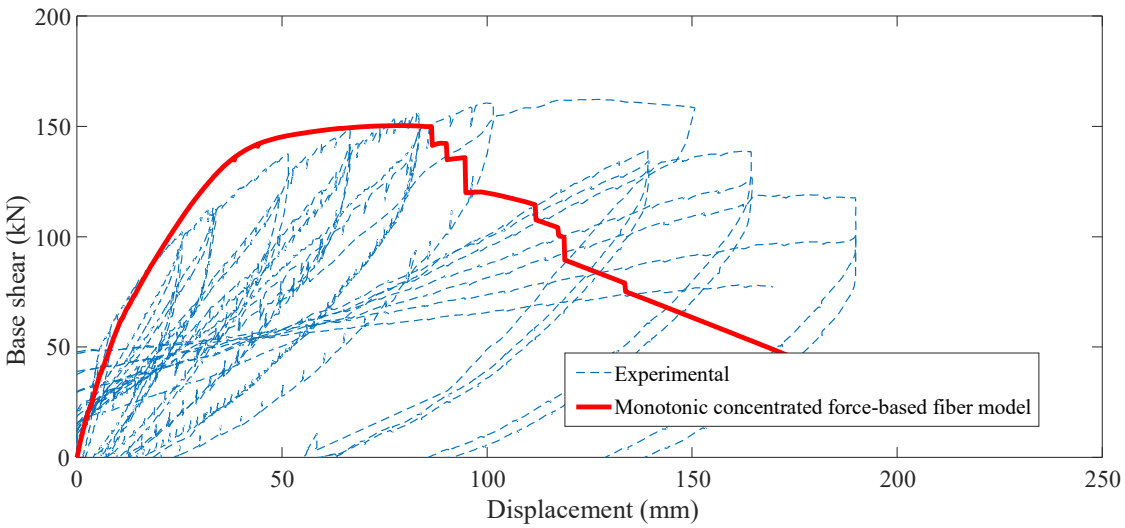

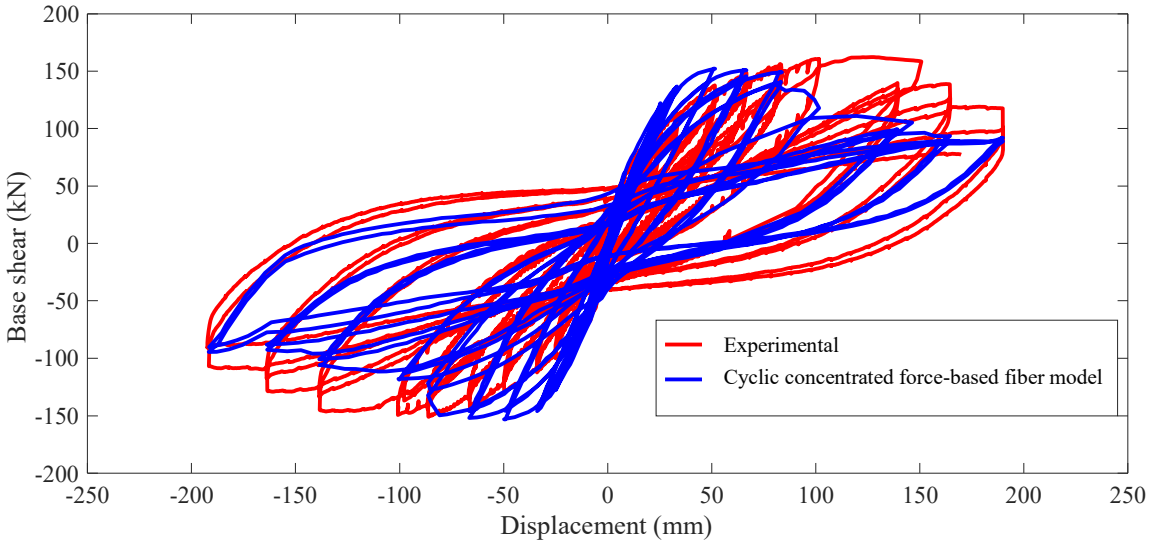

Figure 5-13 Monotonic and cyclic response using concentrated force-based (BeamWithHinges) fiber models.

6 CONCLUSIONS AND RECCOMENDATIONS

6.1 Conclusions

The thesis aims to evaluate the performance of the numerical nonlinear models used in earthquake engineering. Experimentally tested cantilever columns and reinforced concrete frames were taken as case studies. For section exhibiting strain-softening and strain-hardening behavior, the study comes up with these following conclusions.

- For strain-hardening behavior, the distributed force-based fiber models with one element per member provides accurate response of beam-column members. The distributed displacement-based fiber models require several elements per member to capture the actual global response of beam-column members; however, the local moment-curvature response does not converge to the same solution with an increase in mesh refinement. The force-based plastic hinge methods (BeamWithHinges) accurately predict the inelastic response of beam-column members. The Lumped plasticity with zero-length hinge models captures the initial stiffness well, but the models fail to predict cracking, the onset of yielding and underestimate the maximum base shear.
- For sections exhibiting softening behavior, both distributed force-based and displacement-based fiber models produce nonobjective responses at the global and local levels. Of the four force-based plastic hinge (BeamWithHinges) methods, the inelastic response obtained using the Gauss-Radau-Two integration method is nonobjective or mesh dependent results at global and local levels. However, the force-base plastic hinge (BeamWithHinges) based on the modified Gauss-Radau method successfully overcome the localization issue.
- Material regularization based on the constant energy successfully tackle the localization in the distributed fiber beam-column models. Comparison of partial and full material regularization shows that if the strain-softening behavior results from both fiber materials, regularization for both steel and concrete materials is required. The study identified two types of localization in the fiber section: linear softening and sudden loss of strength, which resulted from the concrete softening and steel localization, respectively.

- For the distributed displacement-based elements, the suggested crushing energy values by Pugh (2012) for slender concrete wall was found to overcome mesh dependent result for cantilever bridge column too.
- From the nonlinear analysis of the multistory RC frames, the distributed force-based fiber models have shown to be very accurate and efficient. The displacement-based fiber models with four elements per member overestimate the real capacity; however, when the first element of the members assumed as 15% of the member's length best level of accuracy was achieved. The force-based plastic hinge (BeamWithHinges) based on the modified Gauss-Radau method yields a comparable result with the distributed force-based fiber models in terms of maximum base shear capacity; however, for the three-story RC frame, the post-peak response showed high softening.

6.2 Suggested nonlinear beam-column models

Finally, before going directly to the nonlinear analysis, it is suggested that the analysts should understand the strength and weaknesses of the models.

6.2.1 For section exhibiting strain-hardening behavior

- For section showing strain-hardening behavior, the distributed plasticity models have proven to be more accurate and efficient in describing the inelastic behavior of beam-column members. There are two-element formulations in distributed plasticity: force-based and displacement-based. The detailed analysis shows the distributed force-based models with a single element and 5 IPs or above yields an accurate response. However, the distributed displacement-based models with several elements per member are required to capture the inelastic response of beam-column members.

6.2.2 For section exhibiting strain-softening behavior

- For section showing strain-softening behavior, the distributed plasticity models have proven to be affected by localization issues. Therefore, the models require material regularization for both steel and concrete. If material regularization seems to be complicated, especially in multi-story structures, the force-base plastic hinge (BeamWithHinges) based on the modified Gauss-Radau method is the best choice.

6.3 Recommendations for future works

Due to restrictions in the time of the master's program, the study suggests the following important topics for future work.

- The study confirmed that material regularizations overcome localization issues; however, for strain-hardening behavior, Pugh (2012) has shown that material regularization affects the drift capacity of the members. Furthermore, this study indicates that both materials have different softening characteristics. Therefore, the study suggests further investigation for the three cases, when to apply material regularization: (1) only to concrete (2) only to steel and (3) to both materials. This helps the analyst to make decisions on when regularization is required.
- The study focuses on structures in which their failure governed by flexure; therefore, the work requires further investigation on extending the models to include nonlinear shear effects and shear-flexural interaction.

References

Addessi, D., and Ciampi, V. (2007). "A regularized force-based beam element with a damage-plastic section constitutive law." *International Journal For Numerical Methods In Engineering*, 70(5), 610–629.

Alfarah, B. (2017). "Advanced computationally efficient modeling of RC structures nonlinear cyclic behavior." PHD Thesis, University of Barcelona.

Applied Technology Council (ATC). (2005). "Improvement of nonlinear static seismic analysis procedures." *FEMA 440*, prepared by the Applied Technology Council for the Federal Emergency Management Agency, Redwood City, California.

Ashtari, S. (2018). "Evaluating the performance-based seismic design of RC bridges according to the 2014 Canadian highway bridge design code." PHD thesis, University of British Columbia.

Bazant, Z. p, Belytschko, T. B., and Chang, T. (1984). "Continuum Theory for Strain-Softening." *Journal of Engineering Mechanics*, 110(12), 1666–1692.

Bazant, Z. p, Pan, J., and Pajaudier-Cabot, G. (1987). "Softening in reinforced concrete beams and frames." *Journal of Structural Engineering*, 113(12), 2333–2347.

Berry, M., and Eberhard, M. (2008). "Performance modeling strategies for modern reinforced concrete bridge columns." *PEER Report 2007/07*, Pacific Earthquake Engineering Research Center, University of California, Berkeley.

Berry, M., Parrish, M., Eberhard, M. (2004). "PEER structural performance database user's manual." *PEER user's manual*, 2004(01).

Calabrese, A., Almeida, J. P., and Pinho, R. (2010). "Numerical issues in distributed inelasticity modeling of RC frame elements for seismic analysis." *Journal of Earthquake Engineering*, 14(S1), 38–68.

Calderone, A. J., Lehman, D. E., and Moehle, J. P. (2001). "Behavior of reinforced concrete bridge columns having varying aspect ratios and varying lengths of confinement." *PEER Report 2000/08*, Pacific Earthquake Engineering Research Center, University of California, Berkeley.

Clough, R. W., Benuska, K. ., and Wilson, E. (1965). "Inelastic earthquake response of tall buildings." *Proc., The 3rd World Conference on Earthquake Engineering*, Wellington, New Zealand.

Coleman, J., and Spacone, E. (2001). "Localization issues in force-based frame elements." *Journal of Structural Engineering*, 127(11), 1257–1265.

Correia, A. A., Almeida, J. P., and Pinho, R. (2008). "Force-based versus displacement-based formulations in the cyclic nonlinear analysis of RC frames." *Proc., The 14th World Conference on Earthquake Engineering*, Beijing, China.

Federal Emergency Management Agency (FEMA). (2000). "Prestandard and commentary for the seismic rehabilitation of buildings." *FEMA 356*, Washington, D. C.

Feng, D.-C., and Ren, X.-D. (2017). "Enriched force-based frame element with evolutionary plastic hinge." *Journal of Structural Engineering*, 143(10).

Filippou, F. C., and Fenves, G. L. (2004). "Methods of analysis for earthquake- resistant structures." *Earthquake engineering:From engineering seismology to performance-based engineering, Y. Bozorgnia and V. V. Bertero, eds,Chap. 6,* CRC, Boca Raton, Fla.

Filippou, F. C., and Issa, A. (1988). "Nonlinear analysis of reinforced concrete frames under cyclic load reversals." *EERC report 88-12*, Earthquake Engineering Research Center, Berkeley.

Fillippou, F. C., Popove, E. P., and Bertero, V. V. (1983). "Earthquake engineering research center effects of bond deterioration on hysteretic behavior report to the national science foundation." *EERC Report 83-19*, Earthquake Engineering Research Center, Berkeley.

Fragiadakis, M., and Papadrakakis, M. (2008). "Modeling , analysis and reliability of seismically excited structures." *International Journal of Computational Methods*, 5(4), 483–511.

Gharakhanloo, A. (2014). "Distributed and concentrated inelasticity beam-column elements used in earthquake engineering." Maters thesis, Norwegian University of Science and Technology.

Gilberson, M. F. (1967). "The response of non-linear multi-storey structures subjected to earthquake excitations." PhD thesis, California Institute of Technology, Pasadena, Calif.

Ibarra, L. F., Medina, R. A., and Krawinkler, H. (2005). "Hysteretic models that incorporate strength and stiffness deterioration." *Earthquake engineering and structural dynamics*, 34(12), 1489–1511.

Jansen, D. C., and Shah, S. P. (1997). "Effect of length on compressive strain softening of concrete." *Journal of Engineering Mechanics*, 123(1), 25–35.

Kaba, S. A., and Mahin, S. A. (1984). "Refined modelling of reinforced concrete columns." *EERC Report 84-03*, Eearthquake Engineering Research Center, California, Berkeley.

Kent, D., and Park, R. (1971). "Flexural members with confined concrete." *Journal of the Structural Division Proc. of the American Society of Civil Engineers*, 97(7), 1969–1990.

Kostic, S. M., and Deretic-Stojanovic, B. (2016). "Fiber element formulation for inelastic frame analysis." *Building Materials And Structures*, 59(2), 3–13.

Kunnath, S. K., El-Bahy, A., Taylor, A., and Stone, W. (1997). "Cumulative seismic Damage of reinforced concrete bridge piers,." *Technical Report NCEER-97-0006*, National Center for Earthquake Engineering Research, Gaithersburg.

Lai, S. S., Will, G. T., and Otani, S. (1984). "Model for inelastic biaxial bending of concrete members." *Journal of Structural Engineering*, 110(11), 2563–2584.

Lehman, D. E., and Moehle, J. P. (2000). "Seismic performance of well-confined concrete bridge columns seismic performance of well-confined concrete bridge columns." *PEER Report 1998/01*, Pacific Earthquake Engineering Research Center, University of California, Berkeley.

Mander, J. B., Priestley, M. J. N., and Park, R. (1988). "Theoretical stress-strain model for confined concrete." *Journal of Structural Engineering*, 114(8), 1804–1826.

McKenna, F., Fenves, G. L., Scott, M. H., and Jeremić, B. (2000). "Open system for earthquake engineering simulation <http://opensees.berkeley.edu >(May 2019).

Marini, A., and Spacone, E. (2006). "Analysis of reinforced concrete elements including shear effects." *ACI Structural Journal*, 103(5), 645–655.

Martlnez-rueda, E. J., and Elnashai, A. S. (1997). "Confined concrete model under cyclic load." *Materials and Structures*, 30, 139–147.

Menegotto, M., and Pinto, E. P. (1973). "Method of analysis for cyclically loaded R . C . plane frames including changes in geometry and non-elastic behaviour of elements under combined normal force and bending." *Proc., IABSE Symposium on Resistance and Ultimate Deformability of Structures Acted on by Well Defined Repeated Loads*, Lisbon, 15-22.

Meyer, C., Roufaiel, M. S., and Arzoumanidis, S. G. (1983). "Analysis of damaged concrete frames for cyclic loads." *Engineering and Structural Dynamics*, 11, 207–228.

Neuenhofer, A., and Filippou, F. C. (1997). "Evaluation of nonlinear frame finite-element models." *Journal of Earthquake Engineering*, 123(7), 958–966.

NIST. (2010). "NEHRP seismic design technical brief No. 4: Nonlinear structural analysis for seismic design, A guide for practicing engineers." *NIST GCR 10-917-5*, prepared by the NEHRP Consultants Joint Venture, a partnership of the Applied Technology Council and the Consortium of Universities for Research in Earthquake Engineering for the National Institute of Standards and Technology, Gaithersburg, Maryland.

Paulay, T., and Priestley, M. J. N. (1992). *Seismic design of reinforced concrete and masonry buildings*, Wiley, New York.

Pugh, J. S. (2012). "Numerical simulation of walls and seismic design recommendations for walled buildings." PHD dissertation, University of Washington.

Roufaiel, M. S. L., and Meyer, C. (1987). "Analytical modeling of hysteretic behavior of R/C frames." *Journal of Structural Engineering*, 113(3), 429–444.

Seismosoft (2018) "SeismoStruct 2018 - A computer program for static and dynamic nonlinear analysis of framed structures," available from http://www.seismosoft.com.

Scott, M. H., and Fenves, G. L. (2006). "Plastic hinge integration methods for force-based beam–column elements." *Journal of Structural Engineering*, 132(2), 244–252.

Soleimani, D., Popov, E. P., and Bertero, V. V. (1979). "Nonlinear beam model for R/C frame analysis." *Seventh ASCE Conference on Electronic Computation*, St. Louis.

Spacone, E., Fillippou, F. C., and Taucer, F. F. (1996a). "Fibre beam–column model for non-linear analysis of r/c frames: part II. applications." *Earthquake Engineering & Structural Dynamics*, 25, 727–742.

Spacone, E., Fillippou, F. C., and Taucer, F. F. (1996b). "Fibre beam-column model for non-linear analysis of R/C frames: part II. formulation." *Earthquake engineering and structural dynamics*, 25(7), 711–726.

Takeda, T., Sozen, M., and Nielsen, N. (1970). "Reinforced concrete response to simulated earthquakes." *Journal of the Structural Division*, 96(12), 2553–2573.

Tanaka, H. (1990). "Effects of lateral confining reinforcement on the ductile behavior of reinforced concrete columns." Doctoral Dissertation, University of Canterbury, New Zealand.

Taucer, F. F., Spacone, E., and Filippou, F. C. (1991). "A fiber beam-column element for seismic response analysis of reinforced concrete." *Report No. UCB/EERC-91/17*, Earthquake Engineering Research Center, University of California, Berkekey.

Vecchio, F. J., and Emara, M. B. (1992). "Shear deformations in reinforced concrete frames." *ACI Structural Journal*, 89(1), 46–56.

Wong, Y., Paulay, T., and and Priestley, M. J. (1993). "Response of circular reinforced concrete columns to multi-directional seismic attack." *ACI Structural Journal*, 90(2), 180–191.

Zeris, C. A., and Mahin, S. A. (1988). "Analysis of reinforced concrete beam-columns under uniaxial excitation." *Journal of Structural Engineering*, 114(4), 804–820.

Zeris, C. A., and Mahin, S. A. (1991). "Behavior of reinforced concrete structures subjected to biaxial excitation." *Journal of Structural Engineering*, 117(9), 2657–2673.

Appendices

A. Properties of the test specimens

A.1 Specimen A2

Table A1 detail properties of specimen A2

Name:	Kunnath et al. 1997, A2
Type:	Spiral
Comments:	
Material Properties	
Concrete Strength:	29 (MPa)
Transverse Steel:	Yield Stress: 434 (MPa)
Longitudinal Steel:	Yield Stress: 448 (MPa) Strength: 690 (MPa)
Geometry	
Diameter:	305 (mm) Cross-Section: Circular
Length:	L-Inflection: 1,372 (mm) L-Measured: 1,372 (mm)
Test Configuration:	Cantilever
Loading	
Axial Load:	200 (kN)
P-D:	Shear provided
L-Bottom:	0
Longitudinal Reinforcement	
Diameter:	9.5 (mm)
Number of Bars:	21
Reinforcement Ratio:	0.0204
Transverse Reinforcement	
Diameter Spiral:	4 (mm)
Hoop Spacing, Sv:	19 (mm)
Cover to Center of Hoop Bar:	14.5 (mm)
Reinforcement Ratio:	0.94
Non-Dimensional Properties	
Span-to-Depth Ratio:	4.5
Axial Load Ratio:	0.094
Test Results	
Failure Type:	Flexure
Damage Observation:	Concrete Crushing: 0 (mm) Significant Concrete Spalling: 40 (mm) Long Bar Buckling: 68.3 (mm) Long Bar Fracture: 0 (mm) Spiral Fracture: 76.2 (mm) Loss of Axial Load Capacity: 0 (mm)

A.2 Specimen No.3

Table A2 detail properties of specimen No.3

Name:	Wong et al. 1990, No. 3
Type:	Spiral
Comments:	
Material Properties	
Concrete Strength:	37 (MPa)
Transverse Steel:	Yield Stress: 300 (MPa)
Longitudinal Steel:	Yield Stress: 475 (MPa) Strength: 625 (MPa)
Geometry	
Diameter:	400 (mm) Cross-Section: Circular
Length:	L-Inflection: 800 (mm) L-Measured: 800 (mm)
Test Configuration:	Cantilever
Loading	
Axial Load:	1,813 (kN)
P-D:	Shear provided
L-Bottom:	0
Longitudinal Reinforcement	
Diameter:	16 (mm)
Number of Bars:	20
Reinforcement Ratio:	0.032
Transverse Reinforcement	
Diameter Spiral:	10 (mm)
Hoop Spacing, Sv:	60 (mm)
Cover to Center of Hoop Bar:	20 (mm)
Reinforcement Ratio:	1.42
Non-Dimensional Properties	
Span-to-Depth Ratio:	2
Axial Load Ratio:	0.39
Test Results	
Failure Type:	Flexure
Damage Observation:	Concrete Crushing: 0 (mm) Significant Concrete Spalling: 9.7 (mm) Long Bar Buckling: 25.9 (mm) Long Bar Fracture: 0 (mm) Spiral Fracture: 0 (mm) Loss of Axial Load Capacity: 0 (mm)

A.3 Specimen 415

Table A2 detail properties of specimen 415

Name:	Lehman et al. 1998, 415
Type:	Spiral
Comments:	
Material Properties	
Concrete Strength:	31 (MPa)
Transverse Steel:	Yield Stress: 606.8 (MPa)
Longitudinal Steel:	Yield Stress: 462 (MPa) Strength: 630 (MPa)
Geometry	
Diameter:	609.6 (mm) Cross-Section: Circular
Length:	L-Inflection: 2,438.4 (mm) L-Measured: 2,438.4 (mm)
Test Configuration:	Cantilever
Loading	
Axial Load:	653.86 (kN)
P-D:	P Ram rotation decreases V
L-Bottom:	450
Longitudinal Reinforcement	
Diameter:	15.9 (mm)
Number of Bars:	22
Reinforcement Ratio:	0.0149
Transverse Reinforcement	
Diameter Spiral:	6.4 (mm)
Hoop Spacing, Sv:	31.8 (mm)
Cover to Center of Hoop Bar:	22.2 (mm)
Reinforcement Ratio:	0.7
Non-Dimensional Properties	
Span-to-Depth Ratio:	4
Axial Load Ratio:	0.072
Test Results	
Failure Type:	Flexure
Damage Observation:	Concrete Crushing: 38.1 (mm) Significant Concrete Spalling: 0 (mm) Long Bar Buckling: 127 (mm) Long Bar Fracture: 178 (mm) Spiral Fracture: 135 (mm) Loss of Axial Load Capacity: 0 (mm)

B. OpenSees Scripts

```
#2D Model of Cantilever Column pushover analysis; Metric units mm, g, N, sec
  wipe;
   set dataDir Data;              # set up name for data directory
   file mkdir $dataDir/;          # create data directory
   set GMdir "../GMfiles";        # ground-motion file directory
   set eleType 1;
   # Type 1 for force-based Element
   # Type 2 for Displacement Based
   # Type 3 for Concentrated plasticity with Modified Radau Integration method
   # Type 4 for Concentrated plasticity Radau Two integration points  method
   # Type 5 for Concentrated plasticity with Mid Points Integration method
   # Type 6 for Concentrated plasticity with End Points  Integration method
   if { $eleType == 1 } {
      set NoEle 1
      set nIP 6
   } elseif { $eleType == 2 } {
   set NoEle 2
   set nIP 2
   } elseif { $eleType == 3 } {
   set NoEle 1
   } elseif { $eleType == 4 } {
   set NoEle 1
   } elseif { $eleType == 5 } {
   set NoEle 1
   } elseif { $eleType == 6 } {
   set NoEle 1
   }
# Start of model generation
# create Model Builder (with 2-dimensions and 3 DOF/node)
    model BasicBuilder -ndm 2 -ndf 3
#input parameters
   set HEle 1372; #column height
```

```
    set DCol 305.00; #column diameter
    set clear Cover 12.5; #clear cover of concrete
    set PI 3.14;
    set ACol [expr $DCol**2*$PI/4.0]; #area of the column cross-section
    set IzCol [expr 1./12.*$DCol*pow($DCol,3)];
    set cocncreteweigt 25e-06;
   set g 9810;
   set mass [expr $cocncreteweigt/$g];
   set massDens [expr $cocncreteweigt/$g*$ACol*$HEle]
   set Weihtofcol [expr $cocncreteweigt*$ACol*$HEle]
# Define geometry for model
# nodal coordinates:
    node  1     0.0  0.0
    for { set i 0 } { $i < $NoEle } { incr i } {
    node  [expr $i+2]   0.0  [expr ($i+1)*$HEle]
    }
# set the boundary conditions
# fix tag DX DY Rot
     fix  1   1  1  1
# Define uniaxial materials
# define material tags
    set coreTag 1
    set coverTag 2
    set steelTag 3
#define longitudinal reinforcement and transverse reinforcement
    set db 9.5; #longitudinal bar diameter
    set barArea [expr 3.14159*($db/2.0)*($db/2.0)];
    set numBars 21; #number of longitudinal bars
    set fy 448; #yield strength of longitudinal bars
    set Es 200000.00; #modulus of elasticity of steel
    set Esf [expr $Es*0.015]; # tangent at initial strain hardening
    set dh 4; #diameter for  the spiral
    set NH 1; #number of hoops in the bundle
    set as1 12.56; #area of transverse reinforcement bar
```

```
set S 19; #the centerline distance between spirals along the height of the column
set fyh 434; #yield strength of the hoop
#unconfined concrete
set fc 29; # compressive strength of the concrete on the day of the test
set Ec [expr 5000*sqrt($fc)];
set fc      $fc;          # Unconfined concrete maximum stress
set eps1U  [expr 2.0*$fc/$Ec];      # strain at maximum strength of unconfined concrete
set fc20     [expr 0.2*$fc];      # ultimate stress
set eps2U  0.008;         # strain at ultimate stress
#confined concrete
# Mander's equations for calculating confined concrete compressive strength#
set sp [expr $S-$NH*$dh]; #clear distance between spirals
set ds [expr $DCol-2.0*$clearCover-$dh]; #diameter of the confined core
set Asp [expr $as1*$NH]; #total area of transverse reinforcement
set As [expr $barArea*$numBars]; #total area of the longitudinal bar
set Ac [expr $ds*$ds *$PI/4.0]; #area of core
set rho_cc [expr $As/$Ac]; #ratio of area of longitudinal reinf. to area of core of section
set k [expr (1.0 - $sp/2.0/$ds)/(1.0-$rho_cc)];#confinement effectiveness
set rho_t [expr 4.0*$Asp/$ds/$S]; # ratio of transverse reinforcement
set fh [expr 1.0/2.0*$k*$rho_t*$fyh]; #effective lateral confining stress on the concrete
set    fcc    [expr    $fc*(-1.254+2.254*sqrt(1.0+7.94*$fh/$fc)-2.0*$fh/$fc)];#confied strength
set epscc [expr $eps1U*(1.0+5.0*($fcc/$fc-1.0))]; #strain that corresponds to fcc'
set fcc20      [expr 0.2*$fcc];      # ultimate stress
set epscu [expr 0.004+0.14*$fyh/$fc*$rho_t]; #ultimate strain
# Define uniaxial materials
uniaxialMaterial Concrete02 $coverTag  -$fc  -$eps1U  -$fc20  -$eps2U  0.1 [expr -0.5* sqrt($fc)] [expr 0.5* sqrt($fc)/(2.0*$fc/$Ec)] ; #  plain concrete
uniaxialMaterial Concrete02 $coreTag  -$fcc  -$epscc  -$fcc20  -$epscu 0.1 [expr -0.5* sqrt($fcc)] [expr 0.5* sqrt($fcc)/(2.0*$fcc/$Ec)]; # confined concrete
uniaxialMaterial  Steel02    [expr  $steelTag+1]    $fy  $Es  0.010  20.00  0.925  0.15; # Menegotto-Pinto uniaxial steel model
uniaxialMaterial MinMax    $steelTag  [expr $steelTag+1]  -min -1.0e16 -max 0.09
```

```
    #Define Section
    set secnTag 1
    set nfCoreT 16
    set nfCoreR 10
    set nfCoverT 12
    set nfCoverR 8
    set total_conc_fibers [expr $nfCoreT*$nfCoreR+$nfCoverT*$nfCoverR]
    set ro [expr $DCol/2.0]; #radius of the column cross-section
    set rl [expr $ro-$clearCover-$dh-($db/2.0)]; #distance from the column centroid to the centroid of the long. bar
    set ri [expr ($ds-$sprime/4.)/2.]; #radius of the effectively confined core
# define circular fiber section
    section fiberSec $secnTag {
        # Define the core patch
        patch circ $coreTag $nfCoreT $nfCoreR 0 0 0 $ri 0.0 360.0
        # Define the cover patch
        patch circ $coverTag $nfCoverT $nfCoverR 0 0 $ri $ro 0.0 360.0
        # Define the reinforcing layer
        set theta [expr 360.0/$numBars]
        layer circ $steelTag $numBars $barArea 0 0 $rl [expr $theta/2.] [expr 360.0-$theta/2.]
    }
    set transfTag 1
    geomTransf Corotational $transfTag
# Define elements and element connectivity:
    set maxIters 6;
    set tol 10e-10;
    set LpJ 0;
    set LpI [expr 0.08*$HEle+ 0.022*$fy*$db]

for { set i 0 } { $i < $NoEle } { incr i } {
        if { $eleType ==1 } {
        element forceBeamColumn  [expr $i+1]  [expr $i+1] [expr $i+2]  $nIP $secnTag $transfTag
        } elseif { $eleType == 2 } {
```

```
        element dispBeamColumn  [expr $i+1]  [expr $i+1] [expr $i+2]  $nIP $secnTag $transfTag
        } elseif { $eleType ==3  } {
        element  forceBeamColumn  [expr  $i+1]  [expr  $i+1] [expr  $i+2]  $transfTag "HingeRadau $secnTag $LpI $secnTag $LpJ $secnTag"       }
  elseif { $eleType ==4  } {
        element  forceBeamColumn  [expr  $i+1]  [expr  $i+1] [expr  $i+2]  $transfTag "HingeRadauTwo $secnTag $LpI $secnTag $LpJ $secnTag"       }
elseif { $eleType ==5  } {
        element  forceBeamColumn  [expr  $i+1]  [expr  $i+1] [expr  $i+2]  $transfTag "HingeMidpoint $secnTag $LpI $secnTag $LpJ $secnTag"       }
elseif { $eleType ==6  } {
        element  forceBeamColumn  [expr  $i+1]  [expr  $i+1] [expr  $i+2]  $transfTag "HingeEndpoint $secnTag $LpI $secnTag $LpJ $secnTag"       }
    }
#Define Recorders
   recorder Node -file $dataDir/DFree.out -time -node 2 -dof 1 2 3 disp;      # displacements of free nodes
   recorder Node -file $dataDir/DBase.out -time -node 1 -dof 1 2 3 disp;      # displacements of support nodes
   recorder Node -file $dataDir/RBase.out -time -node 1 -dof 1 2 3 reaction;      # support reaction
   recorder Drift -file $dataDir/Drift.out -time -iNode 1 -jNode 2 -dof 1   -perpDirn 2 ;  # lateral drift
   recorder Element -file $dataDir/curvatu1a.out -time -ele 1 section 1  deformation;
   recorder Element -file $dataDir/curvatu1b.out -time -ele 1 section 2 deformation;
   recorder Element -file $dataDir/curvatu1c.out -time -ele 1 section 3 deformation;
   recorder Element -file $dataDir/curvatu1d.out -time -ele 1 section 4  deformation;
#Define Gravity Load
    set IDctrlNode [expr $NoEle+1];
    set ColWeight [expr $massDens*$g/$HEle];
    pattern Plain 1 Linear {
       load 2 0. -200000 0.;   # node#, FX FY MZ
    }
```

```
set Tol 1.0e-8;
constraints Transformation;
numberer Plain;
system BandGeneral;
test NormDispIncr $Tol 100 ;
algorithm Newton;
set NstepGravity 10;
set DGravity [expr 1./$NstepGravity];
integrator LoadControl $DGravity;
analysis Static;
analyze $NstepGravity;
loadConst -time 0.0
puts "Model built
 # LATERAL LOAD
set Tolerance 1.0e-8;
set MaxIterations 10;
set MaxDisplacement [expr 0.055*$HEle];
set DisplacementIncrement [expr $MaxDisplacement/1000];
set ControlDOF 1;
constraints Plain;
numberer RCM;
system BandGeneral;
test NormDispIncr $Tolerance $MaxIterations;
algorithm Newton;
integrator DisplacementControl $IDctrlNode $ControlDOF $DisplacementIncrement;
analysis Static;
set Load [expr $Weihtofcol];
pattern Plain 2 Linear {
load $IDctrlNode $Load 0.0 0.0;
}
# analysis
analyze 1000; #Steps
```